Helsinki University of Technology Reports in Electron Physics 2004/31

Espoo, September 2004

OPTICAL ACTIVATION OF COPPER IN SILICON STUDIED BY CARRIER LIFETIME MEASUREMENTS

Marko Yli-Koski

Dissertation for the degree of Doctor of Science in Technology to be presented with due permission of the Department of Electrical and Communications Engineering, for public examination and debate in Auditorium S4 at Helsinki University of Technology (Espoo, Finland) on the 12th of November, 2004, at 12 o'clock noon.

Helsinki University of Technology
Department of Electrical and Communications Engineering
Electron Physics Laboratory

Teknillinen korkeakoulu
Sähkö- ja tietoliikennetekniikan osasto
Elektronifysiikan laboratorio

Distribution:
Helsinki University of Technology
Electron Physics Laboratory
P.O.Box 3500
FIN-02015 HUT
Tel. +358-9-451 2322
Fax. +358-9-451 5008
http://www.hut.fi/Units/Electron/

© Marko Yli-Koski

ISBN 951-22-7233-4
ISBN 951-22-7234-2 (pdf)

ISSN 0781-4984

Otamedia Oy
Espoo 2004

HELSINKI UNIVERSITY OF TECHNOLOGY
P.O. BOX 1000, FIN-02015 HUT
http://www.hut.fi

ABSTRACT OF DOCTORAL DISSERTATION

Author

Name of the dissertation

Date of manuscript

Date of the dissertation

Monograph

Article dissertation (summary + original articles)

Department
Laboratory
Field of research
Opponent(s)
Supervisor
(Instructor)

Abstract

Keywords

UDC

Number of pages

ISBN (printed)

ISBN (pdf)

ISBN (others)

ISSN

Publisher

Print distribution

The dissertation can be read at http://lib.hut.fi/Diss/

Preface

The work for this thesis has been carried out at the Electron Physics Laboratory of Helsinki University of Technology mainly during the years 1999-2003. I would especially like to thank Professor Juha Sinkkonen, who has supervised my work. I would also like to thank the personnel of the Electron Physics Laboratory. I wish to thank the personnel of the Microelectronics Centre at Helsinki University of Technology for the use of their clean room facilities and equipment. I would like to thank everyone who has participated in the board or the guidance group of the “Oxygen precipitation in silicon wafers and its technical applications (Happii)” -project or the “Recombination lifetime of minority charge carriers” -project.

Graduate School of Silicon Technology and Microsystems, National Technology Agency (TEKES), Okmetic Oyj, Micro Analog Systems Oy, VTI Technologies Oy and the Foundation of Technology in Finland are acknowledged for the financial support of this work.

Espoo, September 2004
Marko Yli-Koski

Author's contribution

The author carried out the processing of samples, the optical activations, the lifetime measurements (µPCD) and (SPV), the interpretation of measurement results, the simulations and most of the planning. The author planned part of the experiments together with Hele Savin and Antti Haarahiltunen. TID measurements and the electric contacts for TID measurements were carried out by Hele Savin. TXRF measurements were carried out by Okmetic Oyj. SIRM measurements were carried out by the Laboratory of Physical Metallurgy and Materials Science at Helsinki University of Technology.

List of Symbols

A	area
A_m	amplitude of m's decay
$\bar{c}$	average solute impurity concentration
c_0	initial impurity concentration
c_n	electron capture coefficient
C_n	electron Auger coefficient
C_p	hole Auger coefficient
c_p	hole capture coefficient
c_{prec}	precipitated impurity concentration
c_{prec1}	the concentration of impurity atoms precipitated at oxygen defects
c_{prec2}	the concentration of impurity atoms precipitated at microscopic lattice defects
c_S	impurity solubility at the precipitate interface
D	impurity diffusivity
d	the thickness of plate-shaped precipitate
D_{a}	ambipolar diffusivity
D_{eff}	effective diffusivity
D_{int}	intrinsic diffusivity
D_n	the diffusivity of minority charge carriers
e	elementary charge
E_{c}	the energy of conduction band edge
E_{F}	Fermi level
E_{Fn}	electron quasi-Fermi level
e_n	electron emission constant
e_p	hole emission constant
E_{t}	the energy level of a localized energy state in the bandgap
E_{v}	the energy of the valence band edge
$f(E_{\mathrm{t}})$	the probability that a localized energy state is occupied by an electron
f_{D}	Fermi-Dirac distribution function
$f_{\mathrm{SS}}(E_{\mathrm{t}})$	the probability that a localized state is occupied by an electron at steady-state
G	generation rate of electron-hole pairs due to external excitation
i	index
$\mathbf{J}_n$	electron current density
$\mathbf{J}_p$	hole current density
k	Boltzmann's constant
k_{prec}	volume recombination coefficient
k_{prec1}	volume recombination coefficient of impurity atoms precipitated at oxygen defects
k_{prec2}	volume recombination coefficient of impurity atoms precipitated at microscopic lattice defects
L_n	minority charge carrier diffusion length
m	index
n	the density of the precipitates
n	the density of free electrons
n_0	thermal equilibrium electron concentration

N_a^-	ionized acceptor dopant concentration
N_a	acceptor dopant concentration
N_c	the effective conduction band density of states
N_d^+	ionized donor dopant concentration
n_i	intrinsic carrier density
N_v	the effective valence band density of states
n_{prec1}	the density of the precipitates at oxygen defects
n_{prec2}	the density of the precipitates at microscopic lattice defects
n_s	electron concentration at the interface
n_S	the density of precipitates in the surface recombination model
N_t	the density of localized energy levels
N_{dis}^{total}	the concentration of dissolved impurity atoms
$N_{dis}^{immobile}$	the concentration of immobile dissolved impurity atoms
N_{dis}^{mobile}	the concentration of mobile dissolved impurity atoms
P	the light power density of bias-light
p	the density of free holes
p_0	thermal equilibrium hole concentration
p_s	hole concentration at the interface
$Q_t^{0/-}$	charge density at acceptor level
$Q_t^{+/0}$	charge density at donor level
Q_t	charge density at localized energy levels
r	the radius of the precipitates
R_A	fitting parameter, the saturation of copper related recombination rate
R_{Auger}	Auger recombination rate
R_C	capture radius
R_{ct}	electron capture rate from conduction band
R_{Cu}	recombination rate at light-induced copper precipitates
$R_{intrinsic}$	intrinsic recombination rate
R_n	net electron capture rate from conduction band
R_{others}	recombination rate at other defects than light-induced copper precipitates
R_p	net hole capture rate from valence band
R_{prec}	recombination rate at precipitates
R_{prec1}	recombination rate at precipitates at oxygen defects
R_{prec2}	recombination rate at precipitates at microscopic lattice defects
R_{rad}	radiative recombination rate
R_S	recombination rate at surface states
r_S	the radius of precipitates in the surface recombination model
R_{SS}	the steady-state recombination rate of charge carriers
R_{tc}	electron emission rate into conduction band
R_{vt}	hole capture rate from valence band
R_{tv}	hole emission rate into valence band
R_{prec}^S	recombination rate at the surface of the precipitates
S	surface recombination velocity
S_{Cu}	copper solubility

S_{prec}	surface recombination velocity at the precipitate surface
S_{prec1}	the surface recombination velocity at precipitates at oxygen defects
S_{prec2}	the surface recombination velocity at precipitates at microscopic lattice defects
$\overline{\mathbf{n}}$	surface normal vector
T	sample thickness
T	temperature
t	time
$\Delta\overline{c}$	the change of solute impurity concentration at time interval
v_n	the thermal velocity of electrons
v_p	the thermal velocity of holes
v_{th}	carrier thermal velocity
Δn	excess electron concentration
Δn_{ss}	steady-state excess charge carrier concentration
Δp	excess hole concentration
Δt	time interval
$\Delta\sigma$	excess conductivity
Ω	equilibrium constant
α	abbreviation
ε	the relative permittivity of silicon
ε_0	the permittivity of free space
μ_n	electron mobility
μ_p	hole mobility
ρ	the density of impurity atoms in the precipitate
σ	conductivity
σ_n	electron capture cross-section
σ_p	hole capture cross-section
τ_0	precipitation time constant
τ_2	carrier lifetime after the optical activation
τ_{A}	fitting parameter, the precipitation time constant
τ_{b}	charge carrier recombination lifetime in bulk
τ_{C}	the capture time constant of mobile dissolved atoms
τ_{Cupair}	the dissociation time constant of copper-pairs
τ_{diff}	diffusion time constant
τ_{diss}	the dissociation time constant of immobile dissolved atoms
τ_{eff}	effective carrier lifetime
$\tau_{\text{eff.d}}$	differential effective carrier lifetime
τ_{extended}	recombination lifetime for extended recombination sites in the bandgap
τ_i	multiphonon recombination lifetime for localized energy state i
$\tau_{\text{intrinsic}}$	intrinsic charge carrier recombination lifetime at steady-state
τ_{LL}	low-injection level carrier lifetime
τ_m	decay time constant
τ_{max}	maximum measured lifetime
τ_n	excess electron lifetime
τ_{od}	out-diffusion time constant
τ_p	excess hole lifetime
τ_{PCD}	carrier lifetime determined by means of the μPCD technique

τ_{SS} charge carrier recombination lifetime at steady-state

Abbreviations

ASTM	American society for testing and materials
DLTS	deep level transient spectroscopy
EBIC	electron beam induced current
GF-AAS	graphite furnace atomic absorption spectroscopy
HF	hydrofluoric acid
HCl	hydrochloric acid
HNO_3	nitric acid
H_2O_2	hydrogen peroxide
ICP-MS	inductively coupled plasma mass spectrometry
NH_4OH	ammonium hydroxide
SHR	Shockley-Hall-Read
SIRM	scanning infrared microscope
SPV	surface photovoltage
TEM	transmission electron microscope
TID	transient ion drift
TXRF	total reflection X-ray fluorescence spectroscopy
µPCD	microwave photoconductive decay
VPD	vapour phase decomposition

Contents

Preface ... iv
Author's contribution ... v
List of Symbols ... vi
Abbreviations ... x
Contents ... xi
1 Introduction ... 1
2 Copper in silicon ... 4
2.1 Diffusivity ... 4
2.1.1 Intrinsic diffusivity ... 4
2.1.2 Effective diffusivity ... 4
2.1.3 Donor-acceptor pairing ... 4
2.2 Solubility ... 6
2.3 Behaviour during heat treatment ... 7
2.3.1 General ... 7
2.3.2 Copper concentration above 10^{17} cm^{-3} ... 7
2.3.3 Copper concentration between 10^{13}-10^{17} cm^{-3} in p-type silicon ... 7
2.3.4 Copper in n-type silicon ... 8
2.4 Electrical properties ... 9
2.4.1 Interstitial copper ... 9
2.4.2 Copper-pairs ... 9
2.4.3 Copper precipitates ... 9
2.5 Charge carrier lifetime and copper contamination ... 10
3 Theory ... 13
3.1 Charge carrier lifetime ... 13
3.1.1 General ... 13
3.1.2 Multiphonon recombination ... 13
3.1.3 Intrinsic recombination ... 17
3.1.4 Bulk lifetime ... 17
3.1.5 Surface recombination ... 17
3.1.6 Effective lifetime ... 18
3.1.7 Low-injection-level lifetime ... 19
3.2 μPCD technique ... 20
3.2.1 Time constant of decay ... 20
3.2.2 Differential effective lifetime ... 21
3.3 Precipitation kinetics ... 21
3.3.1 Fixed radius ... 21
3.3.2 Growing radius ... 22
3.3.3 Density and radius of defects ... 23
3.4 Recombination at precipitates ... 23
3.4.1 Volume recombination model ... 23
3.4.2 Surface recombination model ... 24
3.4.3 Comparison of recombination models ... 24
3.4.4 Volume recombination at two kinds of defects ... 26
3.4.5 Surface recombination at two kinds of defects ... 27

4 Experimental.. 28
4.1 Wafers 28
4.2 Thermal oxidation.. 28
4.3 Copper surface contamination.. 29
4.4 Copper in-diffusion.. 29
4.5 Corona charge generation 30
4.6 Optical activation.. 30
4.7 Charge carrier lifetime measurement equipment............................. 30
4.8 Determination of recombination rate 31
4.9 Determination of the precipitation time constant and the saturation of the recombination rate.. 32
4.10 TXRF.. 33
4.11 TID 33
4.12 SIRM 33
4.13 SPV... 33
5 Results and discussion 34
5.1 Copper concentration.. 34
5.2 Oxygen defect density 35
5.3 Carrier lifetime 35
5.3.1 Carrier lifetime dependence on copper contamination level.......... 35
5.3.2 Recombination activity of interstitial copper 37
5.4 Recombination dependence on activation time................................. 38
5.4.1 Examples 38
5.4.2 Measurement inaccuracy.. 41
5.4.3 Comparison of measurements and theory 42
5.5 Out-diffusion of copper by means of negative corona charge 42
5.6 In-diffusion of copper by means of positive corona charge............... 44
5.7 Precipitation time constant dependence on light intensity................. 45
5.8 Properties of copper precipitates... 47
5.8.1 Saturation of the recombination rate and the precipitation time constant................ 47
5.8.2 Density and radius.. 48
5.8.3 Recombination activity 49
5.8.4 Influence of copper concentration.. 50
5.8.5 Influence of oxygen defects 53
5.9 Models with two kinds of recombination sites.................................. 55
5.9.1 Volume recombination.. 55
5.9.2 Surface recombination 56
5.10 Determination of copper concentration.. 57
5.10.1 General.. 57
5.10.2 Volume recombination model.. 57
5.10.3 Surface recombination model... 60
6 Conclusion... 62
Appendix A Recombination activity of copper precipitates..................... 66
A.1 Calculations for comparison 66
Appendix B Simulation 68
B.1 Excess charge carrier concentration 68

B.1.1 Measurement conditions 68
B.1.2 Optical activation conditions 69
Bibliography 70

1 Introduction

The fabrication of modern integrated circuits requires clean production equipment and a clean environment in order to avoid defects in devices. Due to constant miniaturization smaller and smaller quantities of impurities are tolerated in devices and so improvements in the technology of impurity detection are needed. The main detrimental metal impurities in processed silicon wafers are iron, copper and nickel [1]. Trace copper contamination on the surface of silicon wafers can be measured quantitatively by means of total reflection x-ray fluorescence (TXRF) [2]. Trace copper contamination in bulk silicon can be measured by chemical analysis methods, such as graphite furnace atomic absorption spectroscopy (GF-AAS) [3] and inductively coupled plasma mass spectrometry (ICP-MS) [4, 5]. These measurement techniques are slow and expensive. The interstitial copper concentration in bulk silicon can be measured by means of the transient ion drift technique (TID) [6], in which electrical contacts are needed.

The charge carrier recombination in silicon is a physical phenomenon, which is characterized by the charge carrier lifetime. Iron contamination in silicon is commonly identified quantitatively by means of carrier lifetime measurements. Therefore, carrier lifetime measurement equipment already exists in production plants. However, there is not yet a method to determine copper contamination in silicon quantitatively by means of carrier lifetime measurements. Copper contamination in silicon is identified qualitatively by analyzing the charge carrier lifetime in p-type and n-type silicon. Copper contamination decreases the lifetime in n-type silicon but not in p-type silicon [7]. The copper contamination level is estimated by means of carrier lifetime values in n-type silicon.

Henley *et al.* [8] reported a new copper related phenomenon in 1999 that shows promise for the quantitative detection of copper in p-type silicon by means of lifetime measurements. They found that light and heat treatments decreased the charge carrier diffusion length in boron doped Czochralski silicon that had been contaminated by copper in an oxidizing atmosphere. Ramappa [9] reported on the same phenomenon in boron doped float-zone silicon in 2000. The optical activation procedure involved exposing the sample to light with a photon energy above the silicon bandgap.

Flink *et al.* [10] found that copper predominantly diffuses from bulk silicon to the silicon surface at room temperature after a quench. Shabani *et al.* [3] found that copper stays in bulk silicon of an air-cooled sample, if a silicon dioxide layer covered the surfaces. Shabani *et al.* [11] suggested that the surface band bending influences copper diffusion to the sample surfaces. Excess charge carriers decrease the surface band bending during optical activation of copper. Therefore, the question is how to prevent the copper diffusion to the silicon surface during light treatment.

The recombination activity of copper has been reported to be quite low at trace copper contamination levels after optical activation. Raineri *et al.* [12] reported that they did not find any change of the charge carrier diffusion length in copper contaminated p-type silicon due to light treatment when the copper dose was below 10^{13} cm^{-2}. Tarasov *et al.* [13] detected the decrease of the diffusion length from 312 μm to 264 μm in a rapidly cooled silicon sample contaminated by a copper concentration of 10^{12} cm^{-2}. Oxygen defects are known to increase the

influence of copper contamination on the lifetime, because oxygen defects increase copper precipitation in the bulk during the cooling period [14]. Do oxygen defects increase the recombination activity of light-induced copper precipitates?

Ramappa [9] reported that light intensity has an influence on the rate by which the lifetime decreases due to illumination. The light generates excess charge carriers in silicon, which change the occupation of energy levels in the bandgap. The charge state of copper precipitates affects the precipitation behaviour of copper atoms, which is confirmed by Flink *et al.* [10]. Is the change of charge state of copper precipitates the reason for the growth of light-induced copper precipitates?

The aim of the research done here is to develop the sample preparation method for the determination of trace copper contamination by means of charger carrier lifetime measurements. The objective is to study the influence of corona charge, light intensity and oxygen defects on the recombination activity of copper and on the formation of copper precipitates.

The experimental study includes the processing of the copper contaminated samples. Copper precipitates are induced in silicon through the use of high intensity light. The recombination activity of copper is measured by means of the microwave photoconductive decay technique (μPCD). The TXRF technique is used to determine the copper surface concentration and the TID technique is used to determine the interstitial copper bulk concentration. The theoretical study includes the interpretation of lifetime measurement results using the diffusion-limited precipitation model.

The scope of this research is the measuring of the recombination activity of copper precipitates, mainly using the microwave photoconductive decay technique under high injection level conditions. The emphasis of this study is on copper concentration levels below 10^{13} cm^{-3}. The copper contaminated samples are air-cooled, i.e. the samples are not quenched.

An outline of the dissertation

Chapter 2 is a review in the field of copper properties in silicon. It emphasizes the diffusivity and solubility of copper, copper precipitation, the electrical properties of interstitial copper and copper precipitates, and charge carrier lifetime dependence on copper contamination.

Chapter 3 deals with the theories and models used in this work. Chapter 3.1 and chapter 3.2 cover the theory of carrier lifetime for microwave photoconductive decay measurements. Chapter 3.3 deals with the models for diffusion-limited precipitation. Chapter 3.4 presents the volume recombination and surface recombination models for copper precipitates.

Chapter 4 describes the experimental work done on sample preparation. The carrier lifetime measurement equipment is outlined.

Chapter 5 presents the charge carrier lifetime and copper contamination measurement results, and the calculated properties for copper defects.

Chapter 6 consists of the conclusion. It addresses the importance of a positive corona charge to keep copper in bulk silicon, which is a precondition for the formation of copper defects by light treatment.

2 Copper in silicon

2.1 Diffusivity

2.1.1 Intrinsic diffusivity

Copper diffuses in silicon as a positively charged interstitial ion [15]. The diffusivity of interstitial copper in n-type and intrinsic silicon is [16]

$$D_{\mathrm{int}} = (3.0 \pm 0.3) \times 10^{-4} \exp\left(-\frac{0.18 \mp 0.01\,\mathrm{eV}}{kT} \right) \qquad \mathrm{cm^2 \cdot s^{-1}}, \tag{2.1}$$

where T is the temperature and k is Boltzmann's constant. The intrinsic diffusivity is 2.4×10^{-7} $\mathrm{cm^2 \cdot s^{-1}}$ at room temperature.

2.1.2 Effective diffusivity

Positively charged copper ions pair with the negatively charged acceptor atoms. The consequence of the pairing reaction is that only a fraction of the dissolved copper atoms are mobile. The copper-acceptor pairs are more likely to form when the acceptor concentration increases. Therefore, the diffusivity of copper decreases when the acceptor concentration increases. The effective diffusivity of copper in boron-doped silicon can be written as a numerical equation when the dissolved copper concentration is much lower than the boron concentration and the boron concentration is below 10^{17} $\mathrm{cm^{-3}}$ [16]. The effective diffusivity of copper is [16]

$$D_{\mathrm{eff}} = \frac{3 \times 10^{-4} \exp(-2090/T)}{1 + 2.584 \times 10^{-20} \exp(4990/T)(N_{\mathrm{a}}/T)} \qquad \mathrm{cm^2 \cdot s^{-1}}, \tag{2.2}$$

where N_{a} is the acceptor concentration in $\mathrm{cm^{-3}}$ and T is in Kelvin. The effective diffusivity is 7.5×10^{-8} $\mathrm{cm^2 \cdot s^{-1}}$ at room temperature when the boron concentration is 10^{15} $\mathrm{cm^{-3}}$ in silicon. This effective diffusivity is about a third of the intrinsic diffusivity. Therefore, the diffusivity of copper in silicon decreases already at a low boron concentration at room temperature. However, the copper diffusivity is still high, the diffusion length of copper is 160 µm per hour.

2.1.3 Donor-acceptor pairing

This section outlines the diffusion theory, which includes the trapping of mobile donors by immobile acceptors. The theory was presented by Reiss *et al.* [17] and utilized by Istratov *et al.* [16] when deriving the numerical equation (2.2) for the effective diffusivity of copper. The equations presented in this section can be used to calculate the copper diffusivity in silicon even when the copper concentration is not much lower than the boron concentration. When the

donor concentration approaches the acceptor concentration, the effective diffusivity should be calculated using other equations [17].

The effective diffusivity of dissolved atoms D_{eff} in presence of a trapping process is [17]

$$D_{\text{eff}} = D_{\text{int}} \frac{N_{\text{dis}}^{\text{mobile}}}{N_{\text{dis}}^{\text{total}}} = D_{\text{int}} (1 - \frac{N_{\text{dis}}^{\text{immobile}}}{N_{\text{dis}}^{\text{total}}}), \tag{2.3}$$

where $N_{\text{dis}}^{\text{mobile}}$ is the concentration of mobile dissolved atoms, $N_{\text{dis}}^{\text{immobile}}$ is the concentration of immobile dissolved atoms and $N_{\text{dis}}^{\text{total}}$ is their sum. D_{int} is the intrinsic diffusivity of dissolved atoms without the trapping process.

A mobile dissolved atom is captured, i.e. immobile, if it is within the capture radius of an acceptor atom. In the theory of Reiss *et al.* [17], the capture radius R_{C} is calculated from the condition that the Coulomb energy is equal to the average thermal energy

$$R_{\text{C}} = \frac{e^2}{4\pi\varepsilon\varepsilon_0 kT}, \tag{2.4}$$

where e is the elementary charge, ε is the relative permittivity of silicon, ε_0 is the permittivity of free space. By inserting the constants into equation (2.4), the calculated capture radius is 4.9 nm at room temperature. At doping levels above 10^{17} cm^{-3}, the capture radius should be calculated using the screened Coulomb potential [16].

The definition of the equilibrium constant Ω for immobile dissolved atoms is [17]

$$\Omega = \frac{N_{\text{dis}}^{\text{immobile}}}{(N_{\text{a}} - N_{\text{dis}}^{\text{immobile}})(N_{\text{dis}}^{\text{total}} - N_{\text{dis}}^{\text{immobile}})}. \tag{2.5}$$

The ratio between the concentration of the immobile dissolved atoms and the concentration of total dissolved atoms, which occurs in equation (2.3), is from equation (2.5) [17]

$$\frac{N_{\text{dis}}^{\text{immobile}}}{N_{\text{dis}}^{\text{total}}} = 0.5 \times \left(\alpha - \sqrt{\alpha^2 - 4N_{\text{a}} / N_{\text{dis}}^{\text{total}}}\right), \tag{2.6}$$

where

$$\alpha = 1 + \frac{N_{\text{a}}}{N_{\text{dis}}^{\text{total}}} + \frac{1}{\Omega N_{\text{dis}}^{\text{total}}}. \tag{2.7}$$

At thermal equilibrium, the dissociation rate of immobile dissolved atoms equals the capture rate of mobile dissolved atoms

$$\frac{N_{\mathrm{dis}}^{\mathrm{immobile}}}{\tau_{\mathrm{diss}}} = \frac{N_{\mathrm{dis}}^{\mathrm{total}} - N_{\mathrm{dis}}^{\mathrm{immobile}}}{\tau_{\mathrm{C}}}, \tag{2.8}$$

where τ_{diss} is the dissociation time constant of immobile dissolved atoms and τ_{C} is the capture time constant of mobile dissolved atoms. For example, the dissociation rate of immobile copper atoms from boron atoms is [16]

$$\frac{1}{\tau_{\mathrm{diss}}} = (2.05 \pm 0.80)\times 10^{13} \exp\left(-\frac{0.61 \pm 0.01\,\mathrm{eV}}{kT}\right) \qquad \mathrm{s}^{-1}. \tag{2.9}$$

In the theory of Reiss *et al.* [17], the capture of mobile dissolved atoms into the acceptor atoms is diffusion limited. The capture time constant is from Fick's law [17]

$$\tau_{\mathrm{C}} = \frac{1}{4\pi D_{\mathrm{int}} R_{\mathrm{C}} (N_{\mathrm{a}} - N_{\mathrm{dis}}^{\mathrm{immobile}})}. \tag{2.10}$$

The term $N_{\mathrm{a}} - N_{\mathrm{dis}}^{\mathrm{immobile}}$ is the concentration of acceptor atoms not containing an impurity atom within the capture radius.

Using equations (2.5) and (2.8) the equilibrium constant can be expressed as

$$\Omega = \frac{\tau_{\mathrm{diss}}}{\tau_{\mathrm{C}} (N_{\mathrm{a}} - N_{\mathrm{dis}}^{\mathrm{immobile}})}. \tag{2.11}$$

Inserting τ_{C} from equation (2.10) leads to

$$\Omega = \tau_{\mathrm{diss}} 4\pi D_{\mathrm{int}} R_{\mathrm{C}}, \tag{2.12}$$

which is in usable form for equation (2.7) and the effective diffusivity can be calculated from equation (2.3).

2.2 Solubility

In non-degenerate silicon, the copper solubility is dominated by the solubility of interstitial copper [15]. The copper solubility in silicon is [18]

$$S_{\mathrm{Cu}} = 5\times 10^{22} \exp\left(2.4 - \frac{1.49\,\mathrm{eV}}{kT}\right) \qquad \mathrm{cm}^{-3}. \tag{2.13}$$

The solubility was determined in a temperature range from 500 ºC to 800 ºC [18]. The solubility is as high as 10^{14} cm^{-3} at 500 ºC. At room temperature the solubility is small, 0.05 cm^{-3}, extrapolating from equation (2.13).

2.3 Behaviour during heat treatment

2.3.1 General

Copper can easily diffuse from a contaminated silicon surface into bulk during thermal processes. The high copper solubility and diffusivity enable a high copper concentration to form in silicon in a short period of time. Because copper atoms have high diffusivity and low solubility at room temperature copper favours defect reactions during the cooling period. The following sections outline the defect reaction dependence on copper concentration and cooling rate.

2.3.2 Copper concentration above 10^{17} cm^{-3}

Seibt *et al.* [19] and Istratov *et al.* [20] have reviewed copper precipitation in silicon containing copper concentrations above 10^{17} cm^{-3}. Transmission electron microscopy (TEM) investigations have revealed planar and spherical copper precipitates in the bulk [21]. The thicknesses of these planar precipitates range from 0.5 nm to 5 nm and the diameters of the precipitates range from 30 nm to 500 nm, with a precipitate density up to 10^{13} cm^{-3} [20, 21, 22]. The size of the planar precipitates depends on the contamination level and the cooling rate [19]. Small spherical copper precipitates grow around planar precipitates [21]. The planar precipitates decompose into spherical precipitates [19] during low temperature annealing, 260 ºC to 400 ºC. The spherical copper precipitates also grow at dislocations and at stacking faults, which are sinks for interstitial silicon atoms. The size of the spherical precipitates has been found to be from a few nanometers [23] to 20 nm [24]. At cooling rates around 25 K·s^{-1} copper forms precipitates at the surface [24]. The precipitates extend below the surface [24]. The diameter of the copper precipitates in copper precipitate colonies varies from 7 nm to 20 nm. The size of copper precipitate colonies ranges from 0.5 µm to 80 µm [24].

2.3.3 Copper concentration between 10^{13}-10^{17} cm^{-3} in p-type silicon

The Fermi-level position determines the amount of precipitated copper in p-type homogeneous silicon when the cooling rate is above 500 K·s^{-1} [10]. Solute copper atoms precipitate when the Fermi-level is above E_c-0.2 eV, where E_c is the energy of the conduction band edge [10]. The copper precipitation dependence on the Fermi-level position has been explained with electrostatic interaction between the positively charged interstitial copper atoms and the copper precipitates [10]. The copper precipitates have been explained to be positively charged when the Fermi-level is below E_c-0.2 eV, and neutral or negatively charged when the Fermi-level is above E_c-0.2 eV [10]. The acceptor doping concentration and the interstitial donor copper concentration determine the Fermi-level, which is above E_c-0.2 eV when the copper concentration exceeds the acceptor doping concentration with more than 10^{16} cm^{-3}. Almost all solute copper atoms can be quenched in interstitial states when the Fermi-level is below E_c-0.2 eV [10]. Copper diffuses from the bulk to the wafer surfaces at room temperature in a few days if the silicon dioxide layer is removed from the silicon surface [3]. It has been suggested that the potential barrier at the surface slows down the out-diffusion [11].

Shabani *et al.* [3] reported that a copper surface contamination of 2.2×10^{13} cm^{-2} was homogeneously distributed in the bulk after air-cooling. The amount of copper at the surface was below 3 % of the total copper in bulk. Hourai *et al.* [25] reported that a copper surface concentration of about 10^{13} cm^{-2} causes shallow etch pits with a density of about 10^{5} cm^{-2}. The silicon surface was etched using a preferential etching solution after the heat treatment. A density of 10^{5} cm^{-2} means strong copper precipitation in the silicon surface. Shabani *et al.* [11] suggested that the silicon surface condition during the cooling down period strongly affects the out-diffusion of copper. It has also been reported that the copper out-diffusion is suppressed when the thickness of the oxide layer is between 3 nm and 4 nm [3]. This may explain the contrary results that have been presented.

Copper forms copper-pairs in p-type silicon. It has been proposed that the copper-pairs form between interstitial copper atoms and substitutional copper atoms [26]. Koveshnikov *et al.* [27] measured a copper-pair concentration of 6×10^{12} cm^{-3} in boron doped Czochralski silicon, which was ion implanted with a copper dose of 10^{12} cm^{-2} and then underwent rapid thermal annealing. The copper-pair concentration was measured using deep level transient spectroscopy (DLTS). The result indicates that almost all the copper was in copper-pairs. Erzgräber *et al.* [28] measured a copper-pair concentration of 7×10^{13} cm^{-3} in boron doped float-zone silicon that had not been quenched. Unfortunately, the copper concentration level was not determined. In general, the dependence of the copper-pair concentration on the copper concentration, the cooling rate and the surface condition of the sample is not known. However, the copper-pair concentration is low in air-cooled silicon containing a copper concentration of 3×10^{14} cm^{-3}. According to Shabani *et al.* [3] the copper out-diffused in two days. The copper out-diffusion would have been delayed, if copper pairs had existed. The dissociation time constant of copper-pairs τ_{Cupair} is [26]

$$\tau_{\mathrm{Cupair}} = 1.47\times10^{-10}\exp\left(\frac{1.02\pm0.07\ \mathrm{eV}}{kT}\right) \quad \mathrm{s.} \qquad (2.14)$$

The dissociation time constant of copper-pairs is from 22 days to 5 years from equation (2.14) at T=297 K. These are extreme values.

2.3.4 Copper in n-type silicon

Istratov *et al.* [29] reported that the maximum achievable interstitial copper concentration in n-type silicon is 10^{13} cm^{-3}, when the cooling rate is about 1000 K·s^{-1}. The interstitial copper concentration was measured by means of DLTS. The time constant for a decrease in the interstitial copper concentration was about six hours at room temperature. The measured activation energy of the time constant was (0.56 ± 0.03) eV. The interstitial copper concentration was $(4\text{-}7)\times10^{11}$ cm^{-3} at steady-state conditions. Shabani *et al.* [3] did not detect any copper out-diffusion in n-type silicon below 200 ºC, when the samples were first air-cooled from 800 ºC. This indicates that copper forms complexes or precipitates during air-cooling in n-type silicon, which prevents copper out-diffusion at room temperature.

2.4 Electrical properties

2.4.1 Interstitial copper

Interstitial copper atoms have low recombination activity compared to interstitial iron atoms. The recombination activity is low because interstitial copper atoms do not form an energy level in the middle of the bandgap of silicon. The interstitial copper in silicon forms the donor level at E_c-(0.15±0.01) eV with an electron capture cross-section of 1.5×10^{-15} cm^2. The energy level and the capture cross-section were determined by means of DLTS [29]. Istratov *et al.* [30] suggested that a dissolved copper concentration of 10^{15} cm^{-3} causes a charge carrier diffusion length of 110 μm in silicon with a boron concentration of 2×10^{15} cm^{-3}. The copper concentration was determined from the compensated boron concentration by means of C-V measurements at 80 K. The diffusion length corresponding to the interstitial copper was determined by measuring the change of the diffusion length.

For comparison, an interstitial iron concentration of 3×10^{11} cm^{-3} causes a charge carrier diffusion length of 110 μm. The diffusion length was calculated using the SHR-equation (3.23) with an energy level at E_v+0.38 eV [31], and an electron and a hole capture cross-section of 4×10^{-14} cm^2 [31] and 7×10^{-17} cm^2 [31], respectively.

2.4.2 Copper-pairs

Copper-pairs in silicon have a donor level at E_v+(0.088±0.006) eV [26], where E_v is the energy of the valence band edge. A value of E_v+0.096 eV has also been presented [27]. The hole capture cross section is between 3×10^{-15} cm^2 [26] and 1.5×10^{-14} cm^2 [28]. It has been proposed that pairs form between interstitial copper atoms and substitutional copper atoms [26]. The copper-pair concentration is not easy to determine by means of DLTS, because iron-boron pairs have almost the same energy level and hole capture cross-section [27].

2.4.3 Copper precipitates

It was presented in chapter 2.3 that copper forms precipitates in silicon. Two reproducible energy levels have been found in copper contaminated samples, E_v+(0.20 to 0.23) eV and E_v+(0.41 to 0.46) eV [20].

Copper precipitates in quenched silicon samples containing copper concentration above 10^{16} cm^{-3} have been characterized by means of TEM, DLTS and electron beam induced current (EBIC) techniques [19, 21, 22, 32]. Istratov *et al.* [22] studied the DLTS spectrum and the minority carrier diffusion length dependence on the size of the copper precipitates. The minority carrier diffusion length was determined using the EBIC technique. The sizes of the precipitates were varied by changing the cooling rate. A copper concentration of 10^{17} cm^{-3} was used to obtain a sufficient precipitate-related DLTS-signal amplitude. TEM studies showed that the diameters of the copper precipitates were 30 nm, 70 nm and 240 nm, with densities of 4.3×10^{12} cm^{-3}, 1.1×10^{12} cm^{-3} and 1.4×10^{9} cm^{-3} for cooling rates of 2000 K·s^{-1}, 1000 K·s^{-1} and 200 K·s^{-1}, respectively. The precipitates were plate-shaped and mostly parallel to silicon (111)

planes. The thicknesses of the precipitates were about 0.5 nm for cooling rates of 2000 $K \cdot s^{-1}$ and 1000 $K \cdot s^{-1}$ and about 5 nm for a cooling rate of 200 $K \cdot s^{-1}$. The DLTS-spectra of copper precipitates obtained after a cooling rate of 2000 $K \cdot s^{-1}$ was almost rectangular, with a width of almost 100 K. From the DLTS spectra it was estimated that copper silicide precipitates form band-like states in the silicon bandgap between E_c-0.15 eV and E_c-0.40 eV [22]. The peak in the DLTS spectra was narrower for slower cooling rates. The minority carrier diffusion length was below 2.2 µm, 2.6 µm and 13 µm when the cooling rates were about 2000 $K \cdot s^{-1}$, 1000 $K \cdot s^{-1}$ and 200 $K \cdot s^{-1}$, respectively. Istratov *et al.* [22] suggested that the high recombination activity of copper precipitates is due to the attraction of charge carriers by space charge regions around the positively charged precipitates and the defect states close to the mid-gap.

Copper forms precipitates at crystal defects in silicon [7]. Copper increases the recombination activity of crystal defects [33]. Shen *et al.* [34] reported that copper precipitates were not observed at the surface of oxygen precipitates. The copper precipitates were next to the oxygen precipitates at dislocations [34]. Correia *et al.* [35] measured a minority carrier diffusion length of 4 µm for a sample with a defect density of 10^{15} cm^{-3}. The defects were suggested to be copper decorated oxygen precipitates. They also found that in stacking faults copper silicide particles are more efficient than oxide particles as recombination sites.

2.5 Charge carrier lifetime and copper contamination

Several studies have concluded that the carrier lifetime in copper contaminated silicon is lower in n-type than in p-type silicon [36, 37, 38]. The copper precipitates were confirmed to be the reason for the decrease of carrier lifetime in copper contaminated silicon [38, 39]. This conclusion was reached from the minority carrier diffusion length dependence on copper contamination in p-type silicon. The diffusion length decreased rapidly when the copper concentration was more than 10^{16} cm^{-3} above the boron concentration. In n-type silicon, the minority carrier diffusion length decreased gradually when the copper concentration increased. The work of Sachdeva *et al.* [38] confirmed the importance of the electrostatic effect between the positively charged interstitial copper atoms and the copper precipitates on the behaviour of copper in silicon. The Coulomb repulsion between the positively charged copper precipitates and the positively charged interstitial copper atoms retards copper precipitation in p-type silicon. The higher Fermi-level in n-type silicon causes the copper atoms to precipitate more easily than in p-type silicon.

Bazzali *et al.* [14] reported in 1996 that copper was efficiently detected in boron-doped silicon containing small oxygen clusters by means of the Elymat technique [40]. The Elymat technique was used to determine the minority carrier diffusion length and the surface recombination velocity. In copper contaminated samples, the minority carrier diffusion length was lower in samples containing small oxygen clusters than in samples without oxygen clusters. In clean samples, the diffusion length was almost equal in both kinds of samples. The reaction of copper with oxygen defects was recognized as causing minority carrier lifetime decrease also in quenched boron doped silicon [38]. However, for a copper concentration of 10^{13} cm^{-3} the minority carrier lifetime change was small. This indicates that the copper reaction rate with

oxygen defects is low at room temperature, because in quenched silicon, for a quenching rate of 2000 $K \cdot s^{-1}$, the defect formation occurs at room temperature. Or at least, the copper reaction time constant is larger than the out-diffusion time constant of copper into surfaces.

Henley *et al.* [8] reported a new phenomenon in 1999. They found that light treatment and low temperature heat treatment decrease the minority carrier lifetime permanently in boron doped copper contaminated Czochralski silicon. The minority carrier diffusion length was measured by means of the surface photovoltage (SPV) technique. The copper contamination was done by applying a drop of the copper contamination solution to selected spots on the bare silicon surface. The copper was diffused into the bulk in an oxidizing atmosphere. Neither light nor heat treatment had any effect on the minority carrier lifetime in phosphorous-doped silicon. The heat treatment was done at 200 ºC for 5 minutes. They suggested that the light and heat treatments dissociate copper-pairs and forms extended substitutional defects in silicon, which have greater recombination activity than the copper-pairs. The suggestion was based on the study of Tarasov *et al.* [13], who found that a light intensity of 0.15 $W \cdot cm^{-2}$ dissociates copper-pairs and introduces new energy levels in the lower and the upper part of the bandgap. It was also based on the study of Koveshnikov *et al.* [27], who found that annealing dissociates copper pairs and introduces new energy levels in the lower part of the bandgap.

By comparing the DLTS-spectra presented by Tarasov *et al.* [13] and Koveshnikov *et al.* [27] it can be concluded that annealing causes different copper related energy levels in the bandgap than optical activation does. This should mean a quantitatively different carrier lifetime in silicon, depending on whether copper contaminated silicon is annealed or optically activated. However, Ramappa [9] reported that the minority carrier diffusion length was almost the same after light and heat treatments. The minority carrier diffusion length was measured by means of the SPV technique. The copper contamination was done by immersing bare silicon wafers in an aqueous solution of copper sulfate, and then oxidizing the wafers. A halogen lamp with intensities of 2.5 $W \cdot cm^{-2}$ and 7.5 $W \cdot cm^{-2}$ was used for the optical activation. It was found that the minority carrier diffusion length decreased at a faster rate with a light intensity of 7.5 $W \cdot cm^{-2}$ than 2.5 $W \cdot cm^{-2}$. Furthermore, the diffusion length decreased at a slower rate with a light intensity of 7.5 $W \cdot cm^{-2}$ when the sample temperature was 0 ºC than for a higher temperature. It was concluded that the formation of copper defects by optical activation is thermally enhanced and the defect formation is accelerated by increasing the light intensity. The heat treatments were done between 50 ºC and 300 ºC for 15, 30 and 45 minutes. It was reported that the activation energy of copper precipitation is 0.419 eV. Assuming at that time an activation energy of copper diffusivity of 0.43 eV, Ramappa [9] concluded that the formation of copper defects is a diffusion limited process. Later, the activation energy of copper diffusivity was determined to be (0.18 ± 0.01) eV [16].

Raineri *et al.* [12] reported that the optical activation did not decrease the charge carrier diffusion length in copper contaminated p-type silicon when the implanted copper dose was below 10^{13} cm^{-2}. They concluded that 10^{13} cm^{-2} is the surface concentration limit for copper detection by means of optical activation in p-type silicon. The diffusion length decreased from about 240 µm to about 200 µm due to optical activation when silicon was contaminated with a copper dose of 10^{13} cm^{-2}. Copper diffusion into bulk was done in an oxidizing atmosphere as in the studies by Henley *et al.* [8] and by Ramappa [9].

Tarasov *et al*. [13] reported that the optical activation decreased the charge carrier diffusion length in copper doped silicon from 170 μm to about 10 μm, and from 312 μm to 264 μm when the copper doses were 10^{13} cm^{-2} and 10^{12} cm^{-2}, respectively. The copper doped samples were either rapid thermal or furnace annealed in a nitrogen atmosphere. Furnace annealed samples were quenched. The diffusion length results indicate that the recombination activity of copper per implanted copper dose was 200 times higher in samples containing a copper dose of 10^{13} cm^{-2} than 10^{12} cm^{-2}. In other words, the recombination activity is not linearly dependent on the copper concentration. In addition, the diffusion length results indicate that the recombination activity of copper was quite low for a copper dose of 10^{12} cm^{-2}. The recombination activity was 1000 times higher in rapidly cooled samples [13] compared to the slow cooled samples [12] in copper doped silicon, when the copper dose was 10^{13} cm^{-2}. The copper out-diffusion was not considered in any of these studies [8, 9, 12, 13].

Mcdonald *et al*. [41] reported that charge carrier recombination at copper-related defects can be modelled using two energy levels. They measured samples containing copper-related defects with carrier lifetime spectroscopy, which is lifetime measurement as a function of temperature and excess charge carrier concentration. Stewart *et al.* [42] reported that charge carrier lifetime in silicon containing copper-related defects depends on the boron and phosphorous concentration.

3 Theory

3.1 Charge carrier lifetime

3.1.1 General

The charge carrier generation and recombination processes are always present in silicon. Recombination lifetime can be thought of as the average time excess carriers exist before electron-hole recombination takes place. Generation lifetime can be thought of as the average time it takes to generate electron-hole pairs thermally. The impurities and lattice imperfections form energy levels in the bandgap, which decrease multiphonon recombination and generation lifetimes. Recombination lifetime in moderately doped silicon is dominated by multiphonon recombination in the bulk and at the surface, because of the indirect bandgap of silicon. The Auger and radiative recombination processes in the bulk silicon are important at high excess charge carrier concentrations. The total recombination is a sum of all recombination processes. Therefore, in general the measured carrier lifetime is the effective lifetime, which is a combination of bulk and surface recombinations.

3.1.2 Multiphonon recombination

The equations describing generation-recombination through localized energy levels in the silicon bandgap were originally derived by Shockley and Read [43] and Hall [44]. The multiphonon generation-recombination process is therefore frequently referred to as the Shockley-Hall-Read (SHR) generation-recombination. The generation-recombination process is characterized by the density of localized energy levels N_t, whose energy is E_t within the bandgap.

In the electron capture process, an electron falls from the conduction band into an empty localized energy level. The process rate is proportional to the density of free electrons n in the conduction band and the density of empty localized energy levels. The density of empty localized energy levels is given by $N_\mathrm{t}(1-f(E_\mathrm{t}))$, where $1-f(E_\mathrm{t})$ is the probability that a localized energy level is empty when the energy of the localized level is E_t, and $f(E_\mathrm{t})$ is the probability that the localized energy level is occupied by an electron. Thus, the electron capture rate from the conduction band is

$$R_\mathrm{ct} = c_n N_\mathrm{t} \left(1 - f(E_\mathrm{t})\right) n , \tag{3.1}$$

where c_n is the electron capture coefficient in $\mathrm{cm}^3 \cdot \mathrm{s}^{-1}$.

In the electron thermal emission process, an electron is excited from the localized energy level into the conduction band due to the thermal energy. The process rate is proportional to the density of the occupied localized energy levels. Thus, the electron emission rate is

$$R_\mathrm{tc} = e_n N_\mathrm{t} f(E_\mathrm{t}) , \tag{3.2}$$

where e_n is the electron emission constant in s^{-1}. In thermal equilibrium, the probability that a quantum state is occupied can be modelled using the Fermi-Dirac distribution function

$$f_{\mathrm{D}} = \frac{1}{1 + \exp\left((E_{\mathrm{t}} - E_{\mathrm{F}})/(kT)\right)}, \tag{3.3}$$

where E_{F} is the Fermi level. In thermal equilibrium, the electron capture rate equals the electron emission rate and the electron emission coefficient is

$$e_n = c_n N_{\mathrm{c}} \exp\left(-(E_{\mathrm{c}} - E_{\mathrm{t}})/(kT)\right), \tag{3.4}$$

where N_{c} is the effective conduction band density of states. In the hole capture process an electron falls from an occupied localized energy level to the valence band. The hole capture rate is proportional to the density of free holes p in the valence band and the density of occupied localized energy levels. Thus, the hole capture rate from the valence band is

$$R_{\mathrm{vt}} = c_p N_{\mathrm{t}} f(E_{\mathrm{t}}) p, \tag{3.5}$$

where c_p is the hole capture coefficient in cm^3·s^{-1}.

In the hole emission process an electron is excited from the valence band into the localized energy level due to thermal energy. The process rate is proportional to the density of unoccupied localized energy levels. Thus, the hole emission rate is

$$R_{\mathrm{tv}} = e_p N_{\mathrm{t}} \left(1 - f(E_{\mathrm{t}})\right), \tag{3.6}$$

where e_p is the hole emission constant in s^{-1}. At thermal equilibrium the hole capture and the emission rates are equal and the hole emission coefficient is

$$e_p = c_p N_{\mathrm{v}} \exp\left(-(E_{\mathrm{t}} - E_{\mathrm{v}})/(kT)\right), \tag{3.7}$$

where N_{v} is the effective valence band density of states. In an electron-hole recombination process through a localized energy level an electron is captured from the conduction band to the unoccupied localized energy level, and then a hole is captured from the valence band to the occupied localized energy level, or vice versa.

The rate equations describing the electron-hole generation-recombination are

$$\frac{dn}{dt} = -R_n + G \tag{3.8}$$

$$\frac{dp}{dt} = -R_p + G \tag{3.9}$$

$$\frac{d\left(N_{\mathrm{t}} f(E_{\mathrm{t}})\right)}{dt} = R_n - R_p \tag{3.10}$$

where

$$R_n = R_{\mathrm{ct}} - R_{\mathrm{tc}} = c_n\left(nN_{\mathrm{t}}\left(1 - f(E_{\mathrm{t}})\right) - N_{\mathrm{c}}\exp\left(-(E_{\mathrm{c}} - E_{\mathrm{t}})/(kT)\right)N_{\mathrm{t}} f(E_{\mathrm{t}})\right) \quad (3.11)$$

$$R_p = R_{\mathrm{vt}} - R_{\mathrm{tv}} = c_p\left(pN_{\mathrm{t}} f(E_{\mathrm{t}}) - N_{\mathrm{v}}\exp\left(-(E_{\mathrm{t}} - E_{\mathrm{v}})/(kT)\right)N_{\mathrm{t}}\left(1 - f(E_{\mathrm{t}})\right)\right) \quad (3.12)$$

and G is the generation rate of electron-hole pairs due to external excitation. The trapping of charge carriers in localized energy levels is taken into account by means of equation (3.10).

In the absence of an electric field charge neutrality is present in semiconductors. Then equation

$$N_{\mathrm{d}}^{+} - N_{\mathrm{a}}^{-} + p - n + Q_{\mathrm{t}}/e = 0 \quad (3.13)$$

has to apply, where N_{a}^{-} is the ionized acceptor dopant concentration, N_{d}^{+} is the ionized donor dopant concentration, and Q_{t} is the charge density in localized energy levels. In an acceptor level the charge density is

$$Q_{\mathrm{t}}^{0/-} = -eN_{\mathrm{t}} f(E_{\mathrm{t}})\,. \quad (3.14)$$

In a donor level the charge density is

$$Q_{\mathrm{t}}^{+/0} = eN_{\mathrm{t}}\left(1 - f(E_{\mathrm{t}})\right). \quad (3.15)$$

The definitions of charge carrier lifetime for excess electrons τ_n and for excess holes τ_p are [43]

$$\tau_n = \Delta n / R_n \text{ and} \quad (3.16)$$

$$\tau_p = \Delta p / R_p\,, \quad (3.17)$$

where Δn and Δp are excess electron and hole concentrations, respectively. The electron and hole concentrations are the sum of thermal equilibrium concentrations and excess concentrations

$$n = n_0 + \Delta n\,, \quad (3.18)$$

$$p = p_0 + \Delta p\,, \quad (3.19)$$

where n_0 and p_0 are thermal equilibrium electron and hole concentrations, respectively.

The general case presented above will be simplified next with the assumption that the trapped carrier concentration at a localized energy level does not change much compared to the minority charge carrier concentration at non-equilibrium conditions. In this case, the electron and hole excess charge concentrations are equal, and the electron and hole lifetime values are equal. The validity of this simplification has recently been analyzed by Macdonald *et al*. [45].

Under steady-state conditions time derivates are zero, and the generation rate of charge carriers equals the recombination rate of charge carriers in equations (3.8) and (3.9). In addition, the net electron capture rate, which is the electron capture rate minus the electron emission rate, equals the net hole capture rate, which is the hole capture rate minus the hole emission rate. Thus,

$$R_{SS} = R_{ct} - R_{tc} = R_{vt} - R_{tv}, \tag{3.20}$$

where R_{SS} is the steady-state recombination rate of charge carriers. The electron occupation probability at a localized energy level $f(E_t)$ under steady-state conditions can be solved from equations (3.1), (3.2), (3.5), (3.6) and (3.20) to obtain

$$f_{SS}(E_t) = \frac{c_n n + c_p N_v \exp(-(E_t - E_v)/(kT))}{c_n [n + N_c \exp(-(E_c - E_t)/(kT))] + c_p [p + N_v \exp(-(E_t - E_v)/(kT))]}. \tag{3.21}$$

The steady-state recombination rate can be solved by inserting the expressions for the electron capture and the electron emission rates and equation (3.21) into equation (3.20) to obtain

$$R_{SS} = \frac{N_t (np - n_i^2)}{(c_p)^{-1} [n + N_c \exp(-(E_c - E_t)/(kT))] + (c_n)^{-1} [p + N_v \exp(-(E_t - E_v)/(kT))]}, \tag{3.22}$$

where n_i is the intrinsic carrier density. Equation (3.22) gives the recombination-generation rate for an impurity, which has a single localized energy level. It is assumed that under non-equilibrium conditions the density of energy levels and the capture and emission coefficients are the same as under thermal equilibrium conditions. Equation (3.22) was derived first by Shockley and Read [43], and Hall [44].

The recombination lifetime for a single impurity element from equations (3.16) and (3.22) is

$$\tau_{SS} = \frac{(c_p)^{-1} [n_0 + \Delta n + N_c \exp(-(E_c - E_t)/(kT))]}{N_t (n_0 + p_0 + \Delta n)} + \frac{(c_n)^{-1} [p_0 + \Delta n + N_v \exp(-(E_t - E_v)/(kT))]}{N_t (n_0 + p_0 + \Delta n)}. \tag{3.23}$$

Equation (3.23) shows that the carrier lifetime is inversely proportional to the density of energy levels N_t.

The electron and hole capture coefficients are

$$c_n = \sigma_n v_n \text{ and} \tag{3.24}$$

$$c_p = \sigma_p v_p, \tag{3.25}$$

where σ_n and σ_p are the electron and hole capture cross-sections and v_n and v_p are the thermal velocities of electrons and holes, respectively. In silicon, the electron thermal velocity is 2.03×10^7 cm·s^{-1} and the hole thermal velocity is 1.68×10^7 cm·s^{-1} at 300 K [46].

3.1.3 Intrinsic recombination

Kerr and Cuevas [47] presented recently the expression for the intrinsic recombination rate at silicon

$$\begin{aligned} R_{\text{intrinsic}} &= R_{\text{Auger}} + R_{\text{rad}} \\ &= np(1.8\times10^{-24} n_0^{0.65} + 6\times10^{-25} p_0^{0.65} + 3\times10^{-27} \Delta n^{0.8} + 9.5\times10^{-15}) \quad \text{cm}^{-3}\cdot\text{s}^{-1}, \end{aligned} \qquad (3.26)$$

where R_{Auger} is the Auger recombination rate and R_{rad} is the radiative recombination rate. The intrinsic carrier lifetime $\tau_{\text{intrinsic}}$ from (3.26) is

$$\tau_{\text{intrinsic}} = \frac{\Delta n}{np(1.8\times10^{-24} n_0^{0.65} + 6\times10^{-25} p_0^{0.65} + 3\times10^{-27} \Delta n^{0.8} + 9.5\times10^{-15})} \ \text{s}. \qquad (3.27)$$

The electron and hole densities should be inserted in cm^{-3} in equations (3.26) and (3.27).

3.1.4 Bulk lifetime

The total excess charge carrier recombination is the sum of all recombination processes. Therefore, the recombination lifetime in bulk silicon τ_{b} is

$$\frac{1}{\tau_{\text{b}}} = \frac{1}{\tau_{\text{intrinsic}}} + \frac{1}{\tau_{\text{extended}}} + \sum_i \frac{1}{\tau_i}, \qquad (3.28)$$

where τ_i is the indirect recombination lifetime from equation (3.23) for different recombination energy levels, and τ_{extended} is the recombination lifetime for extended recombination sites in silicon.

3.1.5 Surface recombination

The silicon surface contains silicon atom dangling bonds, which form energy levels, called interface states, in the silicon bandgap.

The process of carrier recombination at interface states is called surface recombination. The carrier recombination rate at interface states per surface area is [48]

$$R_{\text{S}}(n_{\text{s}}, p_{\text{s}}) = \Delta n\, S(n_{\text{s}}, p_{\text{s}})\,, \qquad (3.29)$$

where S is the surface recombination velocity, which depends on the electron n_{s} and hole p_{s} concentrations at the interface, the interface state distribution in the bandgap and the interface

state capture cross-sections. A comprehensive study of the surface recombination process has been presented by Otaredian [49] and Schuurmans [50].

The surface recombination can be minimized effectively by annealing in forming gas after a thermal oxidation, by a post-metallization aluminum anneal [51], by a plasma enhanced chemical vapour deposited silicon nitride film [52], by a chemical surface passivation with iodine-ethanol [53], by an in-situ immersion in HF [54], by a corona charge [55] and by an external electric field [56]. The thermal silicon dioxide with corona charge [55] and in-situ immersion in HF [54] produce the lowest surface recombination velocities. A surface recombination velocity below 1 $cm \cdot s^{-1}$ has been reported [54, 55]. The corona charge can be used to change the electron and hole densities at the surface. Under accumulation or inversion conditions the surface contains only one type of charge carrier in high concentration, which results in a low surface recombination rate because the electron-hole recombination needs both electrons and holes.

3.1.6 Effective lifetime

The effective carrier lifetime is a combination of bulk and surface recombinations, which depend on the spatial distribution of electron and hole concentrations. The carrier concentration distributions in silicon can be solved with the continuity equations [57]

$$\frac{\partial n}{\partial t} = G - R_n + \frac{1}{e}\nabla \cdot \mathbf{J}_n \text{ and} \qquad (3.30)$$

$$\frac{\partial p}{\partial t} = G - R_p - \frac{1}{e}\nabla \cdot \mathbf{J}_p \,, \qquad (3.31)$$

where $\mathbf{J}_n$ and $\mathbf{J}_p$ are the electron current density and the hole current density, respectively. The boundary conditions at the silicon surface are

$$\mathbf{J}_n \cdot \overline{\mathbf{n}} = -eR_S(n_s, p_s) \text{ and} \qquad (3.32)$$

$$\mathbf{J}_p \cdot \overline{\mathbf{n}} = eR_S(n_s, p_s)\,, \qquad (3.33)$$

where $\overline{\mathbf{n}}$ is the surface normal vector.

In the general case the continuity equations can only be solved numerically. An analytical solution can be found for low excess charge carrier concentrations. Otaredian [49] presented a solution in Cartesian coordinates for a homogeneous wafer, Storgårds [58, 59] presented a solution in cylindrical coordinates for a homogeneous wafer and Väinölä [60, 61, 62] presented a solution in one dimension for a two-layer wafer.

In transient measurements, e.g. microwave photoconductive decay, the carrier lifetime is determined from the time dependence of excess charge carriers. The solution for the continuity equation (3.30) after the pulse excitation with surface recombination boundary conditions (3.32) is, after integration [63],

$$\Delta n(t) = \sum_{m=1}^{\infty} A_m \exp(-t/\tau_m), \tag{3.34}$$

where the coefficients A_m depend on the initial conditions at time zero, and τ_m are the decay time constants. Only one decay time constant dominates after the diffusion time [63]

$$\tau_{\mathrm{diff}} = \frac{T^2}{\pi^2 D_{\mathrm{a}}}, \tag{3.35}$$

where D_{a} is the charge carrier ambipolar diffusivity and T is the thickness of the sample. The diffusion time, from equation (3.35), is 20 μs when the thickness of the wafer is 525 μm, and the excess carrier concentration is 10^{16} cm^{-3}, which causes an ambipolar diffusivity of 15 $\mathrm{cm}^2 \cdot \mathrm{s}^{-1}$ in silicon [64]. After the diffusion time, the dominant time constant of decay in equation (3.34) is given approximately by [48]

$$\frac{1}{\tau_{\mathrm{eff}}} = \frac{1}{\tau_{\mathrm{b}}} + \frac{2S}{T}, \tag{3.36}$$

where τ_{b} is the bulk lifetime given by equation (3.28). Equation (3.36) is accurate to within 4 % for surface recombination velocity conditions [65]

$$S < \frac{D_{\mathrm{a}}}{4T}. \tag{3.37}$$

The surface recombination velocity should be below 70 $\mathrm{cm} \cdot \mathrm{s}^{-1}$, when the thickness of the wafer is 525 μm and the ambipolar diffusivity is 15 $\mathrm{cm}^2 \cdot \mathrm{s}^{-1}$. Equation (3.36) can be used when analyzing the effective carrier lifetime of samples containing silicon dioxide layers and corona charge, because then the surface recombination velocity is below 1 $\mathrm{cm} \cdot \mathrm{s}^{-1}$ [55].

The surface recombination velocity of 1 $\mathrm{cm} \cdot \mathrm{s}^{-1}$ limits the measurable effective lifetime to below 26 ms, which is calculated from equation (3.36) with a wafer thickness of 525 μm. The intrinsic lifetime due to the Auger and the radiative recombination processes is 3.1 ms at an excess carrier concentration of 10^{16} cm^{-3}, when the boron-doping concentration is 6.1×10^{14} cm^{-3}. The intrinsic lifetime was calculated from equation (3.27). Thus, the intrinsic recombination is important compared to the surface recombination under excess carrier concentration conditions above 10^{16} cm^{-3}.

3.1.7 Low-injection-level lifetime

The low-injection level lifetime τ_{LL} is frequently calculated from equation

$$L_n = \sqrt{D_n \tau_{\mathrm{LL}}}, \tag{3.38}$$

where L_n is the measured minority charge carrier diffusion length and D_n is the diffusivity of the minority charge carriers. Under low injection conditions, the excess charge carrier concentration is negligible compared to the majority carrier concentration. The low-injection level lifetime is frequently used to estimate the minority carrier capture cross-section of recombination sites from equation

$$\sigma_n = \frac{1}{N_t \tau_{LL} v_{th}}, \tag{3.39}$$

where N_t is the measured or estimated concentration of recombination centers, and the carrier thermal velocity v_{th} is approximated to be 10^7 cm^{-3}. Equation (3.39) can be derived from equation (3.23) for low excess charge carrier concentrations with the assumption that the localized energy level is near the middle of the bandgap.

3.2 μPCD technique

3.2.1 Time constant of decay

In the microwave photoconductive decay (μPCD) technique the reflected microwave power from a silicon wafer is measured. The microwave reflection coefficient depends on the conductivity of silicon. Adjusted properly the reflected microwave power is proportional to the conductivity of silicon. In the μPCD equipment that was used in this study the proportionality is ensured by adjusting the microwave frequency. The silicon conductivity σ depends on the electron and hole concentrations as [48]

$$\sigma(t) = e\big(\mu_n n(t) + \mu_p p(t)\big), \tag{3.40}$$

where μ_n and μ_p are the electron and hole mobilities, respectively. Therefore, the change in the carrier concentration in silicon can be monitored by measuring the reflected microwave power.

In μPCD measurements excess conductivity is generated with a light pulse and the conductivity transient is measured. The time constant of decay is determined by fitting a mono exponential function to the measured conductivity transient. Thus, the carrier lifetime determined with the μPCD technique τ_{PCD} can be written as

$$\tau_{PCD}(\Delta n, \Delta p) = \frac{\Delta\sigma}{-\frac{\partial \Delta\sigma}{\partial t}} = \frac{\mu_n \Delta n(t) + \mu_p \Delta p(t)}{-\frac{\partial(\mu_n \Delta n(t) + \mu_p \Delta p(t))}{\partial t}}, \tag{3.41}$$

where $\Delta\sigma$ is the excess conductivity. The excess hole and electron concentrations are approximately equal when the charge carrier trapping is negligible, and equation (3.41) reduces to

$$\tau_{\mathrm{PCD}}(\Delta n) = \frac{\Delta n(t)}{-\frac{\partial(\Delta n(t))}{\partial t}} . \tag{3.42}$$

Equation (3.42) includes the assumption that the change of carrier mobility due to the change of hole and electron concentrations is negligible. Equation (3.42) shows that the time constant of the conductivity transient is equal to the time constant of the excess charge carrier concentration.

3.2.2 Differential effective lifetime

Schmidt [66] proved experimentally the theoretical finding that the carrier lifetime determined by using the light-biased μPCD technique is the differential effective lifetime, when the excess carrier concentration generated by the probe light is small compared to the concentration generated by the bias-light. The differential effective lifetime is [67]

$$\tau_{\mathrm{eff.d}} = \left(\frac{\partial R(\Delta n)}{\partial \Delta n} \right)^{-1}_{\Delta n = \Delta n_{\mathrm{ss}}} , \tag{3.43}$$

where the excess charge carrier concentration Δn_{ss} is determined by the bias-light intensity.

The effective lifetime can be determined by integrating the differential effective lifetimes over the bias-light intensities [67]

$$\tau_{\mathrm{eff}} = \frac{1}{P} \int_0^P \tau_{\mathrm{eff.d}}(p) dp , \tag{3.44}$$

where P is the light power density of bias-light. Equation (3.44) shows that the differential lifetime equals the effective lifetime when the effective lifetime does not depend on the excess carrier concentration.

3.3 Precipitation kinetics

3.3.1 Fixed radius

Ham [68] described the theory of diffusion-limited precipitation from a supersaturated solution. The precipitation is driven by the supersaturation of solute impurities. Ham calculated the time-dependence of the unprecipitated fraction of the excess solute. In the following it is assumed that the density of precipitates is a constant during the precipitation process, the initial impurity concentration is uniform, the radius of the precipitates is much smaller than the distance between precipitates, and the precipitates are spherical. The radius of the precipitates is approximately constant at the end of the precipitation process, when over half of the solute has precipitated. The solution for the solute concentration using these assumptions is [68]

$$\bar{c}(t) = (c_0 - c_S)\exp(-t/\tau_0) + c_S, \tag{3.45}$$

where $\bar{c}$ is the average solute impurity concentration, c_0 is the initial impurity concentration before precipitation, c_S is the impurity solubility at the silicon-precipitate interface and t is the precipitation time. The precipitation time constant τ_0 is [68]

$$\tau_0 = \frac{1}{4\pi\, nrD}, \tag{3.46}$$

where n is the density of the precipitates, r is the effective radius of the precipitates and D is the impurity diffusivity. The precipitated impurity concentration c_{prec} is the same as the change in the solute concentration

$$c_{\mathrm{prec}}(t) = c_0 - \bar{c}(t). \tag{3.47}$$

It should be emphasized that equation (3.47) includes the assumption that the impurity concentration decreases only through precipitation. The impurity out-diffusion is excluded. The precipitated impurity concentration from equations (3.45) and (3.47) is

$$c_{\mathrm{prec}}(t) = (c_0 - c_S)(1 - \exp(-t/\tau_0)). \tag{3.48}$$

3.3.2 Growing radius

The analytical solution described by Ham [68] for the time-dependence of the unprecipitated fraction of the excess solute is complex. Therefore, Hieslmair *et al.* [69] have presented an iterative method that takes into account the increase of the radius of the precipitates. The change of the solute impurity concentration $\Delta\bar{c}$ at time interval Δt is [69]

$$\Delta\bar{c}(\Delta t) = \bar{c}(t + \Delta t) - \bar{c}(t) = (c_S - \bar{c}(t))(1 - \exp(-\Delta t/\tau_0)), \tag{3.49}$$

where the precipitation time constant τ_0 is the time constant of the fixed radius solution from equation (3.46). The precipitated impurity concentration in spherical precipitates is

$$c_{\mathrm{prec}}(t) = \frac{4}{3}\pi\, r(t)^3 n\rho, \tag{3.50}$$

where ρ is the density of the impurities in the precipitate. Thus, a change in the radius of the precipitates in the time interval Δt causes a change of the impurity concentration [69]

$$\Delta\bar{c}(\Delta t) = \frac{4}{3}\pi\left(r(t)^3 - r(t + \Delta t)^3\right)n\rho. \tag{3.51}$$

The radius of the precipitates increases during the time interval Δt. From equation (3.51) the radius is [69]

$$r(t+\Delta t)=\left(\frac{3\Delta \bar{c}(\Delta t)}{4\pi n\rho}+r(t)^3\right)^{1/3}. \tag{3.52}$$

The solute concentration dependence on the precipitation time is calculated iteratively from (3.49) and (3.52). The precipitated impurity concentration is calculated from equation (3.47).

3.3.3 Density and radius of defects

The precipitation time constant gives information about the precipitates. The *nr* product of the precipitates can be determined from the precipitation time constant, when the impurity diffusivity is known. The density and the radius of the precipitates can be determined from the precipitation time constant and the precipitated impurity concentration. The radius and the density of the spherical precipitates from equations (3.46) and (3.50) are

$$r=\left(\frac{3D\tau_0 c_{\mathrm{prec}}}{\rho}\right)^{1/2} \tag{3.53}$$

and

$$n=\frac{(D\tau_0)^{-3/2}}{4\pi}\left(\frac{\rho}{3c_{\mathrm{prec}}}\right)^{1/2}. \tag{3.54}$$

3.4 Recombination at precipitates

The electrical properties of the light-induced copper precipitates are not known. Therefore, the energy levels or the carrier capture cross-sections are not used in this study in the recombination models for copper precipitates.

3.4.1 Volume recombination model

The simplest model is the one that is called the volume recombination model in this work. The steady-state charge-carrier recombination rate R_{SS} in the copper precipitates is modelled as

$$R_{\mathrm{prec}}=\Delta n\, k_{\mathrm{prec}} c_{\mathrm{prec}}, \tag{3.55}$$

where R_{prec} is the recombination rate at the copper precipitates and k_{prec} is a proportionality factor. Equation (3.55) defines the volume recombination coefficient k_{prec}. In SHR-recombination statistics the capture coefficient is the counterpart for the quantity k_{prec}.

It should be noted that the recombination rate at the volume recombination model does not depend on the radius of the precipitates but on the total precipitated impurity concentration. However, the precipitation time constant depends on the density and the radius of precipitates. The recombination rate dependence on the precipitation time from equations (3.50) and (3.55) is

$$R_{\mathrm{prec}}(t) = \Delta n\, k_{\mathrm{prec}} \frac{4}{3}\pi\, r(t)^3\, n\rho\,. \tag{3.56}$$

In the fixed radius approximation the recombination rate dependence on the precipitation time from equations (3.48) and (3.55) is

$$R_{\mathrm{prec}}(t) = \Delta n\, k_{\mathrm{prec}} (c_0 - c_{\mathrm{S}})(1 - \exp(-t/\tau_0)). \tag{3.57}$$

3.4.2 Surface recombination model

The second model is in this work called the surface recombination model. The charge carrier recombination rate is modelled to be linearly proportional to the surface area of the precipitates. The surface recombination rate is derived from equation (3.29) by multiplying it with the surface area of the precipitates

$$R^{\mathrm{S}}_{\mathrm{prec}}(t) = \Delta n\, S_{\mathrm{prec}} 4\pi\, r(t)^2\, n\,, \tag{3.58}$$

where S_{prec} is the surface recombination velocity at the precipitate surface. Equation (3.58) can be also derived from the equations presented by Hwang *et al.* [70]. The diffusion time of the charge carriers is neglected in equation (3.58). The diffusion time is negligible, if $D >> S_{\mathrm{prec}}\, r$ [70].

3.4.3 Comparison of recombination models

The volume and surface recombination models are compared in Figure 3.1. The recombination rate is shown as a function of precipitation time. Table 3.1 shows the equations and the values used for the calculations. The volume recombination coefficient k_{prec} and the surface recombination velocity S_{prec} were fitted to achieve almost equal maximum recombination rates. The density of the precipitates was treated as the fitting parameter in the growing radius models.

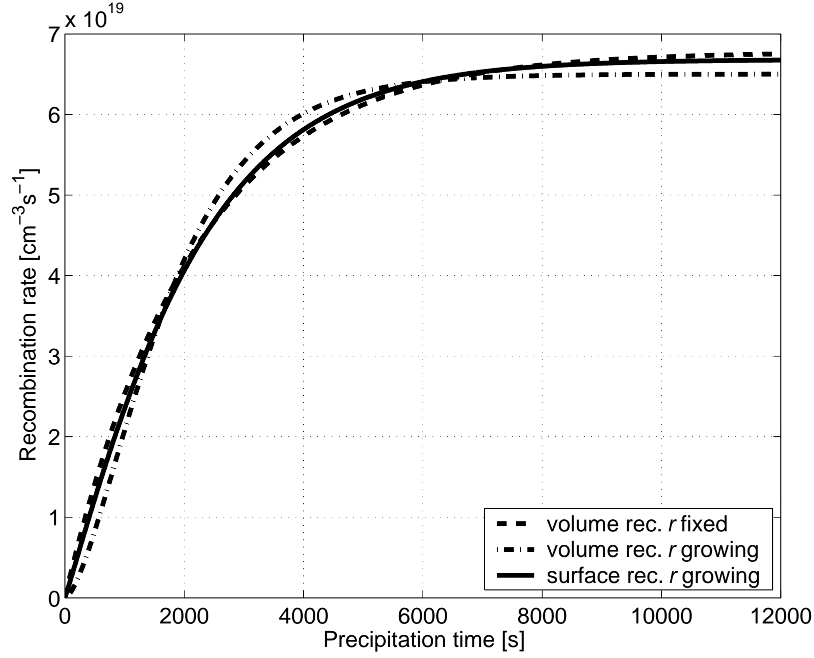

Figure 3.1: The recombination rate at the precipitates as a function of precipitation time. Table 3.1 shows the values and equations used for calculation.

Table 3.1: The values and equations used to calculate the recombination rate as a function of precipitation time, as shown in Figure 3.1. The density of impurity atoms in the precipitates is the density of copper atoms in Cu_3Si precipitates, which have a molecular volume of 46 Å^3 [7, 71]. This gives the density of copper atoms in the precipitate as 6.52×10^{22} cm^{-3}. The diffusivity is the effective diffusivity of copper from equation (2.2) in boron doped silicon at a concentration of 6.1×10^{14} cm^{-3} at 297 K.

quantity	unit	Model		
		volume, r fixed	volume, r growing	surface rec.
$R_{prec}(t)$	cm$^{-3}\cdot$s^{-1}	Eq. (3.57)	Eq. (3.56)	Eq.(3.58)
$r(t=0)$	cm	2.9×10^{-7}, eq. (3.53)	10^{-8}	10^{-8}
$r(t)$	cm	2.9×10^{-7}, eq.(3.53)	Growing	Growing
τ_0	s	2142	-	-
n	cm^{-3}	1.0×10^{9}, eq. (3.54)	2.4×10^{9}, fitted	1.4×10^{9}, fitted
D	cm$^{2}\cdot$s^{-1}	1.28×10^{-7}	1.28×10^{-7}	1.28×10^{-7}
c_0	cm^{-3}	6.5×10^{12}	6.5×10^{12}	6.5×10^{12}
c_S	cm^{-3}	0	0	0
k_{prec}	cm$^{3}\cdot$s^{-1}	1.04×10^{-9}, fitted	1.0×10^{-9}, fitted	-
S_{prec}	cm$\cdot$s^{-1}	-	-	5.7×10^{6}, fitted
Δn	cm^{-3}	10^{16}	10^{16}	10^{16}
ρ	cm^{-3}	6.52×10^{22}	6.52×10^{22}	6.52×10^{22}

Figure 3.1 shows that the recombination rate dependence on the precipitation time is almost identical in the fixed radius volume recombination model and the surface recombination

model. Therefore, the surface recombination can be modelled quite accurately using one time constant. The density of the precipitates in the surface recombination model is $2^{1/2}$ times the density of the precipitates in the fixed radius model. The final radius of the precipitates in the surface recombination model has to be $2^{-1/6}$ times the final radius of precipitates in the fixed radius model in order to give the same result for the total precipitated impurity concentration. Thus, the radius and the density of the precipitates can be approximated in the surface recombination model quite accurately from equations

$$r_\mathrm{S} = 2^{-1/6}\left(\frac{3D\tau_0\, c_\mathrm{prec}}{\rho}\right)^{1/2} \tag{3.59}$$

and

$$n_\mathrm{S} = 2^{1/2}\,\frac{(D\tau_0)^{-3/2}}{4\pi}\left(\frac{\rho}{3c_\mathrm{prec}}\right)^{1/2}. \tag{3.60}$$

Equations (3.59) and (3.60) were derived from equations (3.53) and (3.54) by multiplying them with the factors mentioned.

3.4.4 Volume recombination at two kinds of defects

The charge carrier recombination at the volume of the copper precipitates is modelled using two kinds of recombination sites, called precipitates at oxygen defects and precipitates at microscopic lattice defects. In this model the total precipitated impurity concentration is

$$c_\mathrm{prec} = c_\mathrm{prec1} + c_\mathrm{prec2}\,, \tag{3.61}$$

where c_{prec1} is the concentration of impurity atoms precipitated at oxygen defects and c_{prec2} is the concentration of impurity atoms precipitated at microscopic lattice defects.

The recombination rate at precipitates at oxygen defects is

$$R_\mathrm{prec1} = \Delta n\, k_\mathrm{prec1} c_\mathrm{prec1}\,, \tag{3.62}$$

where k_{prec1} is the volume recombination coefficient of impurity atoms precipitated at oxygen defects. Equation (3.62) defines the quantity k_{prec1}. The recombination rate at the precipitates at microscopic lattice defects is

$$R_\mathrm{prec2} = \Delta n\, k_\mathrm{prec2} c_\mathrm{prec2}\,, \tag{3.63}$$

where k_{prec2} is the volume recombination coefficient of impurity atoms precipitated at microscopic lattice defects. Equation (3.63) defines the quantity k_{prec2}. The total recombination

rate at precipitates is the sum of the recombination rates of both precipitates. The total recombination rate from equations (3.62) and (3.63) is

$$R_{\mathrm{prec}} = \Delta n\left(k_{\mathrm{prec1}}c_{\mathrm{prec1}} + k_{\mathrm{prec2}}c_{\mathrm{prec2}}\right). \tag{3.64}$$

The precipitated impurity concentrations at oxygen defects and at microscopic lattice defects from equations (3.61) and (3.64) are

$$c_{\mathrm{prec1}} = \left(c_{\mathrm{prec}} - \frac{R_{\mathrm{prec}}}{k_{\mathrm{prec2}}\Delta n}\right)\left(1 - \frac{k_{\mathrm{prec1}}}{k_{\mathrm{prec2}}}\right)^{-1} \tag{3.65}$$

and

$$c_{\mathrm{prec2}} = c_{\mathrm{prec}} - c_{\mathrm{prec1}}. \tag{3.66}$$

3.4.5 Surface recombination at two kinds of defects

The charge carrier recombination at the surface of the precipitates is modelled using two kinds of recombination sites, called precipitates at oxygen defects and precipitates at microscopic lattice defects. In this model, the total density of the precipitates n is

$$n = n_{\mathrm{prec1}} + n_{\mathrm{prec2}}, \tag{3.67}$$

where n_{prec1} is the density of the precipitates at oxygen defects and n_{prec2} is the density of the precipitates at microscopic lattice defects. The recombination rate from equation (3.58) is

$$R^{\mathrm{S}}_{\mathrm{prec}} = \Delta n 4\pi r^{2}\left(n_{\mathrm{prec1}}S_{\mathrm{prec1}} + n_{\mathrm{prec2}}S_{\mathrm{prec2}}\right), \tag{3.68}$$

where S_{prec1} is the surface recombination velocity at precipitates at oxygen defects and S_{prec2} is the surface recombination velocity at precipitates at microscopic lattice defects. Equation (3.68) was derived with the assumption that copper precipitates have the same radius at oxygen defects as at microscopic lattice defects.

The densities of the precipitates at oxygen defects and at microscopic lattice defects from equations (3.67) and (3.68) are

$$n_{\mathrm{prec1}} = \left(n - \frac{R^{\mathrm{S}}_{\mathrm{prec}}}{\Delta n 4\pi r^{2} S_{\mathrm{prec2}}}\right)\left(1 - \frac{S_{\mathrm{prec1}}}{S_{\mathrm{prec2}}}\right)^{-1} \tag{3.69}$$

and

$$n_{\mathrm{prec2}} = n - n_{\mathrm{prec1}}. \tag{3.70}$$

4 Experimental

4.1 Wafers

The samples were single side polished Czochralski grown silicon wafers, with a thickness of 525 μm, a diameter of 100 mm and a {100} orientation. The resistivities of boron-doped wafers were 10 Ω·cm and 22 Ω·cm, and of phosphorous-doped wafers were 3 Ω·cm. The influence of oxygen defects on the optical activation of copper was studied using wafers with a resistivity of 22 Ω·cm and an as-grown interstitial oxygen concentration slightly above 14 ppma (ASTM F 1188-93a) before the oxygen precipitation anneals. The resistivities of boron-doped silicon were selected to be 10 Ω·cm or more, because light decreases carrier lifetime in clean boron-doped Czochralski silicon if the resistivity is near or under 1 Ω·cm [72, 73]. It has been proposed that this is a result of boron-oxygen complexes formed by light [72, 73].

4.2 Thermal oxidation

The wafers were pre-oxidized at 1050 ºC for 15 minutes to diminish the effect of the thermal history of the wafer and to form a protective silicon dioxide layer on the surface of the wafers. However, the wafers used for TXRF measurements were oxidized at only 900 ºC for 15 minutes and annealed for 15 minutes in order to decrease the process time in the vapour phase decomposition (VPD) process. Table 4.1 and Table 4.2 show the oxidation processes.

Table 4.1: Oxidation process DRYO1050

wafers in at 800 ºC (10 % O2)
stabilization for 1 min (10 % O2)
ramp up to 1050 ºC, rate 15 ºC/min (10 % O2)
stabilization for 3 min (10 % O2)
oxidation time for 15 min (O2)
stabilization for 0 min (N2)
ramp down to 800 ºC, rate 4 ºC/min (N2)
stabilization for 0 min (N2)
wafers out at 800 ºC (N2)
pull-out speed 25 cm/min (pull-out length 149 cm).

The thickness of the silicon dioxide layer was 28 nm after oxidation at 1050 ºC and 8 nm after oxidation at 900 ºC. The thickness was measured using an ellipsometer, with a light wavelength of 632.8 nm. A refractive index of 1.465 for silicon dioxide and 3.87-i0.017 for silicon were used in the ellipsometer analysis.

Small oxygen precipitates were grown using a two-step thermal treatment process [74]. The nucleation of the oxygen precipitates was done in a nitrogen ambient at 625 ºC for 2, 3, 4 or 16 hours. This was followed by the growth stage of the precipitates in a nitrogen ambient at 800 ºC for 4 hours. Separate samples without a copper contamination were processed for scanning infrared microscope (SIRM) measurements to determine the oxygen defect density.

The SIRM-samples were annealed at 1000 ºC for 4 hours with a ramp-rate of 1 ºC/min in order to increase the size of the oxygen precipitates after the anneal at 800 ºC.

Table 4.2: Oxidation process DRYOX2

wafers in at 800 ºC (10 % O2)
stabilization for 10 min (10 % O2)
ramp up to 900 ºC, rate 8 ºC/min (10 % O2)
stabilization for 0 min (10 % O2)
oxidation time for 15 min (O2)
annealing time for 15 min (N2)
ramp down to 800 ºC, rate 4 ºC/min (N2)
stabilization for 5 min (N2)
wafers out at 800 ºC (N2)
pull-out speed 25 cm/min (pull-out length 149 cm).

4.3 Copper surface contamination

Copper was chemically deposited on the oxide-covered wafer surfaces by immersing them in a diluted copper-sulfate solution with a copper content from 0.3 ppb to 20 ppm. A polypropylene sink was used as a solution container. First 1 liter of DI-water was put in the sink and the copper solution was added, then 2 liters of DI-water were added using a DI-water pistol so that the copper would mix in the solution. After a 10-minute wait wafers were immersed in the solution. The wafers were placed in every second slot in a wafer cassette and the immersion time was 1 hour. The wafers were dried using a nitrogen flow. The sink was cleaned before the first use by filling the sink with a solution 1 ($HCl:H_2O$ 1:30) and a solution 2 ($HNO_3:H_2O$ 1:100), separately. The solutions were stored in the sink over night. The sink was cleaned before every use by rinsing with DI-water and by filling the sink with a standard clean 1 solution ($NH_4OH:H_2O_2:H_2O$ 1:1:5) and a solution 3 ($HCl:H_2O_2:H_2O$ 1:1:30), separately.

4.4 Copper in-diffusion

The copper in-diffusion from the surface of the silicon dioxide layer into the bulk silicon was done in a furnace tube that had been reserved for copper contaminated wafers. Table 4.3 shows the in-diffusion process.

Table 4.3: Copper in-diffusion process CU800N.

wafers in at 300 ºC (N2)
stabilization for 0 min (N2)
ramp up to 800 ºC, rate 8 ºC/min (N2)
stabilization for 0 min (N2)
annealing time for 20 min (N2)
stabilization for 0 min (N2)
wafers out at 800 ºC (N2)
pull-out speed 25 cm/min (pull-out length 148 cm).

The loading temperature of wafers into the furnace was 300 ºC in order to avoid the evaporation of copper from the sample surface as much as possible.

4.5 Corona charge generation

The corona charge generator consists of a grounded metal plate, which is the sample holder, and a sharp metal tip above the sample. The metal tip is biased to a high voltage, which can be selected to be plus or minus 15 kV. The high electric field at the tip ionizes air molecules into CO_3^- and H_3O^+ [75]. The electric field between the tip and the metal plate drive one species of ions into the sample surface depending on the polarity of the voltage. The thickness of the silicon dioxide layer should be over 7 nm in order to prevent electron tunnelling through the oxide layer.

A surface charge density of 1 $\mu C \cdot cm^{-2}$ or –1 $\mu C \cdot cm^{-2}$ was deposited on the wafer surface depending on the aim of the experiment. A positive surface charge was used to prevent copper out-diffusion, and a negative surface charge to maximize the out-diffusion. A high surface charge density was used to eliminate the possibility of significant out-diffusion of copper during high intensity optical activation or storage. It was calculated using a PC1D device simulator [76] that the surface band bending was about 0.2 eV when the light intensity was over 25 $W \cdot cm^{-2}$ and the surface charge density was 1 $\mu C \cdot cm^{-2}$. The surface band bending was about 0.8 eV without light when the surface charge density was 1 $\mu C \cdot cm^{-2}$.

4.6 Optical activation

The optical activation of copper was carried out using a continuous laser light, with a wavelength of 973.5 nm. The spot size was about 1 mm^2. The light intensity was over 25 $W \cdot cm^{-2}$ in most optical activations. It should be noted that UV light is not suitable for optical activation, because UV light increases surface recombination by forming surface states at the silicon-silicon dioxide interface [77]. The optical activation was carried out with the same bias-light source that was used to adjust excess carrier concentration levels during lifetime measurements.

4.7 Charge carrier lifetime measurement equipment

The excess carrier recombination lifetime was measured under high injection level conditions using the standard microwave photoconductive decay technique (µPCD) (Semilab) [78]. Under high injection level conditions, the carrier lifetime depends weakly on the excess charge carrier concentration. The surface recombination is low at an oxidized silicon surface containing corona charge under high excess charge carrier conditions. Therefore, the measured lifetime did not deviate much from differential bulk lifetimes. The kinetics of charge carriers during measurements was described in chapter 3. Figure 4.1 shows the schematic of the equipment used for carrier lifetime measurements. A pulsed laser light, with a wavelength of 904 nm and a pulse length of 200 ns, was applied for the excitation of the excess carriers together with a continuous bias-light. Carrier recombination taking place after application of the pulsed light

causes a photoconductive decay, which was recorded by time-resolved measurements of the microwave power reflected from the silicon wafer. The frequency of the microwave radiation was 10.043 GHz. The time constant of the decay was determined with a mono exponential fit to the photoconductive decay and interpreted as being the recombination lifetime. The pulsed light and bias-light were concentrated at a spot of about 1 mm^2. The injected photons per pulse were 1.2×10^{15} cm^{-2}. The interval of the light pulses was over 10 times the charge carrier lifetime when the lifetime was below 2 ms. The maximum selectable interval was 20 ms. The bias-light intensity was adjusted manually by means of an attenuator to keep the amplitude of transient equal in the different measurements in order to reach a steady-state excess carrier concentration $\Delta n=(6\pm1)\times10^{15}$ cm^{-3}. The measurement apparatus was installed in an ambient temperature of 22 ºC. The sample temperature was 23-27 ºC during lifetime measurements and during prolonged optical activation exposure. The prolonged optical activation increased the sample temperature no more than 3 ºC. The temperature was measured using a thermocouple attached to the surface of a test wafer.

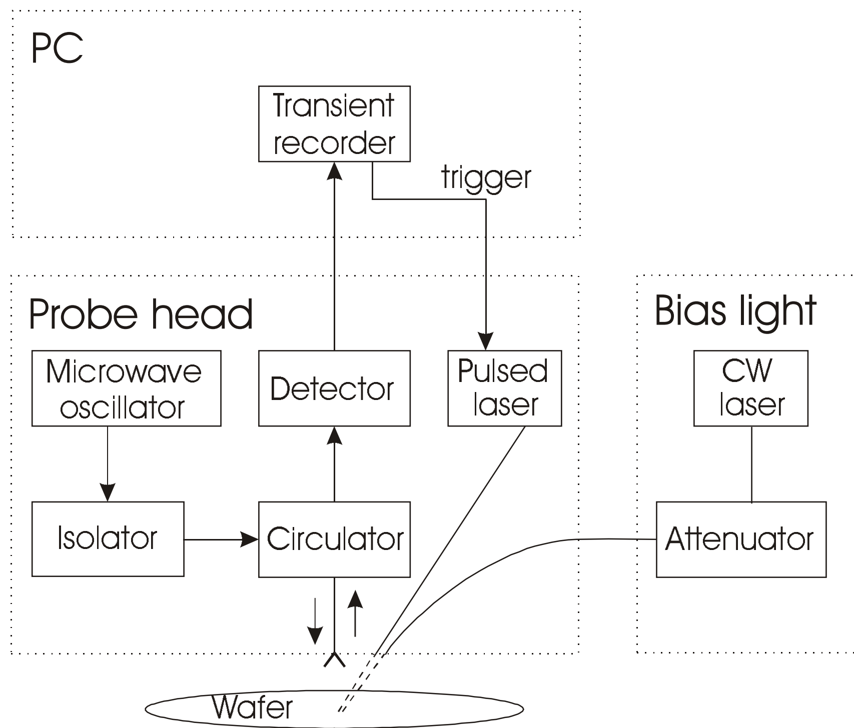

Figure 4.1: The schematic of equipment used for carrier lifetime measurements.

4.8 Determination of recombination rate

The total recombination rate is the sum of recombination rates at light-induced copper precipitates, R_{Cu}, and at other defects, R_{others} as

$$R(t) = R_{\mathrm{Cu}}(t) + R_{\mathrm{others}} . \tag{4.1}$$

In addition to copper, surface defects at the silicon-silicon dioxide interface, oxygen defects, and iron related defects cause recombination. High intensity light dissociates iron-boron pairs

in silicon. This decreases the recombination activity of iron under high excess carrier concentration conditions. The recombination rate of other defects reaches their minimum value when the maximum lifetime value is reached. After that, the recombination rate of other defects is constant as long as the iron atoms are at interstitial positions. However, the measured lifetime depends on the excess charge carrier concentration. Therefore, the excess charge carrier concentration was adjusted for the lifetime measurement by means of the bias-light. The recombination rate due to light-induced copper precipitates is small when the maximum lifetime value is reached, because the dissociation rate of iron-boron pairs is faster than the precipitation time constant of copper. This is because iron atoms diffuse only atomic distances while copper atoms diffuse macroscopic distances. Thus, the maximum measured lifetime τ_{max} approximately gives the recombination rate of other defects

$$R_{\mathrm{others}} = \frac{\Delta n}{\tau_{\mathrm{max}}} . \tag{4.2}$$

The copper related recombination rate R_{Cu} from equations (4.1) and (4.2) is

$$R_{\mathrm{Cu}}(t) = \Delta n \left(\frac{1}{\tau(t)} - \frac{1}{\tau_{\mathrm{max}}} \right), \tag{4.3}$$

where Δn is the excess charge carrier concentration, τ_{max} is the measured maximum charge carrier lifetime and $\tau(t)$ is the measured charge carrier lifetime after optical activation time t. In this work, the copper related recombination rate was determined using equation (4.3) with the excess charge carrier concentration value of 10^{16} cm^{-3}.

4.9 Determination of the precipitation time constant and the saturation of the recombination rate

The precipitation time constant and the saturation value of the light-induced copper related recombination rate were determined by fitting the exponential curve to experimentally determined recombination rates, which were determined from equation (4.3). The exponential curve was

$$R_{\mathrm{Cu}}(t) = R_{\mathrm{A}}(1 - \exp(-t/\tau_{\mathrm{A}})) , \tag{4.4}$$

where R_A is the saturation of the copper related recombination rate and τ_A is the precipitation time constant. These are the fitting parameters. The fitted curve was weighted by the last measurement points when the radius of the precipitates did not change much. The fitting was done by minimizing the difference between the values determined from equation (4.3) and the values calculated from equation (4.4).

4.10 TXRF

The surface concentration of copper on silicon wafers was measured using total reflection X-ray fluorescence spectroscopy (TXRF) (Atomika, TXRF8030W) with a W X-ray tube and SiLi-detector at Okmetic Oyj. Sample preparation was performed with a vapour phase decomposition (VPD) droplet collection system (GeMeTec, PADScan). In the VPD system the SiO_2 layer is decomposed by HF vapour in a teflon chamber with open HF containers. A sample is collected from the wafer surface by scanning a droplet over the wafer. Finally, the droplet is dried on the wafer surface for TXRF analysis. The VPD technique was used to collect metal impurities from a large surface area to a single spot in order to increase the detection sensitivity. Wafers that had high surface contamination were not measured because of the risk of contaminating the facility. The wafers for TXRF analysis and lifetime analysis were contaminated in the same batch. It was not possible to measure charge carrier lifetime in the wafers analyzed by TXRF.

4.11 TID

Interstitial copper concentration in bulk silicon was determined using the transient ion drift (TID) method at Lawrence Berkeley National Laboratory at the University of California. In the TID-measurement, an external reverse pulse is used to drift positive charged interstitial copper to the edge of a depletion region and the change in the capacitance is measured. The interstitial copper concentration is calculated from the measured capacitance change. The details of the measurement technique can be found elsewhere [6]. The TID measurements were only done for a few wafers that had first been measured with μPCD.

4.12 SIRM

The oxygen defect densities were determined using the scanning infrared microscope technique (SIRM) (Semilab, SIRM-300) at the Laboratory of Physical Metallurgy and Materials Science at Helsinki University of Technology. The sizes of the oxygen defects were increased in the SIRM-samples by means of an additional anneal in order to increase the light scattering intensity from the oxygen defects. The oxygen defect density value was taken from values measured at a depth of 40-60 μm from the surface.

4.13 SPV

The charge carrier diffusion length under low excess charge carrier conditions was measured using the surface photovoltage technique (SPV) (Semilab). The principle of this technique can be found elsewhere [79]. The diffusion length was measured for a few samples in order to determine the ratio between the carrier lifetimes measured under low and high excess charge carrier concentration conditions.

5 Results and discussion

5.1 Copper concentration

The copper surface concentration of silicon wafers was measured by means of the total reflectance X-ray fluorescence (TXRF) technique. Table 5.1 presents the copper surface concentration results.

Table 5.1: The copper surface concentration of copper contaminated and reference wafers. Boron doped single side polished oxidized wafers were used. The first column shows the processes after the oxidation. The lot number separates different contamination batches. The ppb value is the copper content in the contamination solution and the text 800 ºC means that in-diffusion heat treatment has been done after contamination. The second column is the measured copper surface concentration.

Process	Copper 10^{10} cm^{-2}
Reference	1.3
0.3 ppb	2.5
1 ppb	8.6
3 ppb + 800 ºC [Lot B1]	9.3
3 ppb [Lot B4]	13.8
3 ppb [Lot B4]	10.7
3 ppb + 800 ºC [Lot B4]	4.3

By comparing the surface copper concentration before and after the in-diffusion heat treatment it was deduced that the surface copper contamination diffused from the sample surface into the bulk silicon. Before in-diffusion the copper surface concentration of two 3 ppb samples in Lot B4 were 13.8×10^{10} cm^{-2} and 10.7×10^{10} cm^{-2}, resulting in the average value of 12.2×10^{10} cm^{-2}. After the in-diffusion the copper surface concentration of the other 3 ppb sample in Lot B4 was 4.3×10^{10} cm^{-2}. Thus, the copper surface concentration decreased by 8×10^{10} cm^{-2} during the heat treatment, which is 64 % of the surface copper concentration before the heat treatment. This percent value was also used when the in-diffused copper concentration was calculated for other samples. The unpolished side of a wafer can contain a higher surface copper concentration than the polished side, because of its larger surface area. However, the TXRF analysis was done only on the polished side of the wafer due to higher sensitivity on that side. Table 5.2 presents the in-diffused copper concentrations determined from the TXRF-results presented in Table 5.1. The bulk concentration was calculated by dividing the estimated in-diffused copper concentration by the thickness of the wafer.

The interstitial copper bulk concentration in a few silicon samples was measured using the transient ion drift (TID) method. Table 5.2 presents the TID results.

Table 5.2: The estimated and measured copper concentrations in bulk silicon. The number in the sample name identifies the anneal time in hours at 625 ºC. The TXRF column is the estimated in-diffused copper concentration from the TXRF-results. The TID column is the interstitial copper concentration measured using the TID technique. The analysis column is the copper concentration used for calculations in this work. The copper concentration for samples B2 and M16 is the average value of samples A0 and G4, which were contaminated in the same batch. The error limits in the TID-results were determined to be 10 %. The error limits in the TXRF-results were estimated to be 20 %.

sample	copper concentration cm^{-3}		
	TXRF	TID	analysis
A0		5.0E+12	5.0E+12
B2			3.9E+12
C3	6.5E+12		6.5E+12
D4	3.0E+11		3.0E+11
E4	6.0E+11		6.0E+11
H4	6.5E+12	1.7E+12	1.7E+12
J4	2.1E+12	2.1E+12	2.1E+12
G4		2.7E+12	2.7E+12
F4	6.5E+12		6.5E+12
K4		1.3E+13	1.3E+13
L16	3.0E+11		3.0E+11
M16			3.9E+12

5.2 Oxygen defect density

The density of the oxygen defects was measured using a scanning infrared microscope (SIRM). The measured absolute density value of oxygen defects was not accurate. However, the results indicated that the sample contained a higher density of oxygen defects when the anneal time at 625 ºC was increased. The density of the oxygen defects was 7×10^{7} cm^{-3}, 5×10^{8} cm^{-3}, and above 2×10^{9} cm^{-3} in samples, which underwent a 3 h, 4 h and 16 h anneal at 625 ºC, respectively. The density of oxygen defects in the sample, which was annealed 16 hours, was above the analysis limit. Thus, 2×10^{9} cm^{-3} is the minimum value for the oxygen defect density for samples annealed for 16 hours.

5.3 Carrier lifetime

5.3.1 Carrier lifetime dependence on copper contamination level

The charge carrier lifetime was measured by means of the microwave photoconductive decay (µPCD) technique. Figure 5.1 presents the lifetime results, which were measured without using the bias-light before the optical activation.

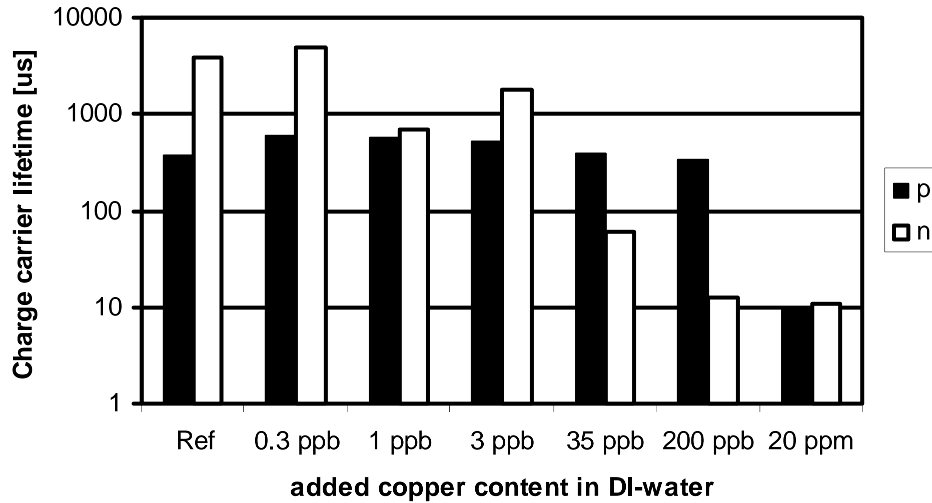

Figure 5.1: The measured average charge carrier lifetime in p-type and n-type silicon. The copper contamination level was varied by changing the copper content in the DI-water used for the contamination. The reference wafers were not intentionally copper contaminated. The charge carrier lifetime was determined under excess charge carrier concentration conditions from 10^{15} cm^{-3} to 3×10^{15} cm^{-3}.

Figure 5.1 shows that the charge carrier lifetime in p-type silicon increased at low copper contamination levels, which can be seen by comparing the results of the reference, 0.3 ppb, 1 ppb and 3 ppb samples. A similar phenomenon has also been reported by Naito *et al.* [36] and Miyazaki [37]. It is assumed that a low copper concentration passivates defects in the silicon-silicon dioxide interface [7]. Figure 5.1 shows that the charge carrier lifetime decreased at high contamination levels in p-type silicon. Figure 5.1 also shows that the charge carrier lifetime in n-type silicon decreased at lower contamination levels than in p-type silicon. This can be seen by comparing the results of the 35 ppb, 200 ppb and 20 ppm samples. The same has also been reported by Naito *et al.* [36], Rotondaro *et al.* [80], Miyazaki [37] and Sachdeva *et al.* [38]. Thus, copper has a stronger impact on the minority carrier lifetime in n-type silicon than in p-type silicon. It was confirmed by Sachdeva *et al.* [38] that the formation of copper precipitates is the reason for the minority charge carrier lifetime decrease in copper contaminated silicon.

In the individual n-type wafers, the measured lifetime was from 0.68 ms to 2.9 ms when the copper surface concentration was around 10^{11} cm^{-2}. In the n-type reference wafers, the carrier lifetime was from 3.5 ms to 4.2 ms. The surface concentrations of other contamination elements were below 10^{10} cm^{-2}, which was checked using TXRF. Therefore, the result indicates that a copper surface concentration of 10^{11} cm^{-2} is high enough to decrease the charge carrier lifetime in n-type silicon. This has also been reported by Naito *et al.* [36] and Miyazaki [37]. They in-diffused copper surface contamination in an oxidizing atmosphere. The oxidation process was done to decrease the surface recombination of charge carriers in order to be able to measure the bulk charge carrier lifetime.

5.3.2 Recombination activity of interstitial copper

The charge carrier lifetime measured in p-type silicon under an excess charge carrier concentration condition of $(6\pm1)\times10^{15}$ cm^{-3} did not depend on the interstitial copper concentration. However, it should be noted that the largest interstitial copper concentration used in the study of the recombination activity of interstitial copper was 1.3×10^{13} cm^{-3}. The highest measured lifetime was 6.4 ms in silicon without any intentional copper contamination. In silicon with an interstitial copper concentration of 1.3×10^{13} cm^{-3}, the measured lifetime was 5.0 ms. The lifetimes were measured after iron-boron dissociation. The iron concentration in p-type silicon was below 10^{10} cm^{-3}, which was determined with the SPV technique. These experimental lifetimes were limited by the Auger and the radiative recombination processes, because the intrinsic bulk lifetime is from 5.0 ms to 7.8 ms in silicon with a boron concentration of 6.1×10^{14} cm^{-3} under excess charge carrier concentration conditions of $(6\pm1)\times10^{15}$ cm^{-3}. The intrinsic lifetime was calculated from equation (3.27). The excess charge carrier concentration of $(6\pm1)\times10^{15}$ cm^{-3} was calculated with a Silvaco device simulator using cylindrical coordinates. More information on this can be found in Appendix B.

The hole capture cross-section of interstitial copper was determined to be below 3×10^{-17} cm^2. This was determined for an electron capture cross-section of 1.5×10^{-15} cm^2 [29], an energy level at E_c-0.15 eV [29], a boron concentration of 6.1×10^{14} cm^{-3}, an interstitial copper concentration of 1.3×10^{13} cm^{-3} and a measured carrier lifetime of 5 ms at an excess charge carrier concentration condition of 6×10^{15} cm^{-3}. The hole capture cross-section was fitted so that a carrier lifetime of 5 ms was calculated from the SHR-equation (3.23). The concentration of interstitial copper paired with boron was estimated to make up 52 % of the total solute copper concentration calculated from equation (2.6). This is the upper limit for the CuB pair concentration, because only a fraction of the immobilized copper ions forms CuB pairs [81]. It is not known if a high excess charge concentration dissociates CuB pairs. Dissociation would decrease the CuB pair concentration. For comparison, the hole capture cross-section is 4.6×10^{-15} cm^2, calculated from the SHR-equation (3.23) using the results of Istratov *et al.* [30]. The hole capture cross-section was in the present study determined with an electron capture cross-section of 1.5×10^{-15} cm^2 [29], an energy level at E_c-0.15 eV [29], a boron concentration of 2×10^{15} cm^{-3} [30], an interstitial copper concentration of 10^{15} cm^{-3} [30] and a minority charge carrier diffusion length of 110 μm [30]. Calculated from equation (2.6), the interstitial copper concentration paired with boron was estimated to make up 70 % of the solute copper concentration, which is the upper limit. The donor state is positively charged before an electron capture process, and neutral before a hole capture process. Thus, it is reasonable that the hole capture cross-section is smaller than the electron capture cross-section, because the Coulomb force does not attract holes, but electrons experience an attractive Coulomb force. Therefore, a hole capture cross-section of 3×10^{-17} cm^2 is physically more reasonable than one of 4.6×10^{-15} cm^2, because the electron capture cross-section is 1.5×10^{-15} cm^2. For comparison, the interstitial iron atoms have electron and hole capture cross-sections of 4×10^{-14} cm^2 and 7×10^{-17} cm^2, respectively [31]. The charge carrier lifetime is inversely proportional to the hole capture cross-section, when the electron capture cross-section is 1.5×10^{-15} cm^2 and the energy level is at E_c-0.15 eV. Therefore, the recombination activity of interstitial copper calculated using the results presented in this study is two orders of magnitude lower than the

recombination activity of interstitial copper calculated using the results presented by Istratov *et al.* [30].

In conclusion, the recombination activity of interstitial copper was found to be low, because the measured carrier lifetime was 5 ms for the interstitial copper concentration of 1.3×10^{13} cm^{-3} in silicon. This means the change in the charge carrier lifetime due to the decrease in the interstitial copper concentration is negligible. Therefore, the decrease in the interstitial copper concentration does not need to be taken into account in the calculation of the copper related recombination rate.

5.4 Recombination dependence on activation time

5.4.1 Examples

Light-induced copper precipitates are studied in this work through charge carrier lifetime measurements using the microwave photoconductive decay technique. Bias-light was used to increase the excess charge carrier concentration during the lifetime measurements and a higher bias-light intensity was used to form copper precipitates in silicon.

Figure 5.2 shows the influence of high intensity light on the charge carrier lifetime of silicon 4 hours and 28 hours after the copper in-diffusion heat treatment. They are called the 4-hour and 28-hour measurements, respectively. A negative corona charge of 1 $\mu C\cdot cm^{-2}$ was deposited on both sides of the silicon wafer on the silicon dioxide surface before the carrier lifetime measurements in order to decrease the surface recombination. The lifetime was measured continuously at different points of the wafer in the 4-hour and 28-hour measurements. However, it was not possible to determine the carrier lifetime when the bias-light intensity was 10 $W\cdot cm^{-2}$, because the transient signal was not detected due to the high excess charge concentration.

Figure 5.2 shows that the carrier lifetime increased rapidly when the bias-light was switched on. This is due to the dissociation of iron-boron pairs. It is known that the recombination rate is lower at interstitial iron atoms than at iron-boron pairs under high excess charge carrier concentration conditions [82]. It is not possible to totally avoid iron contamination during the sample processing. Figure 5.2 shows that the carrier lifetime started to decrease in the 4-hour measurement when the bias-light processing was continued. The lifetime decreased at a faster rate when the bias-light intensity was 10 $W\cdot cm^{-2}$. A contrasting behaviour was seen in the 28-hour measurement, high intensity light did not decrease the carrier lifetime in silicon. This was the first experimental result that showed that the formation of light-induced copper precipitates depends on the time of measurement. The reason for this was the diffusion of positively charged copper atoms to the negatively charged surface. Copper atoms existed and formed precipitates in bulk silicon 4 hours after the heat-treatment. However, after 28 hours all copper atoms had diffused to the surface. Therefore, the high intensity light did not form copper precipitates 28 hours after the heat-treatment.

Figure 5.2 shows that the carrier lifetime was higher at the beginning of the 4-hour measurement than after the high intensity light processing. In addition, the carrier lifetime was higher in the 28-hour than the 4-hour measurement, at the end of the measurement, when the bias-light was switched off. Therefore, light-induced precipitates were still present after the bias-light was switched off.

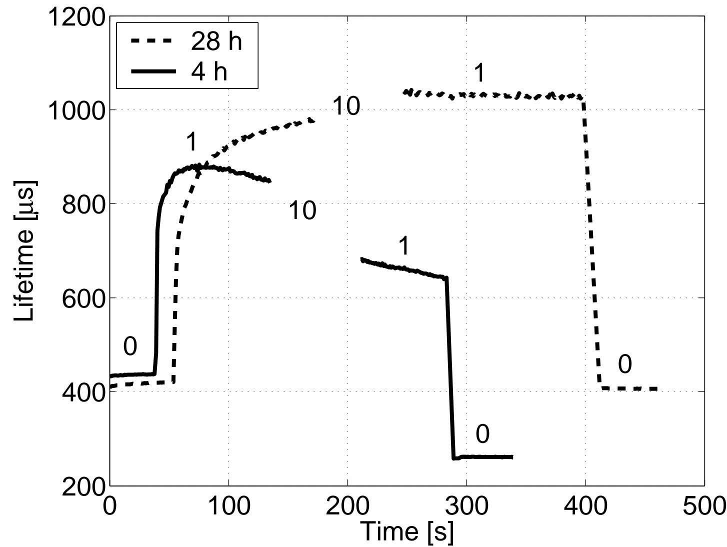

Figure 5.2: The charge carrier lifetime as a function of time in a boron doped copper contaminated silicon sample. The sample was annealed at 625 ºC for 4 hours and at 800 ºC for 4 hours. The heat treatments induced small oxygen precipitates before the copper contamination, which resulted in the bulk copper concentration level of 10^{12} cm^{-3}. The solid line shows the values measured 4 hours after the high temperature process. The dashed line shows the values measured 28 hours after the high temperature process. The bias-light intensity values are shown next to the lines in $W{\cdot}cm^{-2}$. The lifetime was not measurable when the bias-light intensity was 10 $W{\cdot}cm^{-2}$.

Figure 5.3 shows the charge carrier lifetime in silicon as a function of time. The carrier lifetimes were measured 1 day after the heat treatment. A positive corona charge of 1 $\mu C{\cdot}cm^{-2}$ was deposited on the silicon dioxide surfaces before the carrier lifetime measurements in order to decrease the surface recombination. Figure 5.3 shows the time-periods when the high-intensity light was used as zero lifetime values. The average lifetime values between the periods of high-intensity light were extracted from the raw data, and are shown in figure 5.3 as squares. The cumulative time of high-intensity light is called the activation time in the present work.

Figure 5.4 shows the recombination rate at light-induced copper precipitates R_{Cu} as a function of the activation time. The recombination rates are calculated from equation (4.3). The carrier lifetime values were taken from Figure 5.3 and some additional measurement values are also shown. Figure 5.4 also shows the exponential curves, from equation (4.4), which were fitted to the measurement points.

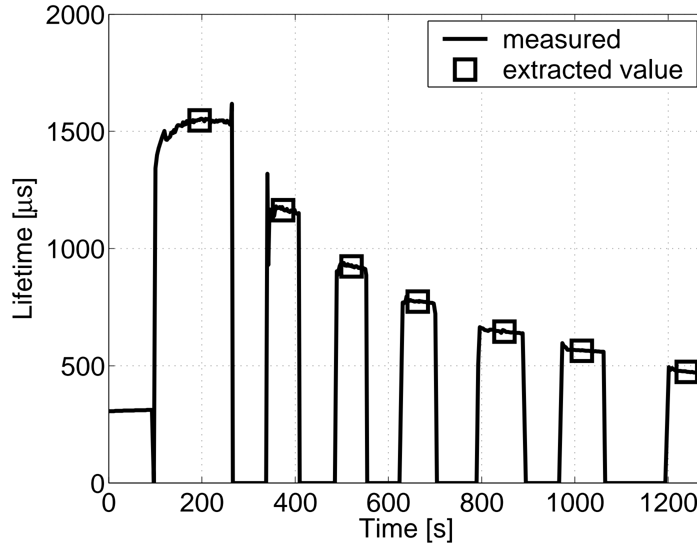

Figure 5.3: The charge carrier lifetime as a function of time in a boron doped copper contaminated silicon sample. The sample was annealed at 625 ºC for 4 hours and at 800 ºC for 4 hours before the copper contamination. The thermal treatments induced small oxygen defects. The copper concentration level was 10^{12} cm^{-3}. The solid line shows the measured values and the squares show the average lifetime values extracted from measured lifetime values. The intensity of the bias-light was 40 $W{\cdot}cm^{-2}$ during the optical activation.

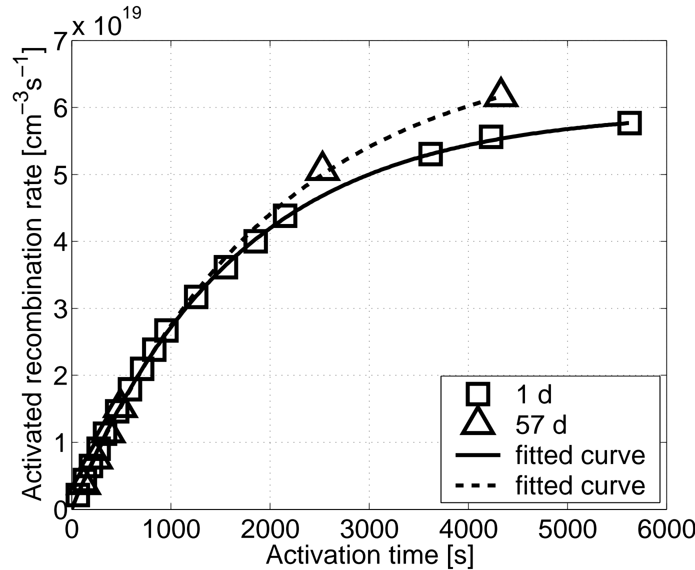

Figure 5.4: The recombination rate at light-induced copper precipitates R_{Cu} as a function of activation time. The values marked with squares were measured 1 day after the high-temperature process and the values marked with triangles were measured 57 days after the high-temperature process. The intensity of the light was 40 $W{\cdot}cm^{-2}$ during the optical activation. The dashed line and the solid line are the curves fitted to the measurement points.

Figure 5.4 shows that the exponential curve is a good fit to the determined recombination rate values, which were measured 1 day after the heat treatment, with a time constant of (1600 ± 100) s with $R_A = 6\times10^{19}$ $cm^{-3}{\cdot}s^{-1}$. The time constant of a later measurement (57 d) was (2000 ± 200) s with $R_A = 7\times10^{19}$ $cm^{-3}{\cdot}s^{-1}$. The time constant and R_A difference between these two

measurements is so small that the formation of copper precipitates can be regarded as equal in those measurements. Thus, the formation of copper precipitates does not depend on the elapsed time after the deposition of positive corona charge. However, the formation of copper precipitates depends on the elapsed time after the deposition of negative corona charge, as seen in Figure 5.2. The polarity of corona charge has an influence on the formation of copper precipitates, because positively charged copper atoms diffuse to the negatively charge surface, but not to the positively charged surface. Traditionally, negative corona charge is used when the carrier lifetime is measured in p-type wafers to form an accumulation layer at the surface.

5.4.2 Measurement inaccuracy

The repeatability of the measurements for charge carrier lifetime was 1 % and 2 % for lifetimes below 0.5 ms and above 1 ms, respectively. The largest source of error was the manual adjustment of the bias-light intensity, which was used to adjust the excess charge carrier concentration in silicon for the lifetime measurements. The charge carrier lifetime depends on the excess charge carrier concentration conditions, but the lifetime was not measured exactly at the same excess charge carrier condition. The feedback for the adjustment of the bias-light intensity was the amplitude of conductivity transient. The repeatability of the lifetime measurements was a significant source of inaccuracy only in the copper out-diffusion experiment when the lifetime change was small at the end of the experiment.

The error estimates for the determined precipitation time constant and the saturation of the recombination rate are 10 % and 5 %, respectively. The error estimates were determined by comparing the calculated recombination rates to the measured values. The calculated recombination rates deviated noticeably from the measured values when the precipitation time constant and the saturation of the recombination rate were changed from the best fit by more than the error estimate. One error source for the precipitation time constant and the saturation of the recombination rate was that the carrier lifetime was not measured after the optical activation time of three hours. The second error source was that the light-induced defect formation at the edge of the light spot was slower than at the middle of the light spot. The defect formation rate depends on the excess charge carrier concentration, which was smaller at the edge of the light spot due to charge carrier diffusion. The third error source was that the charge carrier lifetime was measured at a higher excess charge carrier concentration condition at the beginning than at the end of the optical activation. The charge carrier lifetime was not measured at exactly the same excess charge carrier concentration conditions, because the amplitude of the transient signal also depended on the charge carrier distribution in the silicon sample. The amplitude of the transient signal was used to adjust the excess carrier concentration in silicon.

The carrier lifetime also decreased during lifetime measurements due to the formation of copper precipitates. The lifetime decrease is seen in Figure 5.3 around the square marks. However, the lifetime decreased less during lifetime measurements than during the optical activation. The decrease in lifetimes during the lifetime measurements was not taken into account in the calculations of the activation time. Therefore, the cumulative time of the high-intensity light underestimates the actual activation time. However, this is a negligible error source for the precipitation time constant.

5.4.3 Comparison of measurements and theory

Figure 5.5 shows the comparison of the volume recombination models, the surface recombination model and the measurement data. Figure 5.5 shows that the volume recombination model with growing precipitate radius fits the measurement data best. The surface recombination model and the fixed radius model also fit the measurement data well. The difference between the measurement data and the calculated values is so small that it is possible to use both models to analyze the measurement data.

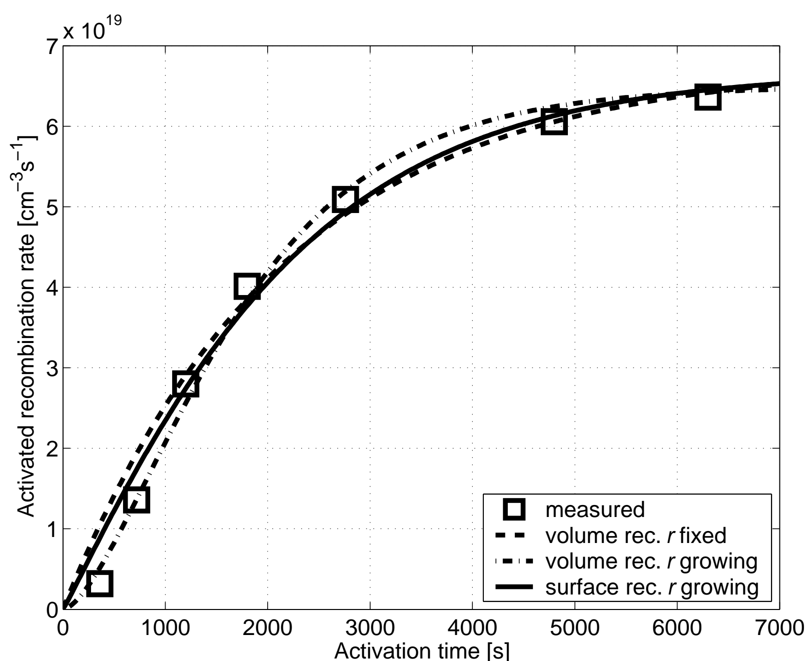

Figure 5.5: The comparison of recombination models and the measurement data of sample F4. Table 3.1 shows the equations and values used for calculations.

5.5 Out-diffusion of copper by means of negative corona charge

In chapter 5.4 it was presented that the formation of copper precipitates depends on the elapsed time after the deposition of negative corona charge. In this chapter, the time constant for the decrease of the light-induced copper related recombination rate is determined and compared with the theoretical out-diffusion time constant of interstitial copper.

In this study, the wafer surfaces were first positively charged after the last furnace process in order to maximize the interstitial copper concentration in bulk silicon and to reach an even interstitial copper distribution. After 12 days, the wafer surfaces were negatively charged and the optical activation was started immediately. A negative corona charge was deposited in order to maximize the diffusion of interstitial copper from bulk into the sample surfaces. At first, the optical activation was carried out for 2 minutes to dissociate iron-boron pairs and the carrier lifetime was measured. Then the optical activation was carried out for 27 minutes and the carrier lifetime was measured again. The same procedure was repeated at 5 other points. Figure 5.6 shows the measurement results and the curve

$$R_{\mathrm{Cu}}(t) = R_{\mathrm{Cu}}(t = 5460\,\mathrm{s}) \times \exp\left(-t/\tau_{\mathrm{od}}\right), \tag{5.1}$$

which was fitted for the last four measurement points. The time-constant τ_{od} is a fitting parameter and t is the elapsed time after the deposition of negative corona charge.

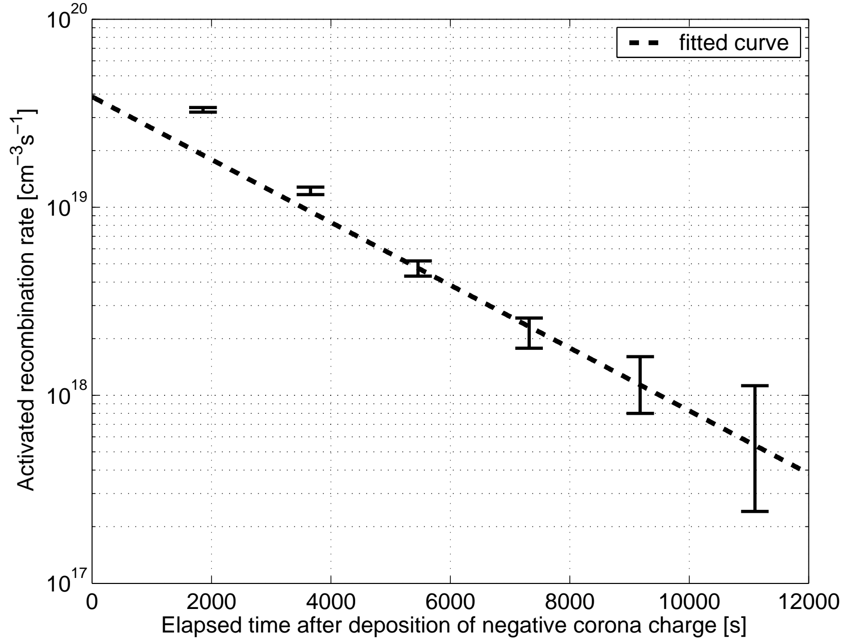

Figure 5.6: The light-induced recombination rate at precipitates at 6 points on the wafer during 27 minutes illumination as a function of elapsed time after the deposition of negative corona charge. The first two measurement points were not included in the fitted curve, because the surface layer is quickly emptied of copper after the deposition of negative corona charge. The light intensity during optical activation was 30 W·cm^{-2}. The measurement data without error bars has been presented in Ref. [83].

Figure 5.6 shows that the time constant (2600 ± 400) s fits the recombination rate decrease well. The time constant for the diffusion limited out-diffusion of particles is

$$\tau_{\mathrm{od}} = \frac{T^2}{\pi^2 D}, \tag{5.2}$$

where T is the thickness of the wafer and D is the diffusivity of particles. The thickness of the sample was 525 µm and the copper diffusion coefficient is 1.3×10^{-7} cm^2·s^{-1}, from equation (2.2), in 22 Ω·cm boron doped silicon at 297 K. The out-diffusion time constant calculated from equation (5.2) is 2180 seconds. The experimental time constant (2600 ± 400) s is close to the theoretical value of 2180 s for copper diffusion into the sample surfaces. Sunakawa *et al.* [84] have applied a negative electric field to attract positive copper atoms into the surface or the vicinity thereof to increase the detection sensitivity of TXRF measurements. In their method, the negative electric field is generated by using non-contact electrodes or corona charge. However, their method does not include a dielectric layer on the silicon surface.

5.6 In-diffusion of copper by means of positive corona charge

It was studied if copper atoms out-diffused by means of a negative corona charge diffuse back into bulk after the deposition of a positive corona charge. In the study, the wafer surface was negatively charged within 20 minutes after the last furnace process in order to enhance the diffusion of interstitial copper atoms from the bulk to the surface. The interstitial copper was allowed to diffuse to the surface for 5 days, which is enough time when compared to the out-diffusion time constant of one hour, calculated from equation (5.2), in silicon with a boron concentration of 10^{15} cm^{-3}. After 5 days, the optical activation was carried out. The surface charge was then changed from negative to positive and the optical activation was repeated. In Figure 5.7 the recombination rate at copper precipitates is presented as a function of optical activation time before and after the surface charge change from negative to positive polarity. It can be seen in Figure 5.7 that the optical activation increases the charge carrier recombination rate again after the change of surface charge polarity. Therefore, the copper atoms that diffused to the surface during the negative surface charge diffuse back into bulk silicon when the surface potential is increased with positive corona charge. However, in-diffusion of copper was not detected in the samples with the lowest copper concentration, if the copper was first out-diffused by means of negative corona charge. The reason for this may be traps, which are present in a low concentration at the surface. This low trap concentration can only trap low copper concentrations but not higher copper concentrations.

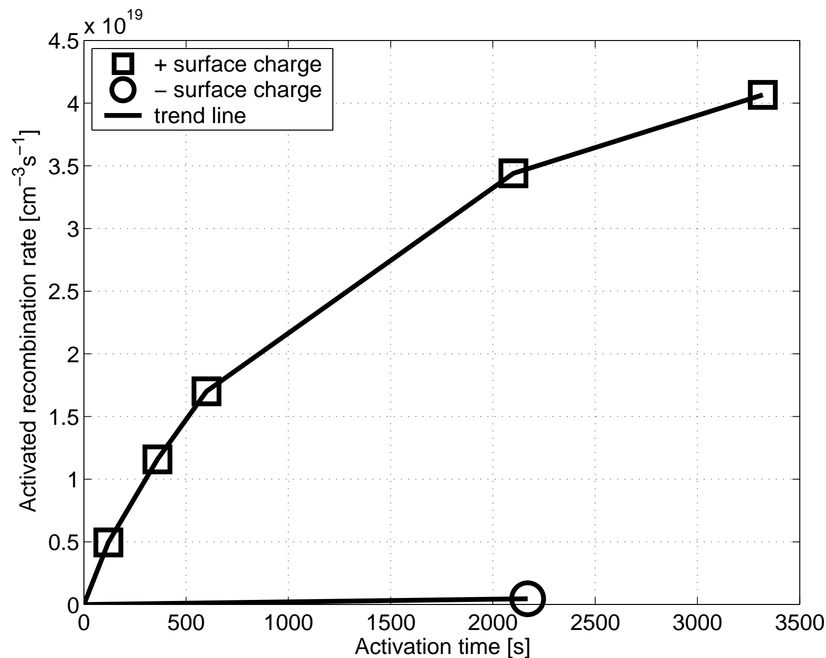

Figure 5.7: The copper related recombination rate as a function of activation time. The key shows the polarity of the surface charge during the optical activation. The result has been presented in Ref. [85].

5.7 Precipitation time constant dependence on light intensity

The dependence of the precipitation time constant on the light intensity was studied in the present work through the following experiment. The copper precipitates were induced by using the high intensity bias-light on different lateral positions of the wafer. The only important difference between the measurements was the different light intensity used for optical activation. The samples contained an oxygen defect density level of 5×10^{8} cm^{-3} and a copper concentration level of 10^{12} cm^{-3}. A positive corona charge of 1 $\mu C\cdot cm^{-2}$ was deposited in order to prevent the copper out-diffusion.

Figure 5.8 presents the experimentally determined precipitation time constant τ_A as a function of the bias-light intensity. Figure 5.8 shows that the precipitation time constant depends strongly on the bias-light intensity. Ramappa [9] has reported that the minority carrier diffusion length decreased at a faster rate with a light intensity of 7.5 $W\cdot cm^{-2}$ compared to a light intensity of 2.5 $W\cdot cm^{-2}$. The light was generated using a halogen lamp.

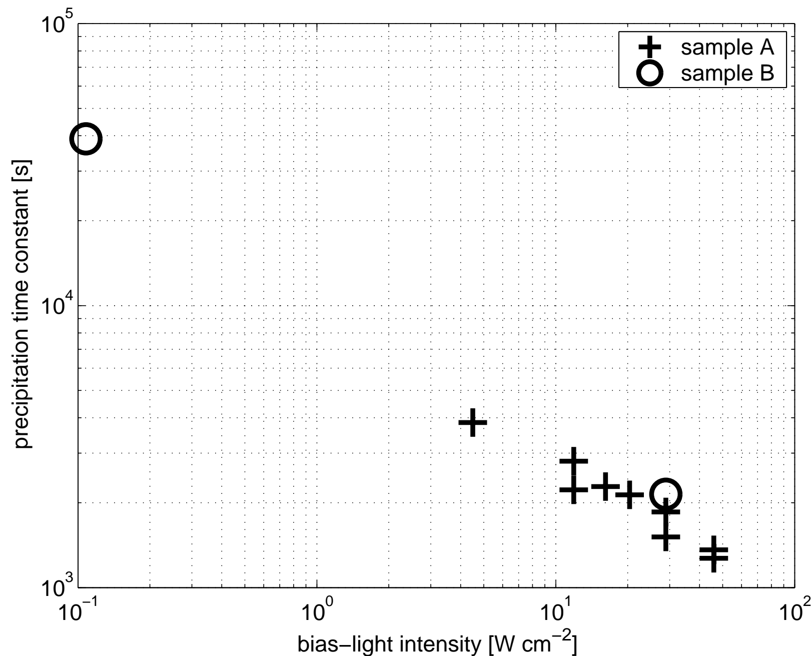

Figure 5.8: The precipitation time constant τ_A as a function of bias-light intensity. The resistivity of sample A was 10 Ω·cm and the resistivity of sample B was 22 Ω·cm.

The electron concentration in semiconductors can be described using an electron quasi-Fermi level. The electron quasi-Fermi level corresponding to the bias-light intensity was calculated with the aid of a Silvaco device simulator using cylindrical coordinates. The 2D simulation was used instead of the 1D simulation, because the charge carrier lifetime was around 100 μs in silicon, which enables significant lateral diffusion for the excess charge carriers. More information on the simulations can be found in Appendix B. The precipitation time constant dependence on the electron quasi-Fermi level, which was calculated in 1D, was presented in Ref. [83].

In Figure 5.9 the precipitation time constant τ_A is shown as a function of the electron quasi-Fermi level. Figure 5.9 shows that the electron quasi-Fermi level should be above E_c-0.2 eV to induce copper precipitates in a reasonable time. However, the optical activation induced copper precipitates when the electron quasi-Fermi level was E_c-0.3 eV. It is suggested here that the optical activation changes the charge state of copper precipitates, which enables copper precipitation at room temperature. The suggestion is based on the results that the copper precipitates are neutral or negatively charged when the Fermi-level is above E_c-0.2 eV, and positively charged when the Fermi-level is below E_c-0.2 eV [22]. Positively charged interstitial copper atoms precipitate with neutral or negatively charged copper precipitates, but not with positively charged copper precipitates due to Coulomb repulsion [10]. This is illustrated in Figure 5.9 by the trend of the precipitation time constant. However, in presence of oxygen defects the copper precipitates even though the Fermi-level is below E_c-0.2 eV [38].

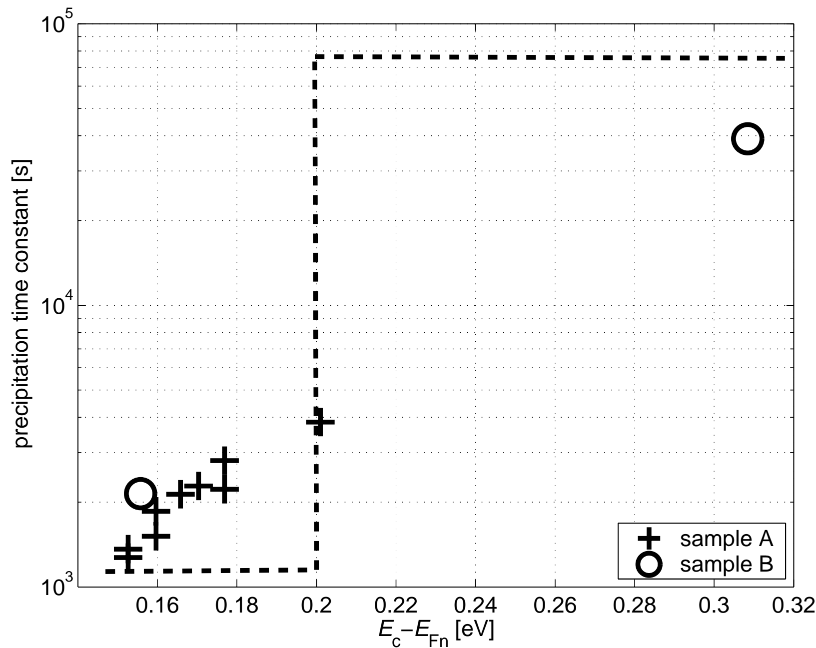

Figure 5.9: The precipitation time constant as a function of the electron quasi-Fermi level position. The resistivity of sample A was 10 Ω·cm and the resistivity of sample B was 22 Ω·cm. The dashed line is the trend of the precipitation time constant as a function of the Fermi-level.

Using the SHR-statistics it was found that the interstitial copper has a high probability to change its charge state when a high excess charge carrier concentration is present in p-type silicon. Therefore, the charge state of interstitial copper may also have an effect on the formation of copper precipitates during the high-intensity illumination. Interstitial copper atoms are positively charged at thermal equilibrium at room temperature, because their donor levels are empty. At an excess charge carrier concentration of 8×10^{16} cm^{-3}, corresponding to an electron quasi-Fermi level at E_c-0.15 eV, 21 % of the donor levels of the interstitial copper atoms are occupied by an electron and therefore neutral. An occupation probability of 21 % was calculated from equation (3.21), with an energy level of interstitial copper at E_c-0.15 eV, an electron capture cross-section of 1.5×10^{-15} cm^2 and a hole capture cross-section of

4.6×10^{-15} cm^2. The occupation probability is 48 % with an electron capture cross-section of 1.5×10^{-15} cm^{-2} and a hole capture cross-section of 2.6×10^{-17} cm^2.

The saturation of the copper related recombination rate did not depend on the light intensity. The saturation of the recombination rate was between 9×10^{19} cm$^{-3}\cdot$s^{-1} and 14×10^{19} cm$^{-3}\cdot$s^{-1} in the measurements of sample A, and 7×10^{19} cm$^{-3}\cdot$s^{-1} in the measurements of sample B.

The saturation of the copper related recombination rate and the time constant dependence on the light intensity suggest that the charge carrier recombination at copper precipitates is dominated by recombination at the bulk of the precipitates. The radius and density of the copper precipitates correlate with the precipitation time constant as $r\propto\tau_0^{0.5}$ from equation (3.53), and $n\propto\tau_0^{-1.5}$ from equation (3.54), respectively. Therefore, the precipitate surface area correlates with the precipitation time constant as $A\propto\tau_0^{-0.5}$. Furthermore, the total surface recombination rate is proportional to the precipitate surface area and the surface recombination velocity. This means that if the charge carrier recombination at copper precipitates is dominated by recombination at the surface of the precipitates, the surface recombination velocity depends on the surface area of the copper precipitates as $S_{prec}\propto A^{-1}$. This kind of dependence is unlikely. However, the surface recombination model was not discarded, because the other results were not against it.

5.8 Properties of copper precipitates

In this chapter the measurement results for the precipitation time constant and light-induced copper related recombination rate for different kinds of samples are presented. The radius and density of the copper precipitates are determined from the precipitation time constant and the copper concentration. The recombination activity of copper is determined from the copper concentration and the light-induced copper related recombination rate. Chapters 5.8.1-5.8.3 show the determined values in tabular form. Chapters 5.8.4 and 5.8.5 show their dependencies on copper concentration and oxygen defects.

5.8.1 Saturation of the recombination rate and the precipitation time constant

Table 5.3 presents the measured precipitation time constant τ_A and the saturation of the recombination rate R_A. They were determined by fitting the curve, from equation (4.4), to the measured recombination rates. The light intensity during the optical activation of copper was 30 W$\cdot$cm^{-2}.

Table 5.3: The copper concentration Cu, the precipitation time constant τ_A and the saturation of the recombination rate R_A. The number in the sample name identifies the anneal time in hours at 625 ºC. The copper concentration values are from chapter 5.1. The error estimate for τ_A is 10 %. The error estimate for R_A is 5 %.

Sample	Cu cm^{-3}	τ_A s	R_A 10^{16} $cm^{-3}\cdot s^{-1}$
A0	5.0E+12	4400	200
B2	3.9E+12	4800	380
C3	6.5E+12	3900	1300
D4	3.0E+11	14000	60
E4	6.0E+11	8500	200
H4	1.7E+12	3700	790
J4	2.1E+12	4900	1200
G4	2.7E+12	2400	3100
F4	6.5E+12	2100	6800
K4	1.3E+13	700	22700
L16	3.0E+11	450	10000
M16	3.9E+12	150	60000

5.8.2 Density and radius

Table 5.4 presents the density and radius of copper precipitates calculated from equations (3.53), (3.54), (3.59) and (3.60) using the values shown in Table 5.3. In the calculations a value of 1.28×10^{-7} $cm^2\cdot s^{-1}$ was used for the effective diffusion coefficient of copper and 6.52×10^{22} cm^{-3} for the density of copper atoms in the precipitates. The calculated densities of the copper precipitates are from 3×10^8 cm^{-3} to 10^{11} cm^{-3}, depending on the sample processing. Istratov *et al.* [9] have reported that copper precipitate densities up to 4.3×10^{12} cm^{-3} are possible. Thus, the determined copper precipitate densities are reasonable. However, the samples of Istratov *et al.* [9] contained a copper concentration of 10^{17} cm^{-3} and were quenched, which made a high precipitation density possible.

The calculated radii of the light-induced copper precipitates are below four nanometers. Elkajbaji *et al.* [23] have detected copper precipitates a few nanometers in size in a fast-cooled sample. In an air-cooled sample, the reported minimum size of the copper precipitates is 7 nm [24].

Table 5.4: The calculated densities and radii of the copper precipitates. The total differential error for the densities is 25 % due to errors in τ_A and R_A. The total differential error for the radii is 15 % due to errors in τ_A and R_A.

Sample	n cm^{-3}	r nm	n_S cm^{-3}	r_S nm
A0	3.9E+08	3.6	5.6E+08	3.2
B2	3.9E+08	3.3	5.6E+08	2.9
C3	4.1E+08	3.9	5.8E+08	3.4
D4	2.8E+08	1.6	4.0E+08	1.4
E4	4.2E+08	1.7	6.0E+08	1.5
H4	8.7E+08	1.9	1.2E+09	1.7
J4	5.2E+08	2.5	7.3E+08	2.2
G4	1.3E+09	2.0	1.9E+09	1.7
F4	1.0E+09	2.8	1.5E+09	2.5
K4	3.8E+09	2.3	5.4E+09	2.1
L16	4.9E+10	0.3	6.9E+10	0.3
M16	7.1E+10	0.6	1.0E+11	0.5

5.8.3 Recombination activity

The copper related recombination is modelled with the volume recombination and the surface recombination models, which are presented in chapters 3.4.1 and 3.4.2, respectively. In Table 5.5 the calculated volume recombination coefficients and the surface recombination velocities at copper precipitates are presented. The volume recombination coefficients were calculated from equation (3.55) using the copper concentrations and the saturation of the recombination rates shown in Table 5.3. The surface recombination velocities are calculated from equation (3.58) using the saturation of the recombination rates, which are shown in Table 5.3, and the density of the copper precipitates n_S and the radii of the copper precipitates r_S, which are shown in Table 5.4. The volume recombination coefficients and surface recombination velocities were calculated in order to compare the recombination activity of copper in different samples after the optical activation.

Table 5.5 shows that k_{prec} is between 4×10^{-11} cm$^3\cdot$s^{-1} and 1.6×10^{-8} cm$^3\cdot$s^{-1} and S_{prec} is between 2.8×10^5 cm$\cdot$s^{-1} and 1.8×10^7 cm$\cdot$s^{-1}, depending on the sample processing. Those values are reasonable when compared to the results of Istratov *et al.* [22] and Sachdeva *et al.* [38]. In Appendix A, k_{prec} and S_{prec} are calculated from the results of Istratov *et al.* [22]. The volume recombination coefficient in p-type silicon was above 7×10^{-9} cm$^3\cdot$s^{-1} and the surface recombination velocity was above 1.1×10^7 cm$\cdot$s^{-1} for plate-shaped copper precipitates. The copper concentration was 2×10^{17} cm^{-3} and the cooling rate was 2000 K$\cdot$s^{-1}. Sachdeva *et al.* [38] reported that the minority charge carrier diffusion length is from 13 μm to 20 μm, corresponding to a carrier lifetime from 0.05 μs to 0.12 μs, when a copper concentration of 10^{16} cm^{-3} is precipitated by quenching. These result in the volume recombination coefficients of copper precipitates 8×10^{-10} cm$^3\cdot$s^{-1} and 2×10^{-9} cm$^3\cdot$s^{-1} from equation (3.55).

The largest surface recombination value calculated in this work is 1.8×10^{7} cm·s^{-1}, which is above the theoretical maximum surface recombination velocity of 5×10^{6} cm·s^{-1} given by the Schottky model [86]. The surface area of the copper precipitates used in the calculations is the minimum limit for the area in which charge carries recombine. Therefore, the calculated surface recombination velocities are the maximum ones. The model does not take into account the surface area of the oxygen defects, which could increase the recombination area. In addition, the surface area of the copper precipitates is larger if the precipitates are not spherical or if the density of the copper atoms in the precipitate is lower than in the Cu_3Si precipitates. The radius and the density of the copper precipitates depend on the density of the copper atoms in the precipitates according to $r\propto\rho^{-0.5}$ from equation (3.59), and $n\propto\rho^{0.5}$ from equation (3.60), respectively. Therefore, the dependence of the precipitate surface area on the density of copper atoms in precipitates is $A\propto\rho^{-0.5}$.

Table 5.5: The volume recombination coefficient k_{prec} and surface recombination velocity S_{prec}. The total differential error of the volume recombination coefficient is 15 % or 25 %, depending on the copper concentration determination method. The total differential error of the surface recombination velocity is 45 % or 60 %, depending on the copper concentration determination method.

sample	k_{prec} cm^{3}·s^{-1}	S_{prec} cm·s^{-1}
A0	4.0E-11	2.8E+05
B2	9.9E-11	6.3E+05
C3	2.0E-10	1.5E+06
D4	2.0E-10	6.1E+05
E4	3.3E-10	1.1E+06
H4	4.6E-10	1.7E+06
J4	5.7E-10	2.7E+06
G4	1.1E-09	4.3E+06
F4	1.0E-09	5.7E+06
K4	1.7E-09	7.8E+06
L16	3.3E-08	1.8E+07
M16	1.6E-08	1.8E+07

5.8.4 Influence of copper concentration

The results in this subsection are for samples with oxygen defect densities that are as equal as possible. Figure 5.10 presents the precipitation time constant dependence on the copper concentration. Figure 5.10 shows that the precipitation time constant τ_A is shorter when the copper concentration is higher. The decrease in the precipitation time constant when the copper concentration increases indicates that the *nr* product increases when the copper concentration increases, see equation (3.46). Figure 5.11 presents the dependence of the density of copper precipitates on the copper concentration, which shows that the density of copper precipitates increases when the copper concentration increases. Figure 5.12 presents the dependence of the

radius of copper precipitates on the copper concentration, which shows that the radius does not depend strongly on the copper concentration. Thus, the results indicate that the decrease in the precipitation time constant is explained by the increase in the density of copper precipitates, when the copper concentration increases.

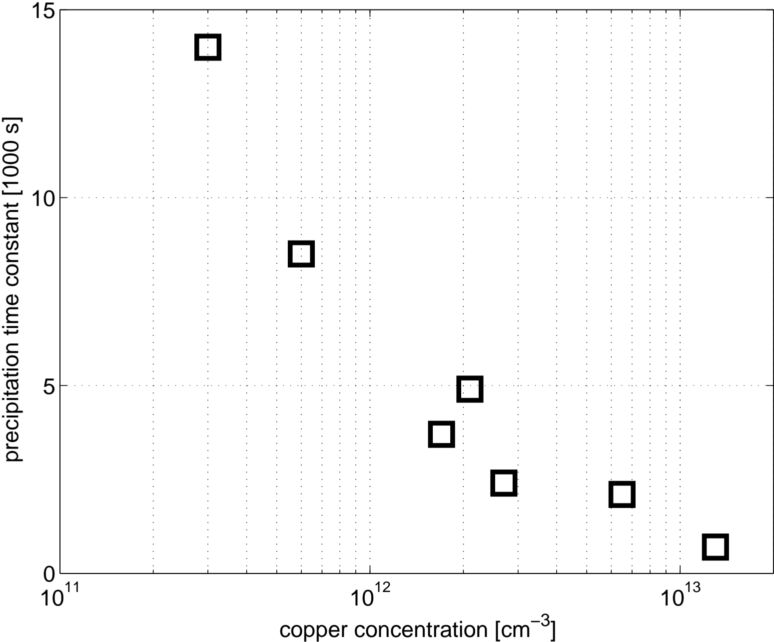

Figure 5.10: The precipitation time constant τ_A as a function of copper concentration.

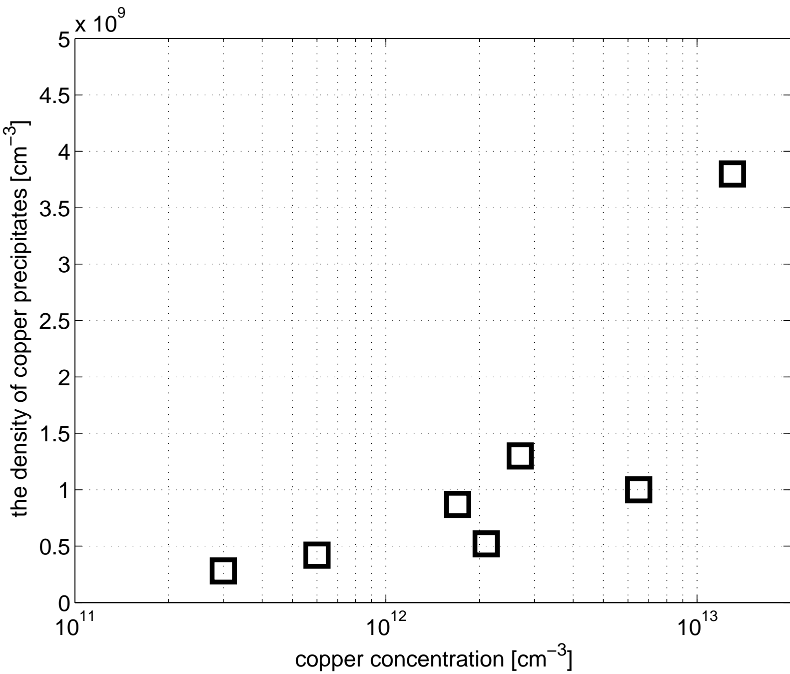

Figure 5.11: The density of the copper precipitates as a function of copper concentration.

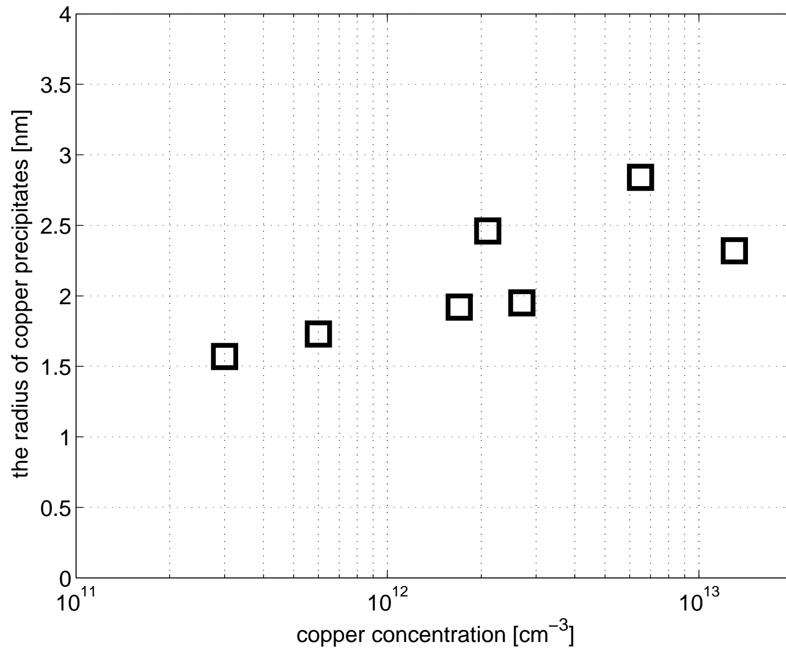

Figure 5.12: The radius of the copper precipitates as a function of copper concentration.

Figure 5.13 shows the saturation values of the recombination rates and the calculated recombination rates as a function of copper concentration. The recombination rates for the volume recombination and the surface recombination models were calculated from equations (3.55) and (3.58), respectively. Table 5.6 shows the values used for the calculations. The volume recombination coefficient k_{prec} and the surface recombination velocity S_{prec} were fitted to achieve quantitative agreement between the calculated values and the measured values for a copper concentration of 10^{12} cm^{-3}. The density and radius of the copper precipitates for the surface recombination model are taken from Table 5.4.

Table 5.6: The values and equations used to calculate the recombination rate as a function of precipitated copper, as shown in Figure 5.13.

quantity	unit	Model	
		volume recombination	surface recombination
R_{prec}	cm^{-3}·s^{-1}	equation (3.55)	equation (3.58)
c_{prec}	cm^{-3}	Table 5.2	Table 5.2
n_S	cm^{-3}	-	Table 5.4
r_S	cm	-	Table 5.4
k_{prec}	cm^{3}·s^{-1}	5×10^{-10}, fitted	-
S_{prec}	cm·s^{-1}	-	2×10^{6}, fitted
D	cm^{2}·s^{-1}	1.28×10^{-7}	1.28×10^{-7}
Δn	cm^{-3}	10^{16}	10^{16}
ρ	cm^{-3}	6.52×10^{22}	6.52×10^{22}

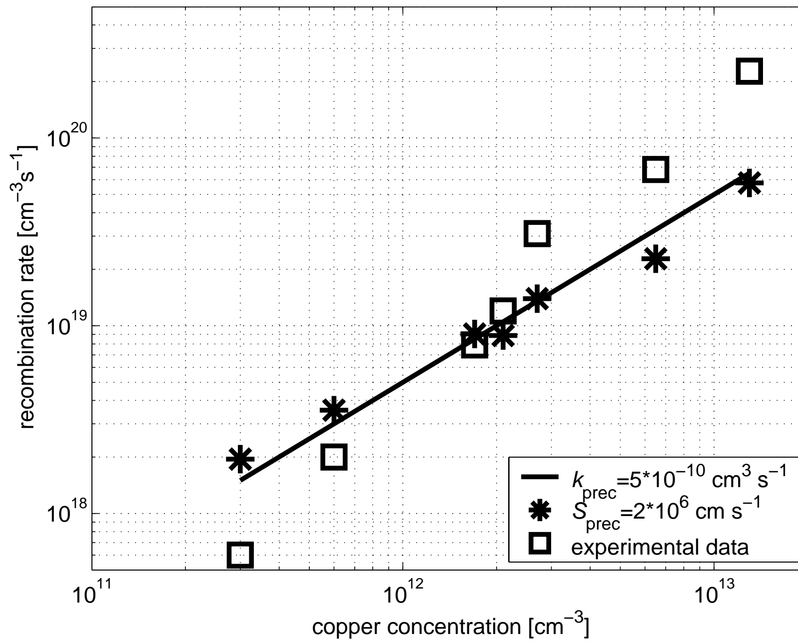

Figure 5.13: The measured and calculated copper related recombination rate as a function of copper concentration. Table 5.6 shows the values and equations used for the calculations. The measured values are in Table 5.3.

Figure 5.13 shows that the measured recombination rate dependence on copper concentration is stronger than the calculated recombination rate dependence on copper concentration. This means that in the recombination models k_{prec} or S_{prec} increases when the copper concentration increases, which can be seen in Table 5.5. The fitted volume recombination coefficient of 5×10^{-10} $cm^3 \cdot s^{-1}$ in the volume recombination model and the fitted surface recombination velocity of 2×10^6 $cm \cdot s^{-1}$ in the surface recombination model are reasonable values when compared to the results of Istratov *et al.* [22] and Sachdeva *et al.* [38], which were presented in chapter 5.8.3. In Figure 5.13 the volume and surface recombination models give almost the same recombination rate dependence on the copper concentration, because the radius of the copper precipitates depends only weakly on the copper concentration, as seen in Figure 5.12.

5.8.5 Influence of oxygen defects

The results in this subsection are for the samples, which contained copper concentrations from 3×10^{12} cm^{-3} to 6×10^{12} cm^{-3}. The oxygen defect density was varied by changing the anneal time at 625 ºC. The oxygen defect densities increased with longer anneal times, which was checked using the SIRM technique. In Figure 5.14 the precipitation time constant and the density of copper precipitates for samples containing different oxygen defect densities are shown. Figure 5.14 shows that the time constants do not change significantly between the samples annealed from 0 hours to 3 hours. However, the time constant is much lower when the anneal time is 16 hours compared to the shorter anneal times. The decrease in the precipitation time constant is explained by the increase in the density of copper precipitates.

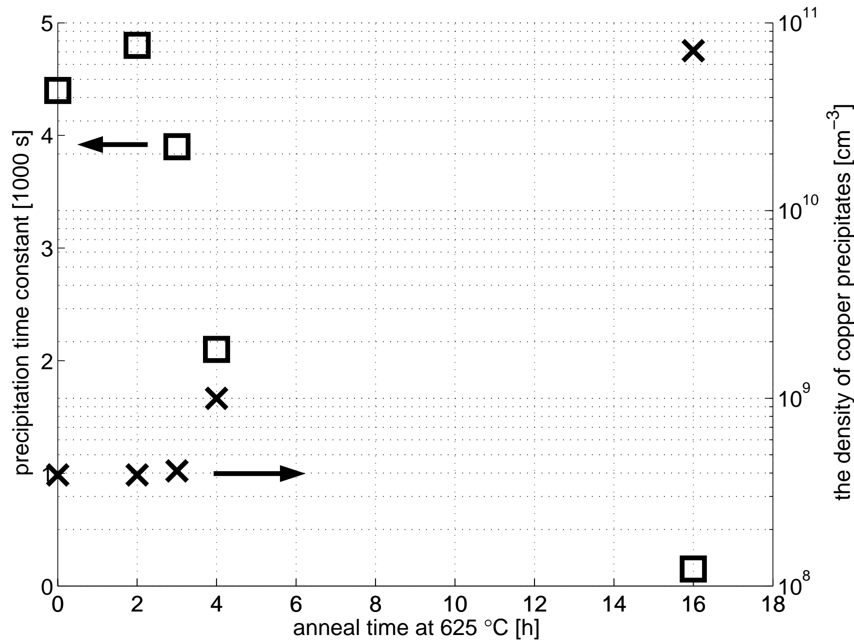

Figure 5.14: The precipitation time constant τ_A and the density of copper precipitates as a function of anneal time at 625 ºC. The squares indicate the time constants. The crosses indicate the densities. The anneal processes were done before the copper contamination processes. The oxygen defect densities increased with longer anneal times.

In Figure 5.15 the copper related recombination rate for samples containing different oxygen defect densities is shown. Figure 5.15 shows that the copper related recombination rate is higher when the oxygen defect density is higher. The difference in the copper concentration between the samples is not the reason for the over two decades difference in the recombination rate. The copper related recombination rate was above two decades higher in sample M16, which had a high oxygen defect density, compared to sample A0, which had a low oxygen defect density. This result indicates that the oxygen defects are precipitation sites for copper at room temperature during the optical activation, because the recombination rate after the optical activation depends strongly on the oxygen defect density in silicon. Oxygen related defects are known to getter copper during the cooling down period, but not at room temperature, at trace copper concentration levels. The decrease of the minority carrier diffusion length was small in the quenched boron doped sample containing oxygen defects and a copper concentration of 10^{13} cm^{-3} [38]. In a quenched sample, the possible copper precipitation at oxygen defects occurs at room temperature.

The following explanation is suggested for the light-induced recombination rate dependence on the density of oxygen defects. The copper related recombination rate depends on whether the copper precipitates are located at microscopic lattice defects or at oxygen related defects or both. The copper precipitates located at oxygen related defects have a more than two decades higher recombination activity than those located at microscopic lattice defects. The suggestion is based on the results that show that the density of copper precipitates stayed about the same, but the recombination rate increased, when the oxygen defect density increased. This can be seen by comparing the densities of the precipitates in Figure 5.14 and the recombination rates in Figure 5.15 for samples A0, B2 and C3, which were annealed 0, 2 and 3 hours, respectively.

Therefore, the increase in the concentration of copper precipitates at oxygen defects is enough to change the total recombination activity without any noticeable change in the total density of copper precipitates. The model, which includes two kinds of copper precipitates, is used in the following chapter to determine the gettering efficiency of copper at oxygen defects.

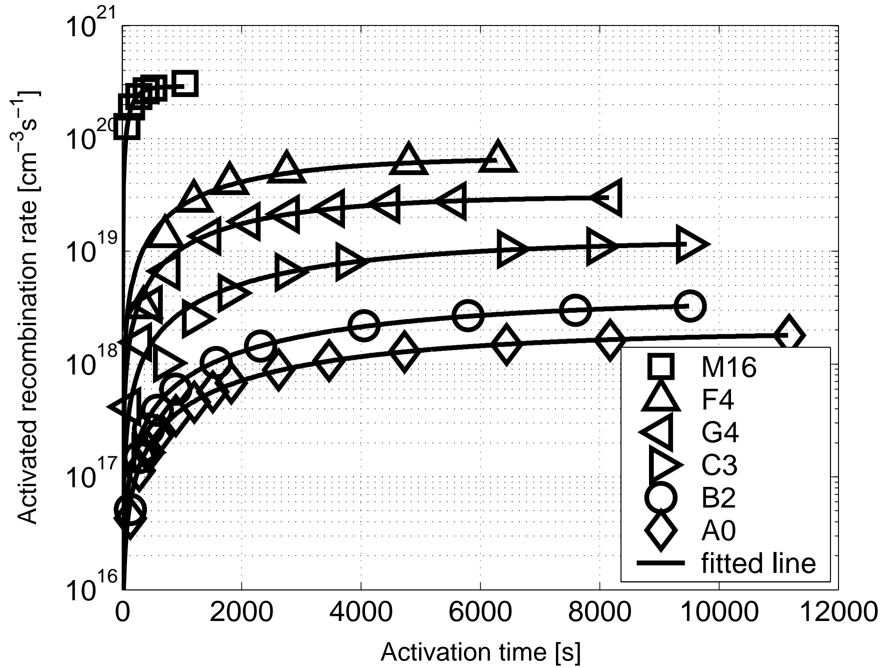

Figure 5.15: The copper related recombination rate dependence on the density of oxygen defects [87]. The number in the sample names equals the anneal time in hours at 625 ºC. The copper concentration in the samples was from 3×10^{12} cm^{-3} to 6×10^{12} cm^{-3}.

5.9 Models with two kinds of recombination sites

The results presented in the previous section indicate that the oxygen defects increase the recombination rate of precipitated copper. This is modelled in the following sections with two kinds of copper precipitates, called here the precipitates at oxygen defects and the precipitates at microscopic lattice defects.

5.9.1 Volume recombination

In chapter 3.4.4 the volume recombination model for two kinds of defects was presented. In this section, the model is used to estimate the ratio of the concentration of copper precipitated at oxygen defects to the concentration of copper precipitated at all kinds of defects. In this work this is called the gettering efficiency of copper at oxygen defects, which is calculated using equation (3.65), with the coefficients $k_{prec1}=2.4\times10^{-8}$ cm^3·s^{-1} and $k_{prec2}=4\times10^{-11}$ cm^3·s^{-1}, and the experimentally determined recombination rates. The volume recombination coefficient of precipitated copper atoms at oxygen defects k_{prec1} is the average value of samples L16 and M16 from Table 5.3. These were samples with a high oxygen defect density. The volume recombination coefficient of precipitated copper atoms at microscopic lattice defects k_{prec2} is

the value of sample A0, in which the oxygen defect density was low. In Figure 5.16 the gettering efficiency of copper at oxygen defects is shown.

Figure 5.16 shows that the gettering efficiency of copper at oxygen defects increases in the volume recombination model from 0.7 % to 7 %, when the copper concentration increases from 3×10^{11} cm^{-3} to 1.3×10^{13} cm^{-3}. Those gettering efficiency values are low. Therefore, precipitation at microscopic lattice defects is more efficient than precipitation at oxygen defects, unless the oxygen precipitation density is high. Hölzl *et al.* [88] reported that the gettering efficiency of copper at oxygen related defects during cooling increased when samples contained a higher oxygen defect density.

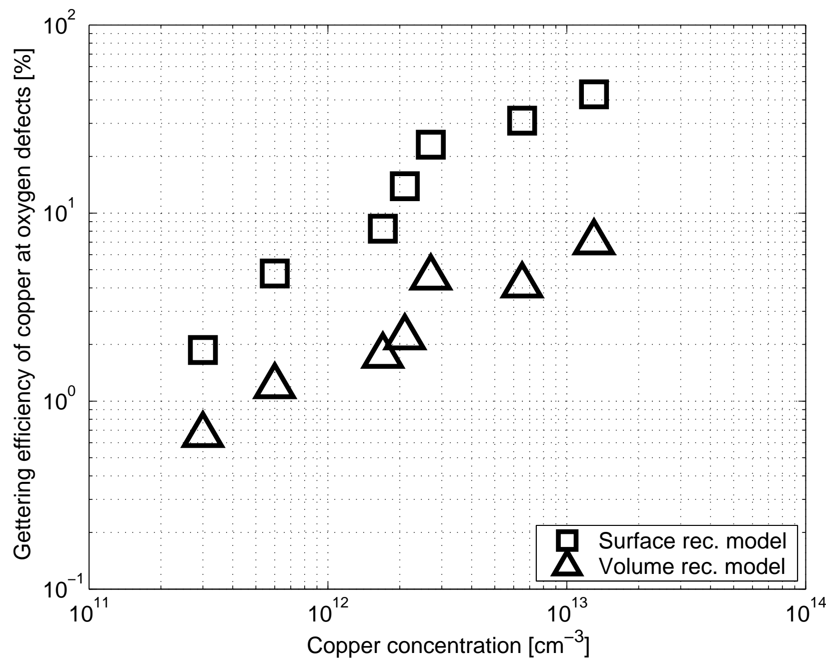

Figure 5.16: The gettering efficiency of copper at oxygen defects as a function of copper concentration. The samples contained an oxygen defect density of about 5×10^{8} cm^{-3}.

The total density of copper precipitates increased from 4×10^{8} cm^{-3} to 10^{9} cm^{-3} when the density of oxygen defects increased from 7×10^{7} cm^{-3} to 5×10^{8} cm^{-3}. This can be seen by comparing the densities of the copper precipitates of samples C3 and F4 from Table 5.4. According to the model for two kinds of defects, the reason for the increase in the total density of copper precipitates is the increase in the density of copper precipitates at microscopic lattice defects. Therefore, it is suggested that the formation of oxygen defects also increases the density of microscopic lattice defects.

5.9.2 Surface recombination

In chapter 3.4.5 the surface recombination model for two kinds of defects was presented. In this section, the surface recombination model is used to estimate the gettering efficiency of copper at oxygen defects. This is calculated by means of equation (3.69), using the surface recombination velocities $S_{prec1}=1.8\times10^{7}$ $cm\cdot s^{-1}$ and $S_{prec2}=2.8\times10^{5}$ $cm\cdot s^{-1}$, and the

experimentally determined recombination rates. The surface recombination velocity at copper precipitates at oxygen defects S_{prec1} is the average value of the samples L16 and M16 from Table 5.3. The surface recombination velocity at the copper precipitates at microscopic lattice defects S_{prec2} is the value of sample A0.

Figure 5.16 shows that the gettering efficiency of copper at oxygen defects increases in the surface recombination model from 2 % to 40 % when the copper concentration increases from 3×10^{11} cm^{-3} to 1.3×10^{13} cm^{-3}. The surface recombination model gives higher gettering efficiencies than the volume recombination model.

5.10 Determination of copper concentration

5.10.1 General

In this chapter the equations for the determination of the copper concentration from the change of charge carrier lifetime are presented. It was shown in chapter 5.8.5 that the recombination activity of copper depends on the density of oxygen defects in silicon. The copper concentration can be determined in cases when copper atoms mainly precipitate at oxygen defects or microscopic lattice defects, but not at both. These situations are present in samples, which do not contain any oxygen defects, or alternatively contain a high density of oxygen defects. These situations are analyzed in the next sections. When a sample contains oxygen defects but not at a high density, the copper concentration can be determined by means of lifetime measurements by using the correlation curves, which are measured through TID measurements. For example, the correlation curve for a sample containing the oxygen defect density of 5×10^{8} cm^{-3} can be determined by means of experimental data, which is shown in figure 5.13.

5.10.2 Volume recombination model

According to the volume recombination model, the precipitated copper concentration in silicon using the optical activation from equation (3.55) is

$$c_{\mathrm{prec}} = \frac{R_{\mathrm{Cu}}}{\Delta n\, k_{\mathrm{prec}}}, \tag{5.3}$$

where the volume recombination coefficient k_{prec} depends on the density of oxygen defects, as presented in chapter 5.8.5. The volume recombination coefficient also depends on the injection level used in the lifetime measurements, which will be presented in this section. The precipitated copper concentration using optical activation, from equations (4.3) and (5.3), is

$$c_{\mathrm{prec}} = \frac{1}{k_{\mathrm{prec}}}\left(\frac{1}{\tau_2} - \frac{1}{\tau_{\mathrm{max}}}\right), \tag{5.4}$$

where τ_2 is the lifetime measured after the optical activation and τ_{max} is the maximum lifetime at the beginning of the measurement.

Without oxygen defects

In a silicon wafer without oxygen defects k_{prec} is 4×10^{-11} $cm^3\cdot s^{-1}$, as presented in section 5.9.1. By inserting this value into equation (5.4), we get the numerical equation

$$c_{prec} = 2.5\times10^{10}\left(\frac{1}{\tau_2} - \frac{1}{\tau_{max}}\right) \quad cm^{-3}, \tag{5.5}$$

where the lifetime values should be inserted in seconds and the lifetime should be determined at a high carrier injection level. The conversion factor in equation (5.5) was determined using a sample in which the copper concentration was 5×10^{12} cm^{-3}. The quantitative detection limit for copper is about 3×10^{12} cm^{-3} in homogeneous boron doped silicon. This interstitial copper concentration decreases the lifetime in silicon from 1 ms to 0.9 ms, if all interstitial copper atoms are precipitated by means of the optical activation.

Henley *et al.* [8] reported that an optical activation decreased the diffusion length in silicon from about 200 µm to 10 µm, corresponding to carrier lifetimes of 13 µs and 30 ns, respectively. Tarasov *et al.* [13] reported an almost equal decrease of the diffusion length in silicon that had been ion implanted with copper to a dose of 10^{13} cm^{-2}. The charge carrier diffusion length decreased from 170 µm to about 10 µm. The copper concentration from equation (5.5) is 10^{18} cm^{-3} for both cases [8, 13]. The interstitial copper concentration can be at a maximum 10^{16} cm^{-3} plus the doping concentration, because copper precipitates at higher copper concentrations [10]. The calculated copper concentration is almost four decades higher than the ion implanted copper dose reported by Tarasov *et al.* [13]. The probable reason for the over-estimation of the copper concentration is that the high copper concentration had induced defects near the surface in the samples of Henley *et al.* [8] and Tarasov *et al.* [13], while equation (5.5) includes the assumption that the copper precipitates are evenly distributed in the bulk. If the copper concentration in silicon is high, copper precipitates near the surface when the sample is air-cooled. The copper related defects can extend up to 40 µm in from surface [24]. TEM figures have indicated that copper precipitated at the surface when the copper dose was 10^{13} cm^{-2}, but did not precipitate at the surface when the copper dose was 10^{12} cm^{-2} [12]. The interstitial copper atoms precipitate at surface defects during the optical activation. The charge carrier diffusion length measurement is based on the charge carrier collection from the bulk to the surface. Therefore, the measured diffusion length is low if the diffusion length is low near the surface region, even when the diffusion length in bulk silicon is high. Therefore, the large copper defect density within 10 µm from the silicon surface is the probable reason for the low diffusion length of 10 µm measured by Henley *et al.* [8] and Tarasov *et al.* [13] after the optical activation.

Tarasov *et al.* [13] reported a charge carrier diffusion length change from 312 µm to 264 µm for a sample doped with a copper dose of 10^{12} cm^{-2}. The calculated copper concentration, from equation (5.5), and the implanted copper concentration are 4×10^{14} cm^{-3} and 2×10^{13} cm^{-3}, respectively. This difference is due to the carrier lifetime dependence on the excess charge

carrier concentration. It was measured in the present work that the charge carrier lifetime at low excess charge carrier concentrations is a tenth of the carrier lifetime at an excess charge carrier concentration of $(6\pm1)\times10^{15}$ cm^{-3}. The diffusion length and lifetime was 120 μm and 47 μs, respectively, after the optical activation. The lifetime was 2.8 ms before the optical activation. Therefore, the conversion factor in equation (5.5) should be about 2.5×10^{9} for SPV measurements. After this correction, the calculated copper concentration is only a factor two higher than the implanted copper concentration. Tarasov *et al.* [13] took into account the influence of iron contamination on the carrier diffusion length. They heat-treated samples at 65 ºC or 80 ºC after the optical activation. The interstitial iron atoms paired with boron atoms during the heat treatment. Therefore, the influence of iron on the carrier lifetime was the same in the first diffusion length measurement before the optical activation as in the last diffusion length measurement after the low temperature heat treatment.

In the study of Raineri *et al.* [12] the charge carrier diffusion length decreased from about 240 μm to about 200 μm due to the optical activation in silicon, which was ion implanted with a copper dose of 10^{13} cm^{-2}. The diffusion length values were extracted from figures presented by Raineri *et al.* [12]. The diffusion lengths correspond to lifetime values of 19 μs and 13 μs, respectively. The copper concentration from equation (5.5) is 7×10^{13} cm^{-3} with the conversion factor 2.5×10^{9}. This copper concentration is the upper limit, because the high-intensity light dissociates possible iron-boron pairs, which also decreases the diffusion lengths in silicon.

Mcdonald *et al.* [41] reported that the lifetime was a factor 1.6 higher when the excess charge carrier concentration was 5×10^{14} cm^{-3} instead of 1.5×10^{13} cm^{-3}, for samples containing plane-shaped copper precipitates. Therefore, the lifetime dependence on the excess charge carrier concentration is weaker in samples containing plane-shaped copper precipitates compared to samples containing light-induced copper precipitates.

High density of oxygen defects

The volume recombination coefficient of precipitated copper atoms at oxygen defects is $k_{prec1}=(2\pm1)\times10^{-8}$ cm$^{3}\cdot$s^{-1}, which was determined for samples containing oxygen precipitates nucleated at 625 ºC for 16 hours and grown at 800 ºC for 4 hours. This process formed a high density of oxygen defects. The copper concentration level of the samples was from 3×10^{11} cm^{-3} to 4×10^{12} cm^{-3}. The coefficient $k_{prec1}=2\times10^{-8}$ cm$^{3}\cdot$s^{-1} gives the conversion factor 5×10^{7}, from equation (5.4). The detection limit for the precipitated copper concentration at oxygen defects is about 5×10^{10} cm^{-3}. This interstitial copper concentration decreases the carrier lifetime in silicon from 100 μs to 90 μs, if the interstitial copper atoms are precipitated using optical activation. The detection limit for copper concentration in silicon without oxygen defects is about 3×10^{12} cm^{-3}. Thus, the detection limit of copper can be increased by almost two decades by the formation of small oxygen defects in bulk silicon.

The volume recombination coefficient of copper atoms precipitated at the oxygen defects probably depends on the size of the oxygen defects. Thus, the volume recombination coefficient $k_{prec1}=(2\pm1)\times10^{-8}$ cm$^{3}\cdot$s^{-1} probably applies only to oxygen precipitates grown at 800 ºC for 4 hours, which results in small oxygen defects.

5.10.3 Surface recombination model

Determining the copper concentration from the change in carrier lifetime with the surface recombination model is more complicated than with the volume recombination model. The precipitation time constant τ_A should be determined when the surface recombination model is used. This is not needed in the volume recombination model. According to the surface recombination model, the copper related recombination rate from equations (3.50) and (3.58) is

$$R_{\mathrm{Cu}} = \Delta n S_{\mathrm{prec}} (4\pi n)^{1/3} \left(\frac{3 c_{\mathrm{prec}}}{\rho} \right)^{2/3} . \tag{5.6}$$

The precipitated copper concentration from equation (5.6) is

$$c_{\mathrm{prec}} = (4\pi n)^{-1/2} \left(\frac{R_{\mathrm{Cu}}}{\Delta n S_{\mathrm{prec}}} \right)^{3/2} \left(\frac{\rho}{3} \right). \tag{5.7}$$

Equations (5.7) and (3.60) can be used iteratively to calculate the precipitated copper concentration, if the precipitation time constant τ_A and the copper related recombination rate R_{Cu} are known.

Without oxygen defects

In a silicon without oxygen defects, S_{prec} is 2.8×10^5 cm·s^{-1} as presented in section 5.9.2. The density of copper precipitates is 5.6×10^8 cm^3·s^{-1} from Table 5.4. By using 6.52×10^{22} cm^3 as the density of copper atoms in the precipitates and inserting these values and equation (4.3) into equation (5.7), we get the numerical equation

$$c_{\mathrm{prec}} = 1.7\times10^9 \left(\frac{1}{\tau_2} - \frac{1}{\tau_{\mathrm{max}}} \right)^{3/2} \quad \mathrm{cm}^{-3}, \tag{5.8}$$

where the lifetime values should be inserted in seconds and the lifetime should be determined at a high excess charge carrier concentration level. Equation (5.8) includes the assumption that the density of copper precipitates is independent of the copper concentration. Therefore, the factor in equation (5.8) is valid for a narrow range of precipitated copper concentrations. In the presented case the factor is calculated for a precipitated copper concentration of 5×10^{12} cm^{-3}·s^{-1}. By comparing equations (5.5) and (5.8), it can be seen that the exponents are 1 and 1.5, respectively. The difference in the exponents should make it possible to identify whether volume or surface recombination dominates on copper precipitates. However, it should be noted that the density of copper precipitates depends on the copper concentration. This decreases the exponent below 1.5 in equation (5.8).

High density of oxygen defects

The surface recombination velocity at copper precipitates at oxygen defects is 1.8×10^{7} cm·s^{-1}, as shown in section 5.9.2. This value should be used when determining the precipitated copper concentration by means of the surface recombination model for a sample containing a high density of oxygen defects. Figure 5.17 shows the precipitated copper concentration as a function of the copper related recombination rate. It was calculated using equation (5.7). Figure 5.17 also shows experimental data for samples, which contained a high density of oxygen defects. This data was used to determine the surface recombination velocity at the copper precipitates at oxygen defects.

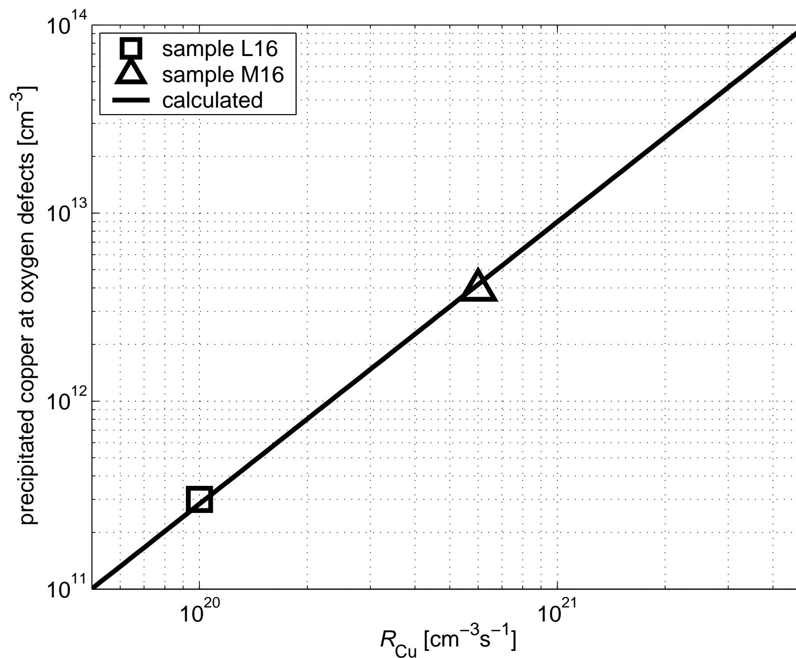

Figure 5.17: The precipitated copper concentration as a function of the copper related recombination rate according to the surface recombination model. The precipitated copper concentration was calculated from equation (5.7) with n=8×10^{10} cm^{-3}, S_{prec}=1.8×10^{7} cm·s^{-1}, Δn=10^{16} cm^{-3} and ρ=6.52×10^{22} cm^{-3}.

Figure 5.17 shows that a copper related recombination rate of about 2×10^{20} cm^{-3}·s^{-1} corresponds to a precipitated copper concentration of 10^{12} cm^{-3}. For example, the recombination rate is 2×10^{20} cm^{-3}·s^{-1} when the lifetime value changes from 100 µs to 33 µs. The measured carrier lifetimes was 110 µs before the optical activation and 52 µs after the optical activation in sample L16, which contained a high oxygen defect density and a copper concentration of 3×10^{11} cm^{-3}. This is still a quite large change in the lifetime. The surface recombination velocity at the copper precipitates at oxygen defects probably depends on the size of the oxygen defects. Thus, the determined surface recombination velocity of 1.8×10^{7} cm·s^{-1} probably only applies to oxygen precipitates grown at 800 ºC for 4 hours.

6 Conclusion

In this work a sample preparation method for copper detection by carrier lifetime measurements in boron-doped silicon was developed. Oxidized silicon wafers were air-cooled, without quenching, after heat treatment. A positive corona charge was deposited on the silicon surface after the heat treatment. An interstitial copper concentration of $(1.3\pm0.1)\times10^{13}$ cm^{-3} was measured by means of TID in a silicon sample one year after the thermal treatment. The silicon sample contained small oxygen precipitates. This result indicates that interstitial copper atoms do not precipitate in boron-doped silicon at room temperature, if the copper concentration is 10^{13} cm^{-3}. Therefore, small oxygen precipitates are not efficient precipitation sites for copper at room temperature. The result also indicates that the out-diffusion of interstitial copper was prevented by a positive corona charge. This means that interstitial copper atoms do not overcome the energy band bending of 0.8 eV, which was induced with a positive corona charge of 1 μC·cm^{-2}. It is proven for the first time that interstitial copper atoms really exist in boron doped bulk silicon after long storage periods. This gives us the possibility to study the properties of interstitial copper and its reactions in silicon.

In this work, the optical activation of copper and the properties of interstitial copper in silicon by means of carrier lifetime measurements using the µPCD technique were studied. The results indicate that the recombination activity of interstitial copper in boron-doped silicon is two decades lower than that determined earlier by Istratov *et al.* [30]. The hole capture cross-section of interstitial copper was determined to be below 3×10^{-17} cm^2. This was determined from the SHR-equation with an interstitial copper energy level at E_c-0.15 eV [29], an electron capture cross-section of 1.5×10^{-15} cm^2 [29], and a carrier lifetime of 5.0 ms in silicon with an interstitial copper concentration of $(1.3\pm0.1)\times10^{13}$ cm^{-3}. The carrier lifetime was measured under an excess charge concentration of $(6\pm1)\times10^{15}$ cm^{-3}. The interstitial copper concentration was measured by means of TID. The recombination activity of interstitial copper is low, because it only has a shallow donor level, E_c-(0.15±0.01) eV [29].

The optical activation of copper was studied in boron-doped silicon. The study was limited to copper concentrations below 1.3×10^{13} cm^{-3}. Silicon wafers containing different amounts of interstitial copper were exposed to high intensity light. The charge carrier lifetime in silicon decreased as a function of the optical activation time. The carrier lifetimes were measured at an excess charge concentration of $(6\pm1)\times10^{15}$ cm^{-3}. The copper related recombination rate was calculated from the change of the inverse charge carrier lifetime. The increase of the copper related recombination rate as a function of the illumination time followed an exponential law. The mono exponential curve was fitted to the experimentally determined copper related recombination rates. The fitting parameters were the saturation of the copper related recombination rate and the precipitation time constant.

The dependence of the precipitation time constant on the light intensity was studied with samples containing oxygen defects. The electron quasi-Fermi level during the high-intense illumination had to be above E_c-0.2 eV in order to induce copper precipitates in a reasonable time. It is suggested here that the optical activation changes the charge state of copper precipitates, which enables copper precipitation at room temperature. The suggestion is based on the results that the copper precipitates are neutral or negatively charged when the Fermi-

level is above E_c-0.2 eV, and positively charged when the Fermi-level is below E_c-0.2 eV [22]. Positively charged interstitial copper atoms precipitate with neutral or negatively charged copper precipitates, but not with positively charged copper precipitates due to Coulomb repulsion [10]. However, in presence of oxygen defects the copper precipitates even though the Fermi-level is below E_c-0.2 eV [38]. Using the SHR-statistics it was found that the interstitial copper has a high probability to change its charge state when a high excess charge carrier concentration is present in p-type silicon. Therefore, the charge state of interstitial copper may also have an effect on the formation of copper precipitates during the high-intensity illumination. It was also found that the saturation of the copper related recombination rate was independent of the light intensity.

The dependence of the copper related recombination rate on the illumination time was modelled with the diffusion-limited precipitation theory. Two models were presented. In the volume recombination model, the recombination rate is proportional to the precipitated copper concentration. In the surface recombination model, the recombination rate is proportional to the surface area of the copper precipitates. Both models fitted the measured copper related recombination rate dependence on the illumination time well. Both models are usable for the calculation of the recombination activity of copper precipitates.

The copper precipitation time constant decreased when silicon contained a higher concentration of interstitial copper or oxygen defects. The results indicate that the precipitation time constant decreased, because the density of copper precipitates increased. The density and radius of copper precipitates were calculated by means of the diffusion-limited precipitation model.

The light-induced copper related recombination rate dependence on the copper concentration and the density of oxygen defects is complicated. The recombination rate depends on the copper concentration superlinearly when silicon contains small oxygen precipitates. The light-induced recombination rate is above two orders of magnitude higher in silicon containing a high oxygen defect density compared to silicon containing a low oxygen defect density. It is suggested here that the reason for this is copper precipitates formed at microscopic lattice defects and at oxygen related defects. It is further suggested that the copper precipitates at oxygen related defects have a more than two decades higher recombination activity than those at microscopic lattice defects. The suggestions are based on the results that the density of the copper precipitates stayed about the same, but the recombination rate increased, when the density of oxygen defects increased from a low density to a density level of 7×10^7 cm^{-3}. Therefore, a low concentration of copper precipitates at oxygen defects is enough to change the total recombination activity of copper without any noticeable change in the total concentration of copper precipitates. It was determined with the diffusion-limited precipitation model that the concentration of the copper precipitates was 10^8-10^9 cm^{-3} when the density of oxygen defects in silicon was 5×10^8 cm^{-3} or below. The radius of the copper precipitates was below 4 nm. Using the volume recombination model it was calculated that the concentration of the copper precipitates at oxygen defects was low compared to the concentration of copper precipitates at microscopic lattice defects. Therefore, oxygen related defects were not efficient gettering sites for copper. In conclusion, the copper related recombination rate depends on whether the copper precipitates are located at microscopic lattice defects or at oxygen related defects or both. The

copper related recombination rate is maximized by using silicon samples containing a high oxygen defect density to aid the formation of copper precipitates at oxygen related defects.

Experimental results for the optical activation of copper are used to estimate the quantitative detection limit of copper in boron doped silicon. The quantitative detection limit of copper is about 3×10^{12} cm^{-3} in boron doped silicon without oxygen defects. The quantitative detection limit of copper is about 5×10^{10} cm^{-3} in boron doped silicon if the bulk silicon contains small oxygen defects at high density.

It should be noted that the determination of copper concentration by means of optical activation of copper is at a preliminary stage. The results in this work are for air-cooled samples at one boron concentration level. However, the results indicate that the copper concentration can be determined by lifetime measurements by using the correlation curves, which are measured with the aid of TID measurements. The correlation curves are the relation between the change of the inverse carrier lifetime due to the optical activation and the interstitial copper concentration.

The decrease of charge carrier lifetime due to optical activation results from the copper contamination. This can be confirmed by out-diffusing copper to the sample surface and repeating the optical activation. The out-diffusion can be done by depositing a negative corona charge on the dielectric surface of silicon. A copper contamination is present in silicon, if a decrease in the lifetime is not seen after the second optical activation. It should be noted that it takes time for the copper to out-diffuse.

The determined out-diffusion time constant of copper was close to the theoretical time constant for copper diffusion to the sample surfaces. The out-diffusion time constant was determined by measuring the copper related recombination rate as a function of the elapsed time after the deposition of the negative corona charge. The result excludes the possibility that the dissociation of copper pairs was the reason for the decrease of the carrier lifetime in the samples studied in the present work. The dissociation time constant of copper pairs is a few weeks at room temperature [26], but the out-diffusion time constant was below one hour in the present work. However, the influence of copper pairs on the light-induced copper related recombination rate in a fast cooled silicon sample, in which almost all copper can be in copper pairs as presented by Koveshnikov *et al.* [27], should be studied.

The detection of copper by means of optical activation contains at least two drawbacks. It takes time for the copper atoms to diffuse to the precipitation places. The diffusion time is in the order of magnitude of 1000 seconds. The copper atoms form precipitates when silicon contains a high excess charge carrier concentration. This can be generated by means of a light intensity of 30 $W\cdot cm^{-2}$. Therefore, the copper detection over a whole wafer area is time-consuming using optical activation.

The charge carrier lifetime depends strongly on the charge carrier injection level in silicon containing light-induced copper precipitates. The charge carrier lifetime is ten times higher under high injection level conditions than under low injection level conditions. Therefore, the SPV technique may be more sensitive for the detection of light-induced copper precipitates than the μPCD technique. However, the μPCD technique is more sensitive than the SPV

technique, if the wafer contains a moderate iron contamination, because the recombination activity of interstitial iron is lower at high excess charge carrier concentrations (μPCD) than low carrier concentrations (SPV).

Appendix A Recombination activity of copper precipitates

A.1 Calculations for comparison

In this appendix the volume recombination coefficient of precipitated copper atoms k_{prec} and the surface recombination velocity at copper precipitates S_{prec} are calculated from measurement data and TEM figures presented by Istratov *et al.* [22]. They determined the size and the density of copper precipitates with transmission electron microscope (TEM) measurements. They determined the minority carrier diffusion length or its upper limit by means of electron beam induced current (EBIC) measurements. Table A.1 shows their measurement results and the calculated precipitated copper concentration, the volume recombination coefficient and the surface recombination velocity. The diameter of the precipitates was determined from the TEM figures. The area of the copper precipitates was calculated by assuming that the precipitates were in the shape of plate circles, from

$$A = 2\pi r^2, \tag{A.1}$$

where r is the radius of the plate-shaped precipitate. The precipitated copper concentration was calculated from equation

$$c_{\mathrm{prec}} = \pi r^2 d\rho n, \tag{A.2}$$

where d is the thickness of the precipitate, ρ is the density of copper atoms in copper precipitates, n is the concentration of the copper precipitates. The volume recombination coefficient of precipitated copper was calculated from equation

$$k_{\mathrm{prec}} = \frac{D_n}{L_n^2 c_{\mathrm{prec}}}, \tag{A.3}$$

where D_n and L_n are the diffusivity and diffusion length of minority charge carriers, respectively. The surface recombination velocity was calculated from equation

$$S_{\mathrm{prec}} = \frac{D_n}{L_n^2 n A}, \tag{A.4}$$

which was solved from the recombination rate equations

$$R = \Delta n\, S_{\mathrm{prec}}\, n\, A = \frac{\Delta n D_n}{L_n^2}. \tag{A.5}$$

Table A.1: The density of copper precipitates n, their diameter $2r$ and thickness d, and the minority carrier diffusion length L_n [22]. The calculated precipitated copper concentration c_{prec}, the volume recombination coefficient of precipitated copper atom k_{prec} and the surface recombination velocity at the copper precipitates S_{prec}. For the density of copper in the precipitates a value of 6.52×10^{22} cm^{-3} was used, and for the hole and electron diffusivities values of 12 cm$^2 \cdot$s^{-1} and 33 cm$^2 \cdot$s^{-1}, respectively.

type	quench K·s^{-1}	n cm^{-3}	$2r$ µm	d nm	L_n µm	c_{prec} cm^{-3}	k_{prec} cm$^3 \cdot$s^{-1}	S_{prec} cm·s^{-1}
n-Si	2000	4.3E+12	0.03	0.5	<2.2	9.9E+16	>2.5E-9	>4.1E+06
n-Si	1000	1.1E+12	0.07	0.5	<2.6	1.4E+17	>1.3E-9	>2.1E+06
n-Si	200	1.4E+09	0.24	5	13	2.1E+16	3.4E-10	5.6E+06
p-Si	2000	4.3E+12	0.03	0.5	<2.2	9.9E+16	>6.9E-9	>1.1E+07

Appendix B Simulation

B.1 Excess charge carrier concentration

The excess charge carrier concentration in silicon was calculated with the aid of a Silvaco device simulator using cylindrical coordinates. The carrier lifetime measurements and optical activation conditions were modelled.

B.1.1 Measurement conditions

In Figure B.1 the excess charge carrier concentration is shown as a function of the distance from the middle point of the light spot. Figure B.1 shows that the excess charge carrier concentration was $(6\pm1)\times10^{15}$ cm^{-3} due to the bias-light, within a radius of 0.07 cm. The simulation parameters for excitation were the radius of the bias light and the pulse light spots, which were 0.056 cm, a bias light intensity of 0.5 W·cm^{-2}, a bias light wavelength of 973.5 nm, a pulse light intensity of 1317 W·cm^{-2} for a duration of 200 ns, a pulse light wavelength of 905 nm. The material parameters were a boron concentration of 10^{15} cm^{-3}, electron and hole Auger coefficients of $C_n=1.5\times10^{-30}$ cm^6·s^{-1} and $C_p=0.6\times10^{-30}$ cm^6·s^{-1}, respectively. They were increased from the default values in order to match the ambipolar Auger coefficient at excess charge carrier concentrations between 10^{15} cm^{-3} and 10^{16} cm^{-3} with the ambipolar Auger coefficient published in Ref. [47]. A interstitial iron concentration of 6×10^9 cm^{-3} was simulated by means of a donor trap by using a level at E_V+0.38 eV, an electron capture coefficient of 5.7×10^{-7} cm^3·s^{-1} and a hole capture coefficient of 1.1×10^{-9} cm^3·s^{-1}.

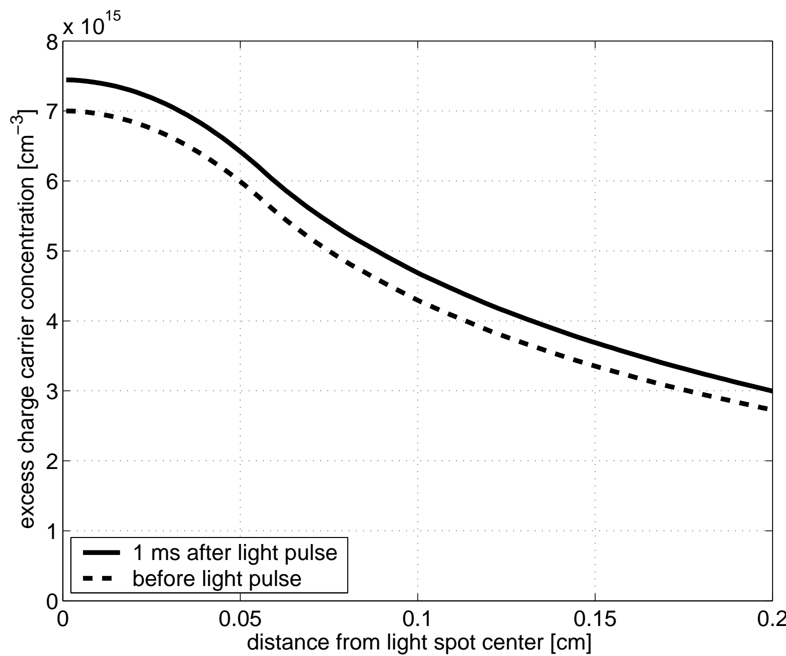

Figure B.1: The excess charge carrier concentration as a function of distance from the center of the light spot.

B.1.2 Optical activation conditions

The excess charge carrier concentration under optical activation conditions was simulated using the following parameters. The simulation parameters for excitation were the radius of the bias light spot, which was 0.056 cm, the bias light intensity varied and the bias light wavelength was 973.5 nm. The material parameters were an interstitial iron concentration of 6×10^{9} cm^{-3}, electron and hole Auger coefficients C_n=1.5×10^{-30} cm$^{6}\cdot$s^{-1} and C_p=0.6×10^{-30} cm$^{6}\cdot$s^{-1}, respectively. An interstitial iron concentration of 6×10^{9} cm^{-3} was simulated by means of a donor trap by using a level at E_v+0.38 eV, an electron capture coefficient of 5.7×10^{-7} cm$^{3}\cdot$s^{-1} and a hole capture coefficient of 1.1×10^{-9} cm$^{3}\cdot$s^{-1}. Light-induced copper precipitates were simulated by means of a donor trap by using a level at E_v+0.56 eV and a concentration of 10^{9} cm^{-3}. The capture cross-sections for the level at E_v+0.56 eV were fitted to get the carrier lifetime calculated from SHR-equation (3.23) to be equal with the measured carrier lifetime at the end stage of the optical activation. The measured lifetimes for samples A and B were 100 µs and 200 µs, respectively, at a high excess charge carrier concentration level. The ratio of capture cross-section was kept a constant 1:9, because carrier lifetimes in silicon containing light-activated copper defects was ten times higher at high excess charge carrier concentration than at low excess charge carrier concentration. Table B.1 shows the boron concentration and the electron and hole capture coefficients for the level at E_v+0.56 eV used in the simulations. The actual recombination parameters for the light-induced copper precipitates are not known.

Table B.1: The parameters used in the simulations. The boron concentration, the electron and hole capture coefficients for the level at E_v+0.56 eV and the light intensity. The simulation result was the average electron quasi-Fermi level E_c-E_{Fn} within a radius of 0.5 mm from the center of the light spot.

sample	N_a cm^{-3}	c_n cm$^{3}\cdot$s^{-1}	c_p cm$^{3}\cdot$s^{-1}	light intensity W$\cdot$cm^{-2}	E_c-E_{Fn} eV
A	10^{15}	1.0E-04	1.1E-05	4.5	0.201
A	10^{15}	1.0E-04	1.1E-05	11.9	0.177
A	10^{15}	1.0E-04	1.1E-05	16.2	0.170
A	10^{15}	1.0E-04	1.1E-05	20.4	0.166
A	10^{15}	1.0E-04	1.1E-05	28.9	0.160
A	10^{15}	1.0E-04	1.1E-05	45.9	0.153
B	6.1×10^{14}	5.0E-05	5.6E-06	0.11	0.308
B	6.1×10^{14}	5.0E-05	5.6E-06	28.9	0.156

Bibliography

[1] K. Graff, "Metal Impurities in Silicon-Device Fabrication," 2nd edition (Springer-Verlag Berlin Heidelberg New York, 2000).
[2] R. S. Hockett, "Ultratrace impurity analysis of silicon surfaces by SIMS and TXRF methods," in Handbook of semiconductor wafer cleaning technology: science, technology, and applications, edited by Werner Kern (Noyes Publications, New Jersey, USA, 1993), pp. 537-592.
[3] M. B. Shabani, T. Yoshimi, and H. Abe, "Low-Temperature Out-diffusion of Cu from Silicon Wafers," J. Electrochem. Soc. **143**, 2025 (1996).
[4] J. Fucsko, S. S. Tan and M. K. Balazs, "Measurement of trace metallic contaminants on silicon wafer surfaces in native and dielectric silicon oxides by vapor phase decomposition flow injection inductively coupled plasma-mass spectrometry," J. Electrochem. Soc. **140**, 1105 (1993).
[5] R. Hoelzl, K.-J. Range, L. Fabry, "Modeling of Cu gettering in *p*- and *n*-type silicon and in poly-silicon," Appl. Phys. A **75**, 525-534 (2002).
[6] T. Heiser and E. R. Weber, "Transient ion-drift-induced capacitance signals in semiconductors," Phys. Rev. B **58**, 3893 (1998).
[7] A. A. Istratov and E. R. Weber, "Physics of Copper in Silicon," J. Electrochem. Soc. **149**, G21 (2002).
[8] W. B. Henley, D. A. Ramappa and L. Jastrezbski, "Detection of copper contamination in silicon by surface photovoltage diffusion length measurements," Appl. Phys. Lett. **74**, 278 (1999).
[9] D. A. Ramappa, "Surface photovoltage analysis of phase transformation of copper in p-type silicon," Appl. Phys. Lett. **76**, 3756 (2000).
[10] C. Flink, H. Feick, S. A. McHugo, W. Seifert, H. Hieslmair, T. Heiser, A. A. Istratov, and E. R. Weber, "Out-Diffusion and Precipitation of Copper in Silicon: An Electrostatic Model," Phys. Rev. Lett. **85**, 4900 (2000).
[11] M. B. Shabani, S. Okuuchi, and Y. Shimanuki, "Kinetics of low-temperature out-diffusion of copper from silicon wafers," in Analytical and Diagnostic Techniques for Semiconductor Materials, Devices, and Processes, edited by B. O. Kolbesen, C. Claeys, P. Stallhofer, F. Tardif, J. Benton, T. Shaffner, D. Schroder, S. Kishino, and P. Rai-Choudhury (PV 99-16, The Electrochemical Proceedings Series, Pennington, NJ, 1999), pp. 510-525.
[12] V. Raineri, D. Cali, M. Camalleri, M. Di Dio and A. Puglisi, "Cu Determination in Silicon Wafers: a Comparison between Electrical and Chemical Measurements," Solid State Phenomena **69-70**, pp. 461-466 (1999).
[13] I. Tarasov, S. Ostapenko and S. Koveshnikov, "Light induced defect reactions in boron-doped silicon: Cu versus Fe," presented at the Eighth workshop on crystalline silicon solar cell materials (National renewable energy laboratory (NREL)/CP-520-25232, 1998) pp. 207-210.
[14] A. Bazzali, G. Borionetti, R. Orizio, D. Gambaro and R. Falster, "Oxygen precipitate precursors and size thresholds for the preferential nucleation for copper and nickel precipitation in silicon: the detection of copper and nickel contamination by minority carrier lifetime methods," Mater. Sci. Eng. B. **36**, 85 (1996).
[15] R. N. Hall and J. H. Racette, "Diffusion and solubility of copper in extrinsic and intrinsic germanium, silicon, and gallium arsenide," J. Appl. Phys. **35**, 379 (1964).

[16] A. A. Istratov, C. Flink, H. Hieslmair, E. R. Weber, T. Heiser, “Intrinsic Diffusion Coefficient of Interstitial Copper in Silicon,” Phys. Rev. Lett. **81**, 1243 (1998).
[17] H. Reiss, C. S. Fuller, and F. J. Morin, “Chemical interactions among defects in germanium and silicon,” The Bell System Technical J. **35**, 535 (1956).
[18] E. R. Weber, “Transition Metals in Silicon,” Appl. Phys. A **30**, 1 (1983).
[19] M. Seibt, H. Hedemann, A. A. Istratov, F. Riedel, A. Sattler, and W. Schröter, “Structural and Electrical Properties of Metal Silicide Precipitates in Silicon,” Phys. Status Solidi A **171**, 301 (1999).
[20] A. A. Istratov, E. R. Weber, “Electrical properties and recombination activity of copper, nickel and cobalt in silicon,” Appl. Phys. A **66**, 123 (1998).
[21] M. Seibt, M. Griess, A. A. Istratov, H. Hedemann, A. Sattler, and W. Schröter, “Formation and Properties of Copper Silicide Precipitates in Silicon,” Phys. Status Solidi A **166**, 171 (1998).
[22] A. A. Istratov, H. Hedemann, M. Seibt, O. F. Vyvenko. W. Schröter, T. Heiser, C. Flink, H. Hieslmair, and E. R. Weber, “Electrical and Recombination Properties of Copper-Silicide Precipitates in Silicon,” J. Electrochem. Soc. **145**, 3889 (1998).
[23] M. Elkajbaji, J. Dessus and J. Thibault, “Structure of copper precipitates in a symmetrical silicon tilt bicrystal: high-resolution electron microscopy and energy-dispersive X-ray analysis,” Philos. Mag. A. **66**, 873 (1992).
[24] M. Seibt and K. Graff, “Characterization of haze-forming precipitates in silicon,” J. Appl. Phys. **63**, 4444 (1988).
[25] M. Hourai, K. Murakami, T. Shigematsu, N. Fujino and T. Shiraiwa, “Behavior of Defects Induced by Metallic Impurities on Si(100) Surfaces,” Jap. J. Appl. Phys. **28**, 2413 (1989).
[26] A. A. Istratov, H. Hieslmair, T. Heiser, C. Flink and E. R. Weber, “The dissociation energy and the charge state of a copper-pair in silicon,” Appl. Phys. Lett. **72**, 474 (1998).
[27] S. Koveshnikov, Y. Pan and H. Mollenkopf, “Investigation of electronic states in copper doped p-type silicon,” Electrochem. Soc. Proc. **96**, 473 (1996).
[28] H. B. Erzgräber and K. Schmalz, “Correlation between the Cu-related luminescent center and a deep level in silicon,” J. Appl. Phys. **78**, 4066 (1995).
[29] A. A. Istratov, H. Hieslmair, C. Flink, T. Heiser and E. R. Weber “Interstitial copper related center in n-type silicon,” Appl. Phys. Lett. **71**, 2349 (1997).
[30] A. A. Istratov, C. Flink, H. Hieslmair , T. Heiser and E. R. Weber “Influence of interstitial copper on diffusion length and lifetime of minority carriers in p-type silicon,” Appl. Phys. Lett. **71**, 2121 (1997).
[31] A. A. Istratov, H. Hieslmair, E. R. Weber, “Iron and its complexes in silicon,” Appl. Phys. A. **69**, 13 (1999).
[32] W. Schröter, V. Kveder, M. Seibt, H. Ewe, H. Hedemann, F. Riedel, A. Sattler, “Atomic structure and electronic states of nickel and copper silicides in silicon,” Mat. Sci. Eng **B72**, 80, (2000).
[33] M. Kittler, W. Seifert and K. Nnobloch, “Influence of contamination on the electrical activity of crystal defects in silicon,” Microelectronic Engineering **66**, 281 (2003).
[34] B. Shen, T. Sekiguchi, J. Jablonski, and K. Sumino, “Gettering of copper by bulk stacking faults and punched-out dislocations in Czochralski-grown silicon,” J. Appl Phys. **76**, 4540 (1994).

[35] A. Correia, D. Ballutaud, A. Boutry-Forveille and J.-L. Maurice, “Effects of copper and oxygen precipitation during thermal oxidation of silicon: An electron-beam-induced current study,” J. Appl. Phys. **78**, 6543 (1995).
[36] S. Naito and T. Nakashizu, “Electric Degradation and Defect Formation of Silicon due to Cu, Fe, and Ni Contamination,” in Defect Engineering in Semiconductor Growth, Processing and Device Technology, edited by S. Ashok, J. Chevallier, K. Sumino and E. Weber (Mater. Res. Symp. Proc. Vol. 262, Materials Research Society, Pittsburgh, 1992) pp. 641-652.
[37] M. Miyazaki, “Influence of Metal Impurities on Lifetime,” in Recombination lifetime measurements in silicon, edited by D. C. Gupta, F. R. Bacher and W. M. Hughes, ASTM STP 1340 (American Society for Testing and Materials, West Conshohocken, PA, 1998) pp. 294-304.
[38] R. Sachdeva, A. A. Istratov, E. R. Weber, “Recombination activity of copper in silicon,” Appl. Phys. Lett. **79**, 2937 (2001).
[39] A. A. Istratov, R. Sachdeva, C. Flink, S. Balasubramanian and E. R. Weber, “Precipitation Kinetics and Recombination Activity of Cu in Si in the Presence of Internal Gettering Sites,” Solid State Phenomena **82-84**, 323-330 (2002).
[40] P. Eichinger, “New developments of the Elymat technique,” in Recombination lifetime measurements in silicon, ASTM STP 1340, edited by D. C. Gupta, F. R. Bacher, and W. M. Hughes (American Society for Testing and Materials, West Conshohocken, PA, 1998) pp. 101-111.
[41] D. Macdonald, A. Cuevas, S. Rein, P. Lichtner, and S. W. Glunz, “Temperature- and injection-dependent lifetime spectroscopy of copper-related defects in silicon,” presented at WCPEC, Osaka, May 11-18, 2003.
[42] K. Stewart, A. Cuevas, D. Macdonald and J. Williams, “Influence of copper on the carrier lifetime of n-type and p-type silicon,” presented at 11th workshop on crystalline silicon solar cell materials and processes, (National renewable energy laboratory (NREL) Estes Park, Colorado, 2001), pp. 212-215.
[43] W. Shockley and W. T. Read, JR., “Statistics of the Recombinations of Holes and Electrons,” The Physical Review, **87**, 835 (1952).
[44] R. N. Hall, “Electron-Hole Recombination in Germanium,” The Physical Review, **87**, 387 (1952).
[45] D. Macdonald and A. Cuevas, “Validity of simplified Shockely-Read-Hall statistics for modeling carrier lifetimes in crystalline silicon,” Phys. Rev. B **67**, 075203 (2003).
[46] M. A. Green, “Intrinsic concentration, effective densities of states, and effective mass in silicon,” J. Appl. Phys. **67**, 2944 (1990).
[47] M. J. Kerr and A. Cuevas, “General parametrization of Auger recombination in crystalline silicon,” J. Appl. Phys. **91**, 2473 (2002).
[48] D. K. Schroder, “Semiconductor Material and Device Characterization,” (J. Wiley & Sons, New York, 1990).
[49] T. Otaredian, “Contactless microwave lifetime measurement,” Ph. D. thesis, Delft University of Technology, Delft, The Netherlands, 1992.
[50] F. Schuurmans, “Surface Passivation of Silicon by PECVD silicon nitride,” Ph. D. thesis, ISBN 90-393-1637-6, Universiteit Utrecht, Utrecht, Nederlands, 1998.
[51] M. J. Kerr and A. Cuevas, “Very low bulk and surface recombination in oxidized silicon wafers,” Semicond. Sci. Tech. **17**, 35 (2002).

[52] M. J. Kerr and A. Cuevas, "Recombination at the interface between silicon and stoichiometric plasma silicon nitride," Semicond. Sci. Tech. **17**, 166 (2002).
[53] T. S. Horányi, T. Pavelka and P. Tüttö, "In situ bulk lifetime measurement on silicon with a chemically passivated surface," Appl. Surf. Science **63**, 306 (1993).
[54] E. Yablonovitch and T. Gmitter, "Auger recombination in silicon at low carrier densities," Appl. Phys. Lett. **49**, 587 (1986).
[55] M. Schöfthaler, R. Brendel, G. Langguth, and J. H. Werner, "High-Quality Surface Passivation by Corona-Charged Oxides for Semiconductor Surface Characterization," IEEE Proceedings of the first World Conference on Photovoltaic Energy Conversion, New York (IEEE, 1994) pp. 1509-1512.
[56] M. Ichimura, A. Tada, E. Arai, H. Takamatsu and S. Sumie, "Bulk carrier lifetime measurement by the microwave reflectance photoconductivity decay method with external surface electric field," Appl. Phys. Lett. **80**, 4390 (2002).
[57] S. M. Sze, "Physics of Semiconductor Devices," 2nd edition (J. Wiley & Sons, New York, 1981) p. 51.
[58] J. Storgårds, "Study of excess carrier lifetime in semiconductor wafers," Master's Thesis, Helsinki University of Technology, 2000.
[59] J. Storgårds, H. Väinölä, M. Yli-Koski and J. Sinkkonen, "3D effects on minority carrier recombination in homogeneous silicon wafers," Physica Scripta Vol. **T101**, 61 (2002).
[60] H. Väinölä, "Study of carrier lifetime in thin silicon layers by photoconductive decay," Master's Thesis, Helsinki University of Technology, 2000.
[61] H. Väinölä, J. Storgårds, M. Yli-Koski and J. Sinkkonen, "Light induced change on the built-in potential of p/p(+) structures and its effect on carrier lifetime measurements," Mater. Sci. Eng. B **91**, 421 (2002).
[62] H. Väinölä, J. Storgårds, M. Yli-Koski and J. Sinkkonen, "Evaluation of effective carrier lifetime in epitaxial silicon layers," Solid State Phenomena **82-84**, 771 (2002).
[63] K. L. Luke and L.-J. Cheng, "Analysis of the interaction of a laser pulse with a silicon wafer: Determination of bulk lifetime and surface recombination velocity," J. Appl. Phys. **61**, 2282 (1987).
[64] M. Rosling, H. Bleichner, P. Jonsson and E. Nordlander, "The ambipolar diffusion coefficient in silicon: Dependence on excess-carrier concentration and temperature," J. Appl. Phys. **76**, 2855 (1994).
[65] A. B. Sproul, "Dimensionless solution of the equation describing the effect of surface recombination on carrier decay in semiconductors," J. Appl. Phys. **76**, 2851 (1994).
[66] J. Schmidt, "Measurement of Differential and Actual Recombination Parameters on Crystalline Silicon Wafers," IEEE Trans. Electron Devices **46**, 2018 (1999).
[67] F. M. Schuurmans, A. Schönecker, A. R. Burgers, and W. C. Sinke, "Simplified evaluation method for light-biased effective lifetime measurements," Appl. Phys. Lett. **71**, 1795 (1997).
[68] F. S. Ham, "Theory of diffusion-limited precipitation," J. Phys. Chem. Solids, **6**, 335 (1958).
[69] H. Hieslmair, A. A. Istratov, T. Heiser, and E. R. Weber, "Evaluation of precipitate densities and capture radii from the analysis of precipitation kinetics," J. Appl. Phys. **84**, 713 (1998).
[70] J. M. Hwang and D. K. Schroder, "Recombination properties of oxygen-precipitated silicon," J. Appl. Phys. **59**, 2476 (1986).

[71] M. Ronay and R. G. Schad, "New Insight into Silicide Formation: The Creation of Silicon Self-Interstitials," Phys. Rev. Lett. **64**, 2042 (1990).
[72] S. W. Glunz, S. Rein and J. Knobloch, "Stable Czochralski Silicon Solar Cells Using Gallium-Doped Base Material," in Proceeding of 16th European Photovoltaic Solar Energy Conference, edited by H. Scheer, B. McNelis, W. Palz, H. A. Ossenbrink and P. Helm (James&James, London, UK, 2000) pp. 1070-1075.
[73] W. Warta, "Defect and impurity diagnostics and process monitoring," Solar Energy Materials & Solar Cells **72,** 389 (2002).
[74] A. Borghesi, B. Pivac, A. Sassella and A. Stella, "Oxygen precipitation in silicon," J. Appl. Phys. **77**, 4169 (1995).
[75] C. Swiatkowski, "Lifetime Measured by Low Injection Level μPCD Technique," in Recombination lifetime measurements in silicon, ASTM STP 1340, edited by D. C. Gupta, F. R. Bacher, and W. M. Hughes (American Society for Testing and Materials, West Conshohocken, PA, 1998), p. 80-87.
[76] D. A. Clugston and P. A. Basore, "PC1D version 5: 32-bit solar cell modeling on personal computers," in Proceedings of 26th IEEE Photovoltaic Specialists Conference, Anaheim, USA (IEEE, 1997), pp. 207-210.
[77] P. E. Gruenbaum, R. A. Sinton, and R. M. Swanson, "Light-induced degradation at the silicon/silicon dioxide interface," Appl. Phys. Lett. **52**, 1407 (1988).
[78] M. Miyazaki, K. Kawai and M. Ichimura, "Measurement of Minority Carrier Recombination Lifetime in Silicon Wafers by Measurement of Photoconductivity Decay by Microwave Reflectance: Result of Round Robin Test," in Recombination lifetime measurements in silicon, ASTM STP 1340, edited by D. C. Gupta, F. R. Bacher, and W. M. Hughes (American Society for Testing and Materials, West Conshohocken, PA, 1998), p. 347-366.
[79] A. M. Goodman, "A method for the measurement of short minority carrier diffusion lengths in semiconductors," J. Appl. Phys. **32**, 2550 (1961).
[80] A. L. P. Rotondaro, T. Q. Hurd, A. Kaniava, J. Vanhellemont, E. Simoen, M. M. Heyns, C. Claeys, G. Brown, "Impact of Fe and Cu contamination on the minority carrier lifetime of silicon substrates," J. Electrochem. Soc., **143**, 3014 (1996).
[81] A. A. Istratov, C. Flink, H. Hieslmair, S. A. McHugo, E. R. Weber, "Diffusion, solubility and gettering of copper in silicon," Mater. Sci. Eng. B. **72**, 99 (2000).
[82] T. S. Horányi, P. Tüttõ, and Cs. Kovacsics, "Identification possibility of metallic impurities in p-type silicon by lifetime measurement," J. Electrochem. Soc. **143**, 216 (1996).
[83] H. Väinölä, M. Yli-Koski, A. Haarahiltunen, J. Sinkkonen, "Sensitive copper detection in p-type CZ silicon using μ-PCD," J. Electrochem. Soc. **150**, G790 (2003).
[84] K. Sunakawa, K. Asako, T. Yagi and Y. Hayamizu, "Method and apparatus for detecting heavy metals in silicon wafer bulk with high sensitivity," U.S Patent No. 6,140,131 (31 October 2000).
[85] M. Yli-Koski, M. Palokangas, A. Haarahiltunen, H. Väinölä, J. Storgårds, H. Holmberg and J. Sinkkonen, "Detection of low-level copper contamination in p-type silicon by means of microwave photoconductive decay measurements," J. Phys.: Condens. Matter **14**, 13119 (2002).
[86] P. S. Plekhanov and T. Y. Tan, "Schottky effect model of electrical activity of metallic precipitates in silicon," Appl. Phys. Lett. **76**, 3777 (2000).

[87] M. Yli-Koski, H. Väinölä, A. Haarahiltunen, J. Storgårds, E. Saarnilehto and J. Sinkkonen, “Light activated copper defects in p-type silicon studied by PCD,” Physica Scripta (in press).
[88] R. Hölzl, L. Fabry and K. J. Range, “Gettering efficiencies for Cu and Ni as a function of size and density of oxygen precipitates in p/p- silicon epitaxial wafers,” Appl. Phys. **A 73**, 137 (2001).